REPORT DOCUMENTATION PAGE

Form Approved
OMB NO. 0704-0188

1. AGENCY USE ONLY (Leave Blank)	2. REPORT DATE	3. REPORT TYPE AND DATES COVERED
	July, 2001	Final Report 01 Jul 97 - 31 Mar 01 ~~July 1997 - December, 2000~~

4. TITLE AND SUBTITLE

High-Performance Multi-Fuel AMTEC Power System

5. FUNDING NUMBERS

DAAG55-97-C-0042

6. AUTHOR(S)

Peter J. Loftus
Roberto O. Pellizzari

7. PERFORMING ORGANIZATION NAME(S) AND ADDRESS(ES)

Arthur D. Little, Inc.
Acorn Park
Cambridge, MA 02140-2390

8. PERFORMING ORGANIZATION REPORT NUMBER

9. SPONSORING / MONITORING AGENCY NAME(S) AND ADDRESS(ES)

U. S. Army Research Office
P.O. Box 12211
Research Triangle Park, NC 27709-2211

10. SPONSORING / MONITORING AGENCY REPORT NUMBER

37536.2-CH

11. SUPPLEMENTARY NOTES

The views, opinions and/or findings contained in this report are those of the author(s) and should not be construed as an official Department of the Army position, policy or decision, unless so designated by the documentation.

12 a. DISTRIBUTION / AVAILABILITY STATEMENT	12 b. DISTRIBUTION CODE

13. ABSTRACT (Maximum 200 words)

AMTEC technology has demonstrated thermal to electric conversion efficiencies and power densities which make it an attractive option for meso-scale power generation. This report details development of an integrated, logistics-fueled, 500 W AMTEC power supply. The development targeted 20% AMTEC thermal efficiency and 16% system efficiency (fuel to net power) in a system that weights 9 kg. The heat source developed was a compact, recuperated combustion system capable of operating with most common liquid or gaseous fuels. Key technical issues that were addressed included: developing a cylindrical multi-tube/single cell AMTEC configuration with effective management of alkali metal flow; scaling down and integrating a multi-fuel micro-combustor technology to achieve soot-free logistics fuel combustion and uniform heat flux to the AMTEC module hot side; and integrating a compact, light-weight recuperator to achieve high thermal efficiency. In addition, we evaluated and tested two alternative AMTEC design and manufacturing concepts aimed at reducing the cost and improving the manufacturability of the technology.

14. SUBJECT TERMS	15. NUMBER OF PAGES
AMTEC, beta-alumina, sodium, direct thermal conversion, wick, artery, condenser, electrode, meso-scale power systems, logistics fuels, recuperator, combustor, combustion, heat transfer, atomization.	105
	16. PRICE CODE

17. SECURITY CLASSIFICATION OR REPORT	18. SECURITY CLASSIFICATION ON THIS PAGE	19. SECURITY CLASSIFICATION OF ABSTRACT	20. LIMITATION OF ABSTRACT
UNCLASSIFIED	UNCLASSIFIED	UNCLASSIFIED	UL

NSN 7540-01-280-5500
(Rev.2-89)
Prescribed by ANSI Std. 239-18

Standard Form 298

298-102

Arthur D Little

20010831 007

High-Performance Multi-Fuel AMTEC Power System

Final Report

ARO Contract DAAG55-97-C-0042

July, 1997 - December, 2000

Peter J. Loftus
Arthur D. Little, Inc.
Cambridge, MA

Robert K. Sievers
Advanced Modular Power Systems, Inc.
Ann Arbor, MI

Table of Contents

List of Figures

List of Figures (continued)

List of Tables

1 Executive Summary

Beginning in July 1997, Arthur D. Little, Inc. (ADL) and Advanced Modular Power Systems, Inc. (AMPS) began working together on the development of a prototype compact, logistics-fueled, 500 Watt power system which integrates alkali metal thermal to electric conversion (AMTEC) technology with an efficient multi-fuel thermal energy source. AMTEC technology had previously demonstrated thermal to electric conversion efficiencies and power densities that made it an attractive option for meso-scale power generation. We established program targets of 20% AMTEC thermal efficiency (i.e. heat to gross electric power) and 16% system efficiency (i.e. fuel to net electric power) in a 500 W system that weighs 9 kg. The heat source we developed was a compact, recuperated combustion system capable of operating with most common liquid or gaseous fuels. The careful integration of the two systems with compact and efficient heat exchanging devices to meet DARPA's challenging power and weight goals was the focus of the activities in the first phase of the program.

Significant progress was made towards development and demonstration of a meso-scale JP-8 fueled power supply, but the embodiment of AMTEC pursued in 1997-8 was deemed not well suited to Army applications. A number of lessons were learned from the fabrication and testing of the Phase I AMTEC cell and the combustion system:

- Beta-alumina solid electrolyte (BASE) assemblies based on AMPS previous designs and developed through sophisticated modeling can be configured in a toroidal cell design.
- The current AMPS technology performs at close to predicted power and efficiencies with minor performance problems.
- Combustion of JP-8 (including cold-start) can be accomplished efficiently and cleanly at small scale with appropriate choice of atomizer technology.
- Challenging heat transfer and surface temperature goals on the AMTEC cell hot sides can be met.
- Charged Injection Corporation's electrostatic atomization system is the most appropriate for these systems, but the development of a proprietary controller is required to achieve long-term performance goals.
- Fabrication of AMPS Phase I BASE tube designs is expensive and time-consuming and paced the overall development program.

The AMTEC cell designs pursued in 1997-8 were complex and raised questions regarding achievement of DARPA and the Army's ultimate cost and reliability targets. Given that the designs contain many components, many manufacturing operations per tube, many complex metal to ceramic and ceramic to ceramic joints, and high-temperature braze seals, they are not amenable to cost-effective mass production. This provoked both Arthur D. Little and AMPS staff to independently re-think AMTEC implementation and design for these terrestrial applications, focusing on improving the manufacturability of the technology. It was recognized that at least one order of magnitude reduction in part count was necessary to achieve the desired

cost targets. These improved concepts were the focus of work in the second phase of the program, starting in July 1999.

An improved system architecture which was compatible with two improved AMTEC converter concepts was developed. The system design draws on lessons learned from the MAPPS combustor development at Arthur D. Little. In particular, the combustor geometric volume is more compatible with the flame envelope volume for the design heat release and the recuperator configuration is much more desirable from a thermal stress management perspective.

The two improved AMTEC converter concepts both incorporate a remote condenser, for reduced heat losses and improved efficiency. The improved tubular concept (developed by AMPS) makes use of fewer, larger BASE tube assemblies, each re-designed with fewer components. In addition, the hot side of the BASE tube operates with a liquid sodium anode (the internal, self-heat pipe, or ISHP) design that isothermalizes the BASE tube and improves performance.

The monolithic AMTEC converter (developed by ADL) has the highest power density and efficiency potential, but represents a much greater departure from AMPS design history and a more significant technical risk. The concept was to fabricate the converter from a monolithic extrusion of beta alumina and avoid the manufacturing overhead of assembling multiple tubes. Efficiency improvements can be obtained from use of thinner solid electrolytes (in the monolith webs) and because much of the active area radiates to itself. The performance penalty for this design comes in the form of increased pressure drop in the monolith channels on the low-pressure side of the converter. The initial design tradeoff analyses indicated that the benefits of the reduced radiative and conductive heat losses more than outweigh the pressure drop penalty.

In the course of refining the monolith design approach and working through the manufacturing issues associated with an initially attractive design, the extruded monolith evolved to become an all-ceramic tube-in-header design. This approach was adopted to allow for easier electrical isolation of individual anode/cathode pairs, which permits cell stacking and operation at a reasonable voltage. One key difference from all previous AMPS BASE tube designs was the incorporation of a glazed joint design which accomplished in one step the sealing and bonding of the BASE tube to a header, as well as to a niobium electrical feedthrough (one per BASE tube).

Arthur D. Little worked with Ionotec on the design, fabrication and testing of the glazed single-tube assemblies with great success. A proprietary barrier coating technology developed by Ionotec overcame potential problems of ion exchange between the glass and the beta-alumina, and the glazed joint proved to be hermetic and survived sodium exposure tests intact. Unfortunately, due to resource limitations at AMPS, no electrochemical performance testing of the glazed single tube assembly was accomplished.

AMPS demonstrated internal self-heat pipe (ISHP) performance for a variety of tube designs. This feature results in improved heat transfer and BASE tube performance due to the isothermalization provided by the heat pipe effect. An eight-BASE-tube, 35 Watt engineering cell incorporating ISHP BASE tube designs was successfully built and tested. The ISHP BASE

tube design used represented a significant reduction in part count and improvement in manufacturability over the BASE tube designs used in the first phase of the program.

Based on the work conducted in the program, it appears that when configured in a JP-8 fired 500 Watt system, AMTEC currently offers system power density of approximately 40 W/kg, net system efficiency of approximately 12% – 14% (fuel to net power out), and manufacturing cost of approximately $8 - $11 per Watt (depending on production volume).

In the course of the program major advances have been made in developing designs and fabrication techniques for AMTEC cells to make the technology better suited to fuel-fired terrestrial applications. In addition, significant progress was made in designing and demonstrating small scale fuel handling, combustion and heat transfer systems for power systems at the 500 W size range. We conclude that AMTEC still has the potential to provide high reliability, long-lived, quiet power at small power ranges (between 10 and a few hundred Watts). Many successful component designs, simulation and modeling tools and fabrication techniques have been demonstrated at small scale in the course of the work. However, fabrication of larger, multi-tube AMTEC modules must still be regarded as at the developmental stage. The glass seals developed in the latter part of the program clearly offer a path to simpler manufacturing processes and more cost-effective and robust designs.

2 Program Objectives

The specific objective of the project was to develop and demonstrate a compact, man-portable electric power generation system capable of producing 500W at 28Vdc. The prototype made use of Alkali Metal Thermal to Electric Conversion (AMTEC) technology in conjunction with a highly recuperated combustion system configured to operate with logistics fuels. Specific system targets established at the onset of the program were a 16% overall efficiency, (based on fuel energy input and net electric output), and a total system weight of 9 kg. The AMTEC cells were being developed by Advanced Modular Power Systems, Inc. (AMPS). The balance of the system was developed by Arthur D. Little, Inc. (ADL).

The focus of this work was the design and demonstration of the first stand-alone AMTEC-based generator that can operate on logistics fuels. The aim was to take a systems-oriented approach to achieving power densities and efficiencies that can meet the military's needs, rather than concentrating on cell-level improvements. The design power level for the demonstration was 500 W, which is at the upper end of the range of interest, but still sufficiently small to pose significant combustion and heat transfer development challenges, especially when low system weight is a primary goal.

Significant lessons were learned from the design, fabrication and testing of the first radial AMTEC cells. These principally related to the manufacturability and cost potential of the technology for terrestrial applications. The objectives of the work in 1999 was to focus on the evaluation of two attractive concepts for reducing the AMTEC converter part count, improving its manufacturability, increasing its performance, and reducing its cost. ADL evaluated a monolithic AMTEC converter concept, with AMPS' support. AMPS evaluated an improved tubular AMTEC converter concept. ADL also continued to provide overall system evaluations.

3 Baseline 500 W MAPPS System Design and Cell Configuration

The original prototype system, shown in Figure 3-1, contains four series-connected annular AMTEC cells. Each cell produces 145 W at 8 V: total power production is 580 W at 32 V. Predicted cell conversion efficiency (thermal to electric) is approximately 18%. Predicted overall system efficiency (fuel to net electric) is approximately 12%. The parasitic power requirements are estimated to be approximately 50 W at start-up and approximately 80 W at full power. An energy balance for the prototype system is shown in Figure 3-2.

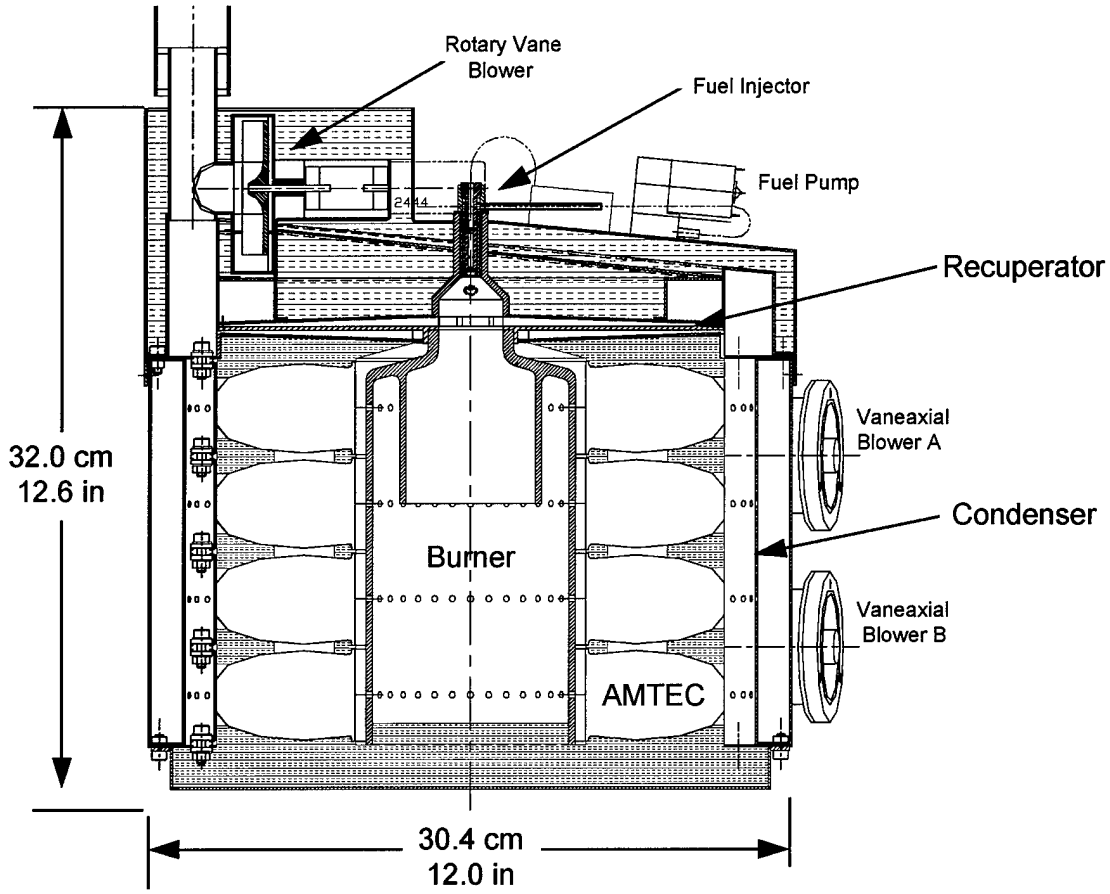

Figure 3-1 Preliminary Design of Baseline Prototype 500 W Power System

The four AMTEC cells are stacked to form the enclosure for the combustion system. The combustion system is composed of an electrostatic fuel atomizer and a radiation shield, which serves to evenly distribute radiative and convective heat to the evaporating walls of the AMTEC cells. The combustor is supplied preheated air by a reverse flow, radially-configured recuperator, which also provides tangential air entry to the combustor for aerodynamic swirl stabilization. The condensing walls of the AMTEC cells are impingement cooled with air supplied from two vane-axial blowers. The spent cooling air is mixed with the recuperator exhaust gasses so as to

reduce thermal signature. A portion of this oxygen rich mixture is drawn from the exhaust stack into the recuperator/combustion system with a rotary vane blower.

The prototype system weight has been estimated at 10.7 kg, within 20% of the Phase I weight goals. The four AMTEC cells account for 49% of the system weight. The heaviest components in the rest of the system are the recuperator (10%), the outer housing/condenser (7%) and the combustor radiation shield (6%).

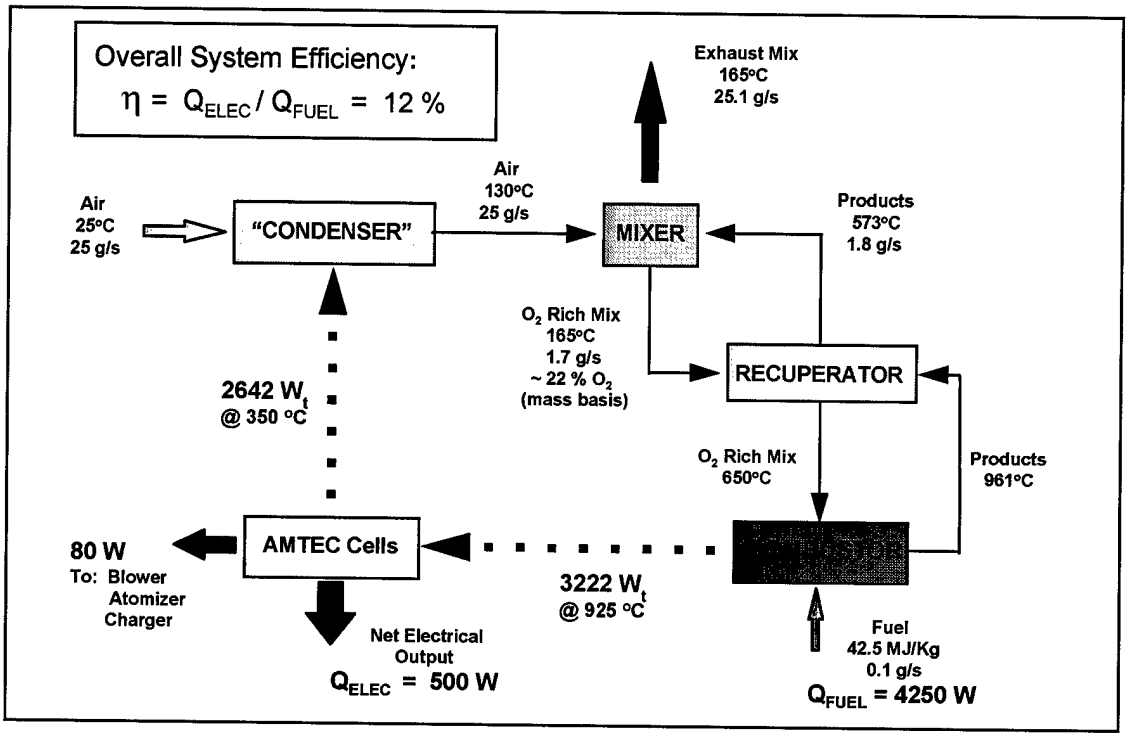

Figure 3-2 Energy Balance for Prototype Power Supply

An optimized design making use of two larger AMTEC cells operating at 15 V each could meet the 9 kg weight goal. The weight savings are attributed to: elimination of several annular cell walls; replacement of the current 0.25" diameter evaporator design with a 0.125" diameter design, thereby allowing 10-12% more BASE tubes per unit area; and reduction of the cell stack height. The prototype MAPPS AMTEC cell is of toroidal design and contains a total of 12 artery/evaporator modules and 96 BASE tube assemblies.

4 Baseline AMTEC Cell Design and Testing

4.1 Baseline MAPPS Cell Configuration

The power supply under development calls for a novel AMTEC cell configuration, see Figure 4-1. The MAPPS cell is of annular configuration, with the inner diameter of the cell being the evaporator or hot side and the outer diameter the condenser or cold side. Each cell contains 96 Beta-Alumina Solid Electrolyte (BASE) tubes and 12 evaporators, arranged in three rings.

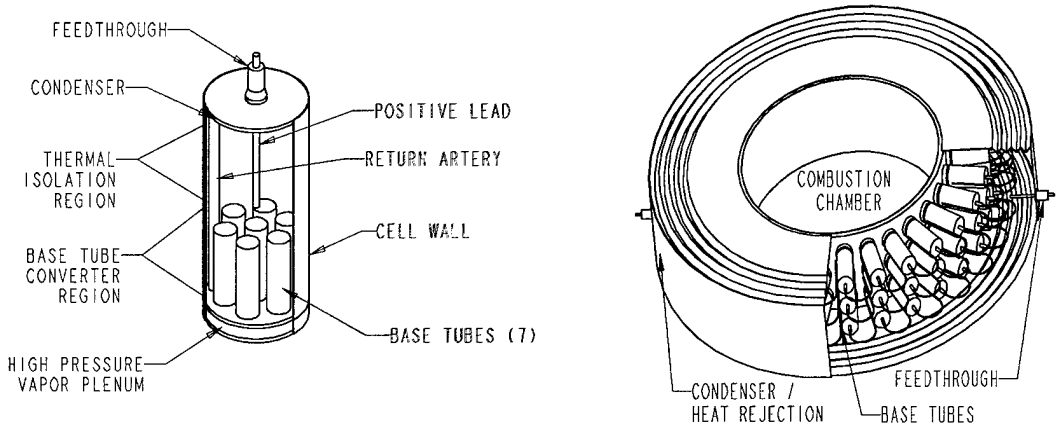

Current Multi-tube Cell Configuration **Proposed MAPPS Cell Configuration**

Figure 4-1 Current Px Cell and Proposed MAPPS Cell Schematics

4.2 Baseline MAPPS Cell Modeling

Flexible, sophisticated thermal/fluid/electrical models of operating AMTEC cells were developed using the SINDA/FLUINT analysis software. These models can accurately simulate AMTEC cell performance at any hot side and cold side temperature combination desired, for any voltage and/or current conditions, and for a broad range of cell design parameters. Design parameters typically include the cell dimensions, the current collector design, the electrode design, electrode performance parameters, and the cell wall and thermal shield emissivities.

This model simulates the thermal radiation network within the AMTEC cell using RadCAD thermal radiation analysis; hot side, cold side and cell wall conductive and radiative coupling; BASE (Beta Alumina Solid Electrode) tube electrochemistry, including electrode over-potentials; the fluid dynamics of the low-pressure sodium vapor flow to the condenser and liquid sodium flow in the wick; sodium condensation at the condenser; and high temperature sodium evaporation in the wick. The model predicts the temperature profiles within the AMTEC cell walls, the BASE tube temperature profiles, the sodium temperature profile in the return artery, temperature profiles in the evaporator, flow of thermal energy throughout the AMTEC cell, all

sodium pressure drops from hot BASE tubes to the condenser, the current, voltage, and power output from the cell and the cell efficiency. The model has been successfully validated against actual cell experimental data.

Model predictions for the MAPPS cell were made for a variety of thermal boundary conditions and cell internal configurations. First the cell wall thickness was optimized. Thicker cell walls increase the parasitic conduction loss, thereby decreasing the cell power output and efficiency for a fixed hot end temperature. However, decreasing cell wall thickness reduces the structural integrity of the cell, so there is a trade-off. Nevertheless, for the cell wall thickness of 0.015" (0.38 mm) for which the cell is structurally sound, the prototype cell is predicted to achieve almost 18% efficiency and a peak power of more than 150 W. This cell design uses chevron shaped heat shields to reduce radiative losses inside the cell and keep the thermal gradient along the length of the BASE tubes as low as possible.

The radial dimension of the cell was also optimized. A smaller cell radial length is advantageous. because of the resulting low cell mass. However, a small cell radial length generally promotes conduction and radiation losses and hence decreases the cell efficiency. The analysis ultimately indicated that a 3" (7.5 cm) cell length produced better overall performance than both the 2.5" and 3.5" cell lengths but that the difference between 2.5" and 3" is marginal. The specific power was highest for the 2.5" (6.35 cm) cell, hence this length was chosen for the present design.

As a result of the analyses conducted, a preferred cell design was selected, see Figure 4-2. and the following accomplishments were achieved:

- A cell weighing less than 1.3 kg which can deliver a peak power of 153 W was designed.
- The temperature margin of more than 20 degrees was obtained at peak power condition.
- The peak efficiency of the cell was 17.8%.
- The design incorporates chevron shields, enhanced BASE tube, thicker current collector, 925°C hot end temperature and Haynes-25 cell wall material.

Structural analyses performed on this cell design included thermal, creep and buckling analyses. The thermal stress analysis results indicated that the cell is structurally good for more than 1000 cycles. The 2% deformation stress was higher than the creep stress and the buckling load factor was greater than 2.

4.3 Engineering Cell Design

Since this is a completely new cell design, there are a number of issues that need to be resolved. Therefore, the first radial cell to be built did not have all the 96 BASE tubes in it. This cell, called the Engineering Cell, has only 24 BASE tubes. Primarily, it was built to identify the manufacturing issues involved in making radial cell configurations. These issues include: sequence of assembly, condenser felt design, effect of welding on cell dimensions, and bake-out and filling of the cell. The testing of the engineering cell is expected to provide information about issues such as sodium management (thermal and fluid) and cell structural integrity. In

addition, the performance data for this cell will be used to validate the SINDA/FLUINT cell model.

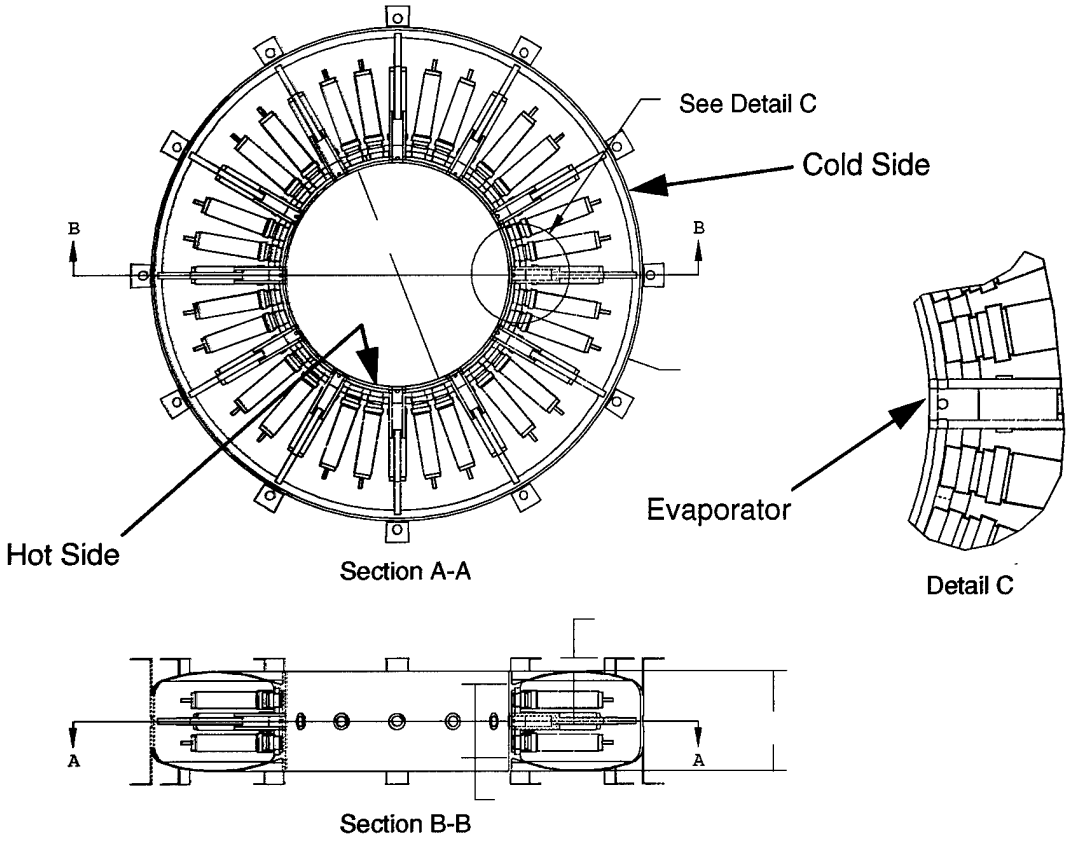

Figure 4-2 Configuration of 96 BASE tube prototype MAPPS cell

The engineering cell is different from the prototype MAPPS cell in the following respects:

- Only a single central ring of BASE tubes;
- State-of-the-art BASE tube design;
- Thicker but shorter current collector;
- State-of-the-art braze materials;
- All 24 BASE tubes are series connected;
- Evaporator pushed back to keep temperature margin positive; and
- Lower power and efficiency.

Since the purpose of constructing the engineering cell was to learn about manufacturing, sodium management, structural performance and model validation, it incorporates the state of the art BASE tubes. The power and efficiency of the engineering cell are reduced relative to the

prototype cell because of enhanced heat loss from the hot end to the cold end (because of the absence of the top and bottom rows of BASE tubes) and because of the pushed-back evaporator (required to keep the temperature margin positive).

The engineering cell was also designed to incorporate a molybdenum sleeve, which has been demonstrated to improve thermal performance in other AMTEC cells. The sleeve is installed on the outside of the BASE tubes. Since the heat input is from the bottom of the BASE tubes, the molybdenum sleeves improve performance by improving thermal conduction along the length of the BASE tube and by cutting down on the radiation heat loss from the BASE tubes (due to the lower emissivity of molybdenum). SINDA/FLUINT model predictions with and without the molybdenum sleeve are given in Table 4-1. As the stand off length (distance between hot end and evaporator) increases, the peak power decreases while the temperature margin increases to positive values. A positive margin must be maintained in order to eliminate the possibility of internally shorting the inner electrode to the mounting plate as a result of sodium condensation. The values of voltage and current are also listed in the table.

Table 4-1 also shows another set of performance predictions for the engineering cell with a molybdenum thermal sleeve. The model predicts a temperature margin of 27°C and peak power of about 21 watts for the cell. This represents a substantial increase both in peak power and the temperature margin over the values reported in Table 4-1 for the corresponding conditions. Interestingly, when using the molybdenum sleeve, the cell without chevron heat shields has better performance than the one with heat shields. The chevron heat shields help to reduce the parasitic heat loss, but increase the pressure drop and consequently make power output lower than for a cell design without chevron heat shields. It may be noted, however, that when the molybdenum sleeve is not present, the chevron heat shields do help to increase the BASE temperature, hence increase the temperature margin and improve cell performance.

Table 4-1 Prediction of engineering cell performance with and without molybdenum sleeve on BASE

Sleeve?	Stand off Length (mm)	Margin Temperature (C)	Peak Power (W)	Voltage (V)	Current (A)	T_{BASE} (K)	T_{ev} (K)
N	16.8	-31.4	20	7.5	2.67	941	972
N	26.2	-1.3	17	7.5	2.24	939	941
N	33.2	26.7	15	6.0	2.50	937	911
Y	16.8	-9.5	25	7.5	3.30	989	998
Y	26.2	26.9	21	7.5	2.80	987	960

4.4 Engineering Cell Fabrication

First of all a mechanical mockup of the engineering cell was fabricated to allow checkout of the cell wall forming process and various other mechanical details and to provide a practice vehicle for other fabrication steps, see Figure 4-3.

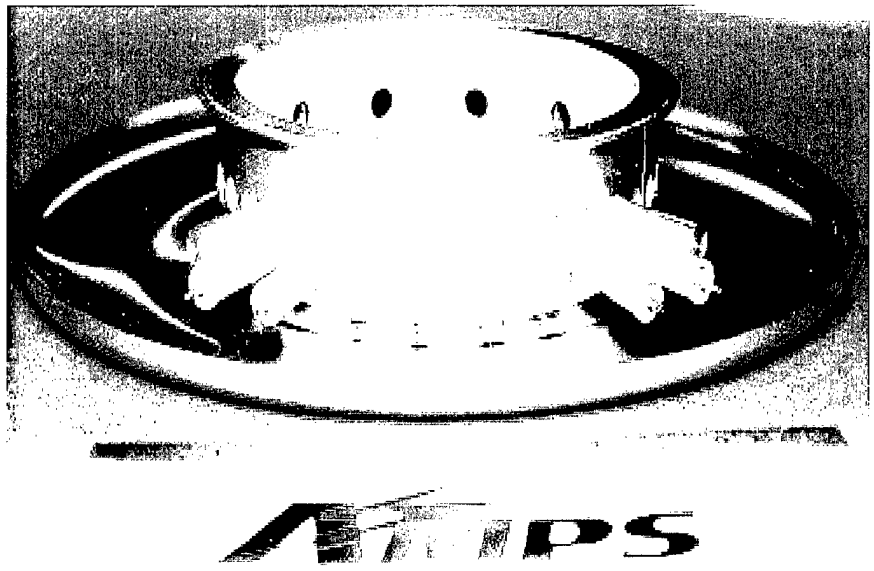

Figure 4-3 Mechanical Mockup of the MAPPS Engineering Cell

Figure 4-4 shows the inner wall and tube-support plates in fabrication. The engineering cell has 12 tube-support plates, each with one evaporator and two BASE tube assemblies. Close-tolerance fitting of all parts is needed for success in welding and to avoid any undesirable mechanical stresses. TIG welding proved to be one of the biggest challenges during the assembly of the cell, particularly the installation of the tube-support plates to the inner wall. These problems are expected to be mitigated through the use of e-beam welding for the prototype cell.

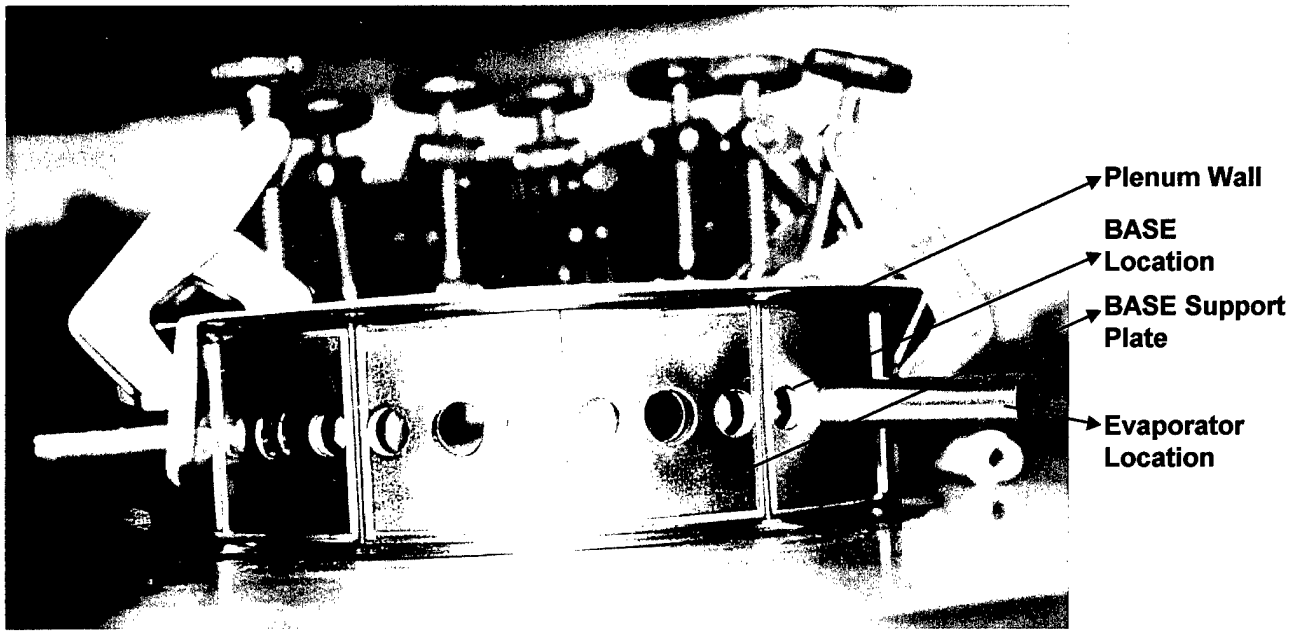

Figure 4-4 Inner wall and tube-support plates of engineering cell in fabrication.

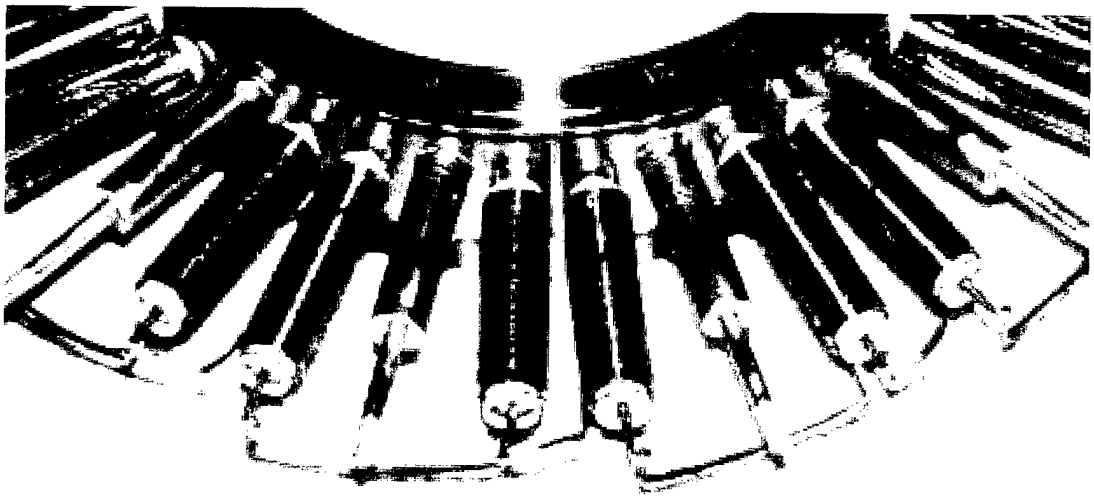

Figure 4-5 Detail of evaporator and BASE tube assemblies in engineering cell.

After assembly of the inner wall and tube-support plate assembly, the 12 evaporators were brazed to the TSP. Then the 24 BASE tubes were assembled, together with the molybdenum sleeves. The connecting wires were cut to length and pre-formed to avoid any additional stress on the BASE tubes during completion of the electrical connections, see Figure 4-5.

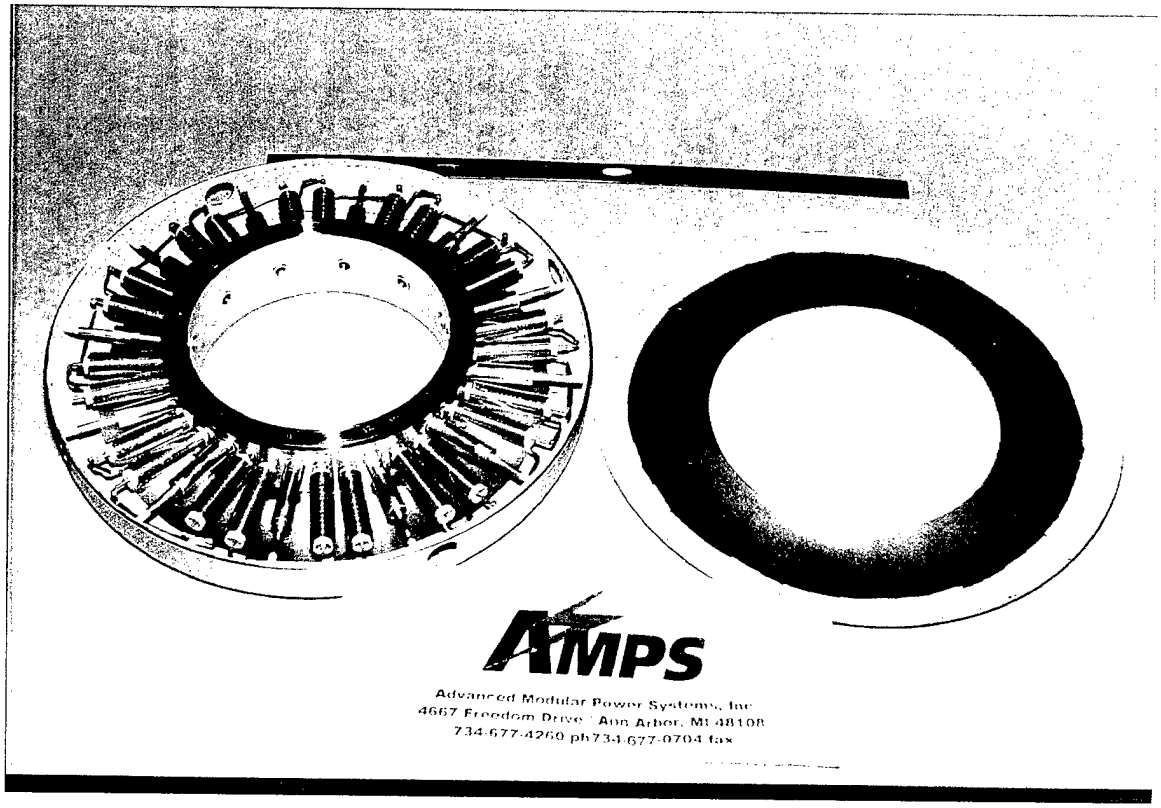

Figure 4-6 Engineering cell before final closure.

The condenser felt, see Figure 4-6, is designed such that (1) there is a large enough reservoir of sodium; (2) the top and bottom halves of the condenser felt have good contact; and (3) the felt extends along the cell walls to capture any condensed sodium. The artery socket is attached to the condenser felt to provide a continuous path for the sodium wick return system.

4.5 Engineering Cell Testing

The arrangement used in the testing of the engineering cell is illustrated in Figure 4-7. The cell was heated using a hot end heater and two cell wall heaters. Figure 4-8 shows the cell equipped with heaters before installation in the test stand. The pump-out ports extending out from the condenser end were also kept hot using heater tapes to prevent any sodium condensation in these tubes. These ports will be pinched off in the prototype cells. The condenser was cooled using an impingement cooling technique. The cell was instrumented with two hot end thermocouples, two cold end thermocouples, two BASE tube thermocouples, two evaporator thermocouples and one tube support plate thermocouple. The thermocouples were placed diametrically opposite in each case to verify radial uniformity. There are two electrical circuits in the cell, each circuit consists of 12 BASE tubes.

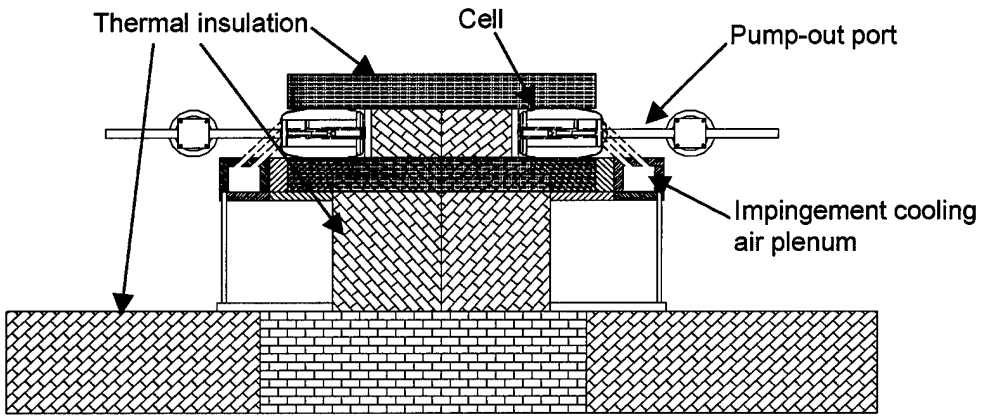

Figure 4-7 Test arrangement for engineering cell performance tests.

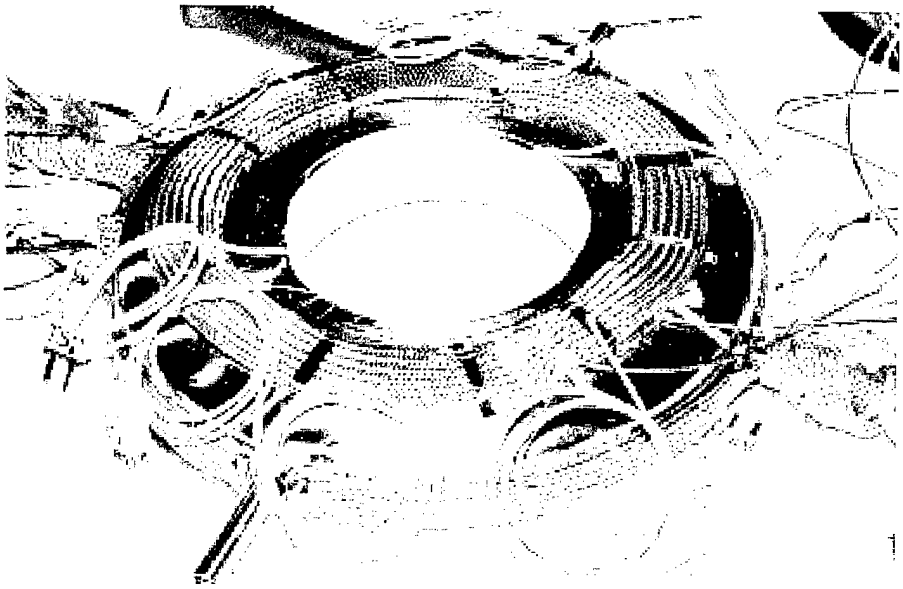

Figure 4-8 Engineering cell fitted with heaters before installation in test stand.

Table 4-2 Temperature Data for MAPPS Engineering Cell

Hot End °C	**TSP °C**	Voltage V	BASE °C	Evaporator °C	**Peak Power W**
900	**843**	3.41	722	645	**6.82**
850	**795**	3.12	680	615	**4.68**
800	**742**		638	594	**3.3**

Temperature data for the cell are listed in Table 4-2. Figure 4-9 shows performance data for one electrical circuit (one half of the cell) at a 900°C hot end temperature condition. For the full cell the power would be about 14 W. The performance data for the engineering cell are summarized in Table 4-3.

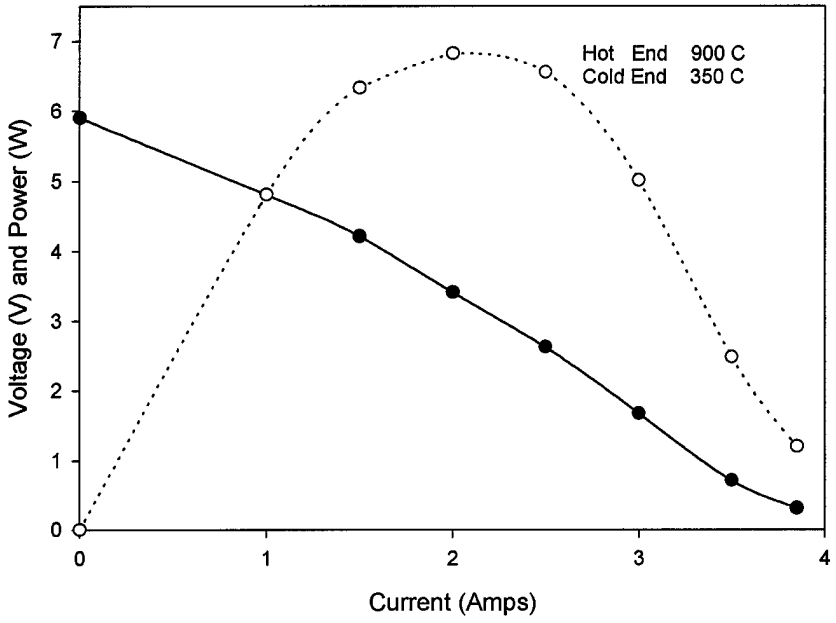

Figure 4-9 Performance of MAPPS Engineering Cell at 900°C Hot End Temperature

Table 4-3 Summary of MAPPS Engineering Cell Test Data

Hot End °C	Cold End °C	Wall °C	BASE °C	Evap °C	Peak Power W
700	300	600	560	505	1.6
750	300	650	595	544	2.3
800	300	650	615	559	2.86
800	350	700	638	594	3.3
850	350	715	680	615	4.68
900	350	735	720	645	6.82

No problems were encountered with sodium flow management in this first-of-a-kind annular AMTEC cell and no circumferential performance non-uniformity could be inferred from the measured temperature distributions. The cell's structural integrity was maintained through several thermal cycles and for prolonged exposure (~600 hours) at maximum working temperatures.

The MAPPS SINDA model was then calibrated using the engineering cell test results. Some minor modifications (such as adjusting the contact resistance and the electrode parameters) were made to the model to improve the accuracy of the prediction for the engineering cell. The model

predictions corresponding to the test data given in Table 4-2 are presented in Table 4-4 and in Figure 4-10. Due to the measurement uncertainly in the hot end temperature, the comparison is based on the tube support plate (TSP) temperature (in bold in both tables).

Table 4-4 Engineering Cell Model Predictions

Hot End °C	**TSP °C**	Voltage V	BASE °C	Evaporator °C	**Peak Power W**
853	**843**	3.75	724	643	**6.85**
803	**794**	3.75	690	624	**5.10**
753	**746**	3.75	656	605	**3.56**

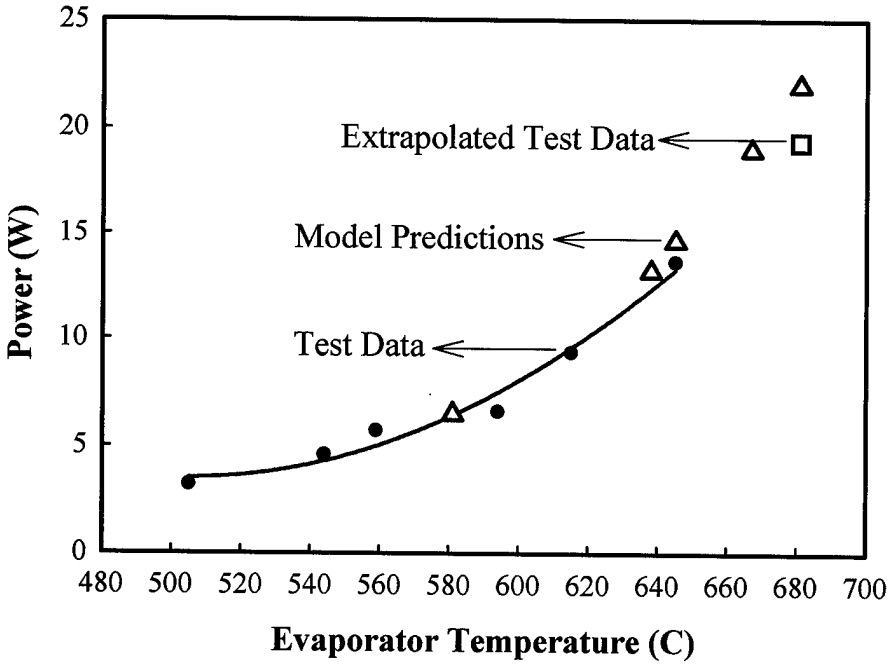

Figure 4-10 Comparison of measured and predicted engineering cell performance.

Using the revised electrode parameters in the model, we then recalculated the prototype MAPPS cell performance. Table 4-5 shows the predictions of the SINDA model for the 96 BASE tube prototype cell.

Table 4-5 Prototype Cell Model Prediction with Molybdenum Sleeve (Tc =350°C)

Hot End °C	Voltage V	Efficiency %	Peak Power W	BASE °C	Evaporator °C	Temp. Margin °C

900	6.75	13.86	129.5	796	776	20

The engineering cell testing was shut down when it was felt that all necessary data had been collected. The cell was X-rayed and prepared for post-test analysis (PTA). The engineering cell was then dissected in a glove box using a DC micro-motor multi-purpose grinder. Figure 4-11 shows the inside view of the cell.

After the cell was pulled out of the insulation from the testing unit, it was noticed that the bottom cell wall was deformed and the convex cell wall had actually become somewhat concave. The top wall was also somewhat deformed, but much less so than the bottom cell wall. It was concluded that the fixturing of the cell during testing allowed the cell to rest on the bottom cell wall rather than on the plenum. This produced additional stresses in the stainless steel wall, causing it to deform.

The cut away view clearly shows that the arteries are bent. Some of the molybdenum connecting wires are touching the artery sockets, causing a short. During testing some shorting had been observed which had been attributed to negative temperature margin. Once the standoff is designed and the cell built, there is generally little that can be done if shorting is observed. But now it is clear that the shorting in the engineering cell was actually due to the molybdenum wires touching the arteries which had bent due to cell deformation. With the Inconel alloy for the cell walls and a better design for supporting the cell, this is not expected to be a problem in the future. The BASE tubes were all in good shape with no braze failures. The feed-through was electrically insulated as is should be and there was no sodium deposition at undesirable locations.

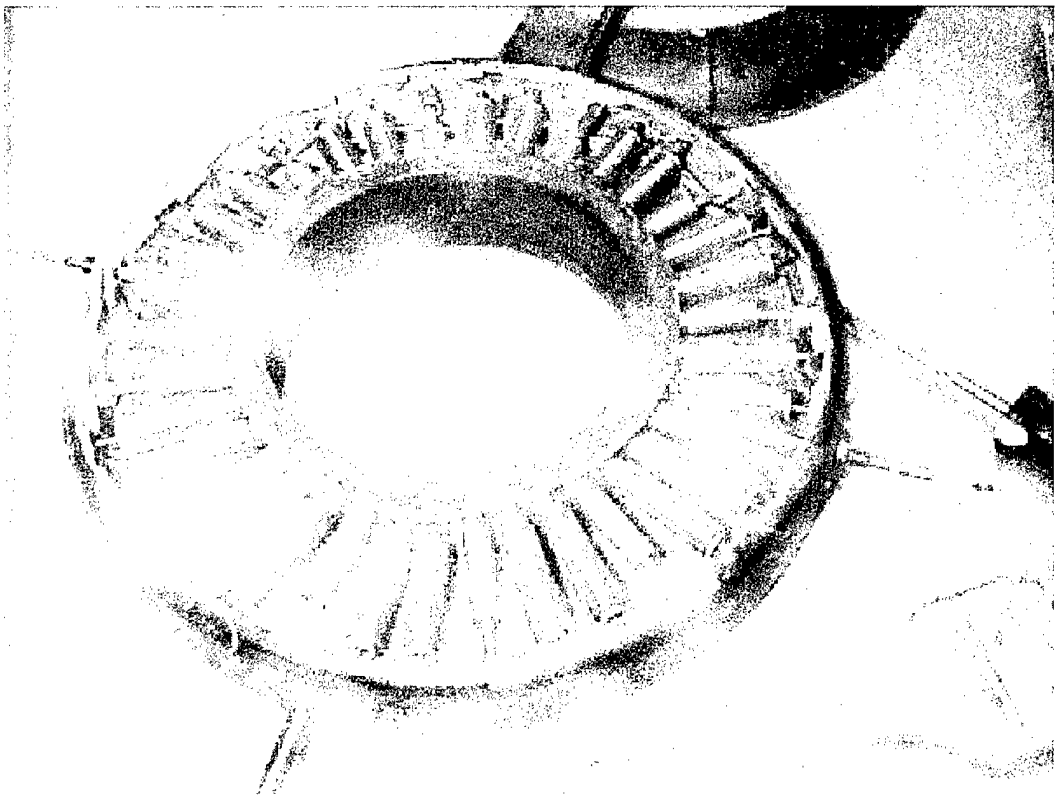

Figure 4-11 Post-Test Analysis of the Engineering Cell.

4.6 Prototype Cell Fabrication

A number of lessons were learned from the engineering cell fabrication and testing, which were incorporated into the prototype cell fabrication. These included:

- TIG welding is not adequate for any of the radial cell components.
- Cell supports must be provided on both the hot and cold walls.
- Improved component and fixture designs were identified for cell wall welding.
- The BASE tube connector height should be reduced.
- A fixture should be designed to permit a leak-check of each BASE tube-evaporator module.
- Feed-through needs sufficient space to prevent shorting.

E-beam welding techniques were developed for the 96-tube prototype radial cell. Some shielding was needed to prevent sputtering of metals onto the insulators. Some difficulties were encountered in completing the inner ring closure welds. It is believed that this was due to the presence of impurities: HCl from cleaning of sputtered metal from e-beam welding and braze materials in the thermocouple wells which contaminated the weld joint. The prototype cell is shown prior to final closure in Figure 4-12.

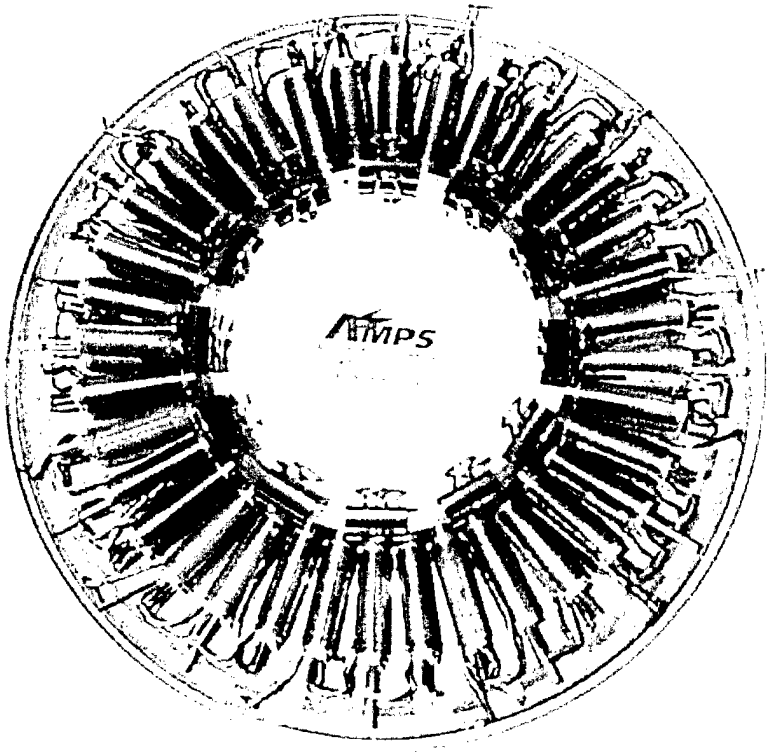

Figure 4-12 Prototype MAPPS cell prior to final closure.

4.7 Prototype Cell Testing

The prototype cell demonstrated a low resistance prior to final bake-out. This indicated internal shorts due to manufacturing processing. The cell was filled and mounted on the same test stand as was used for the engineering cell, but was only capable of 5 – 10 Watts at design temperature. Attempts were made to drive off any deposits on the BASE tubes which could be causing internal shorts by maintaining the cell at a very high temperature for an extended period, but the cell performance did not improve. Subsequent post-test analysis indicated that nickel from the tube support plates had been vaporized during welding and had deposited in the BASE tubes, causing the poor performance.

A number of lessons were learned from the prototype cell build, including:

- The cost of BASE tube parts is substantial.
- A production run will cut the per BASE tube cost significantly even without any major design changes.
- An order of magnitude reduction in part count is necessary to make the cell rugged and inexpensive.
- A new artery design will help in parts count and cost reduction.
- Eliminating the molybdenum sleeves will reduce cost and weight.
- The total number of manufacturing operations needs to be reduced.

5 Baseline Sub-System Design & Testing

5.1 Combustor

Considerable design challenges are posed for the combustion system by the requirements of the AMTEC cells. The required performance characteristics for the combustion system are summarized in Table 5-1. The principal challenges arise from the facts that (1) the volume required to complete the combustion of the design fuel input (the flame envelope) is considerably smaller than the volume enclosed by the four AMTEC cells, and (2) the AMTEC cells require very small cell-to-cell variation in heat transfer flux at a high and very uniform cell wall temperature.

Several combustion chamber configurations were screened using computational fluid dynamics (CFD) analyses before selecting the approach illustrated schematically in Figure 5-1. The combustion air preheat is approximately 650°C, which leads to extremely rapid vaporization of the electrostatically atomized fuel. The swirling inlet flow together with the contoured silicon carbide liner cause an annular flame to be established in the head end of the chamber, with an attendant large central recirculation zone. This promotes heat transfer to the SiC liner, which in turn helps to smooth out the heat transfer profile down the chamber. An impingement configuration was selected for its capacity to tailor the convective heat transfer distribution to the cells much more readily (including enhanced local heat transfer to the evaporator locations, for example), an increased margin in meeting the performance goals, and a design that is much more amenable to experimental optimization.

Table 5-1 MAPPS Combustion System Performance Characteristics.

Parameter	Value
Fuel heat input	4250 W
Fuel flow	0.1 g/s
Air flow	1.7 g/s
Excess air	15%
Combustion air preheat	650°C
Cell hot-side temperature	925±15°C
Max. cell wall temperature	950°C
Hot-side average heat flux	55 kW/m^2
Heat flux variation	±10%
Cell heat input	806 W

Computational fluid dynamics (CFD) models of the MAPPS combustion system were developed using CFX™. A series of designs were modeled and options for tailoring the convective and radiative heat transfer to the AMTEC cells were identified. The results of the computational fluid dynamics (CFD) analyses (see Figures 5-2 to 5-4) indicated that sufficient flexibility exists in this design approach to meet the stringent heat transfer and temperature goals. The

combustor pressure drop necessary to accomplish the desired heat transfer can readily be accommodated by the rotary vane blower chosen for this duty. The CFD analyses conducted also indicated that complete combustion is achieved before the mid-point of the combustor. The volume of the combustor is dictated by the internal diameter and height of the AMTEC cell stack and is considerably larger than is required to effectively complete the combustion process. The subsequent long residence time at elevated temperatures will aid in the burnout of any soot particles produced during the combustion of heavier fuels.

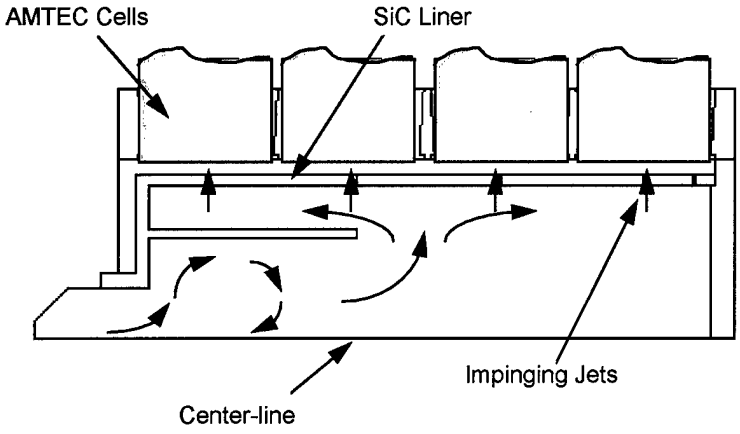

Figure 5-1 Schematic diagram illustrating arrangement of impingement combustor.

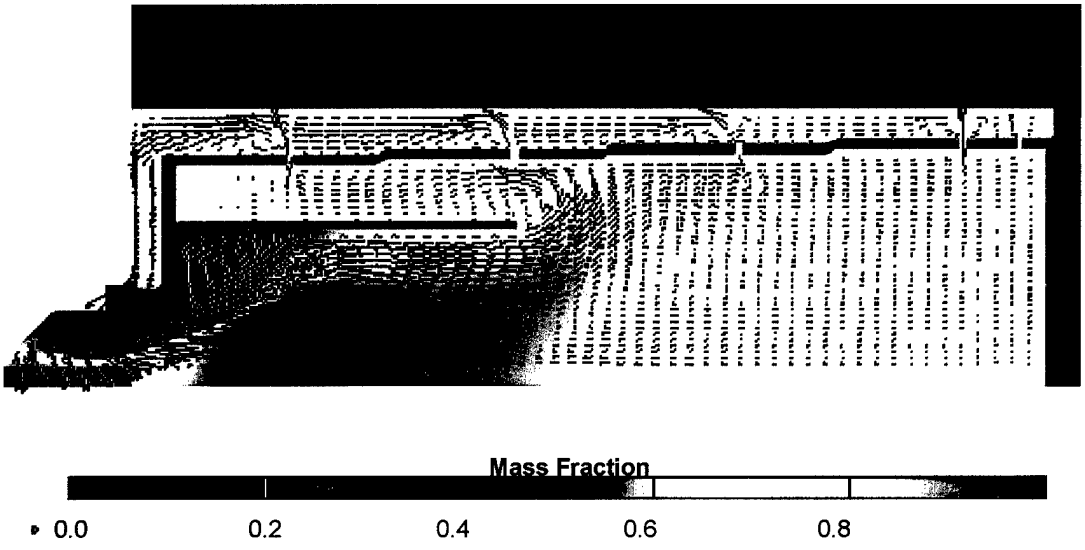

Figure 5-2 Combustion Chamber CFD Modeling - Velocity Vectors and Contours of Combustion Products Mass Fraction

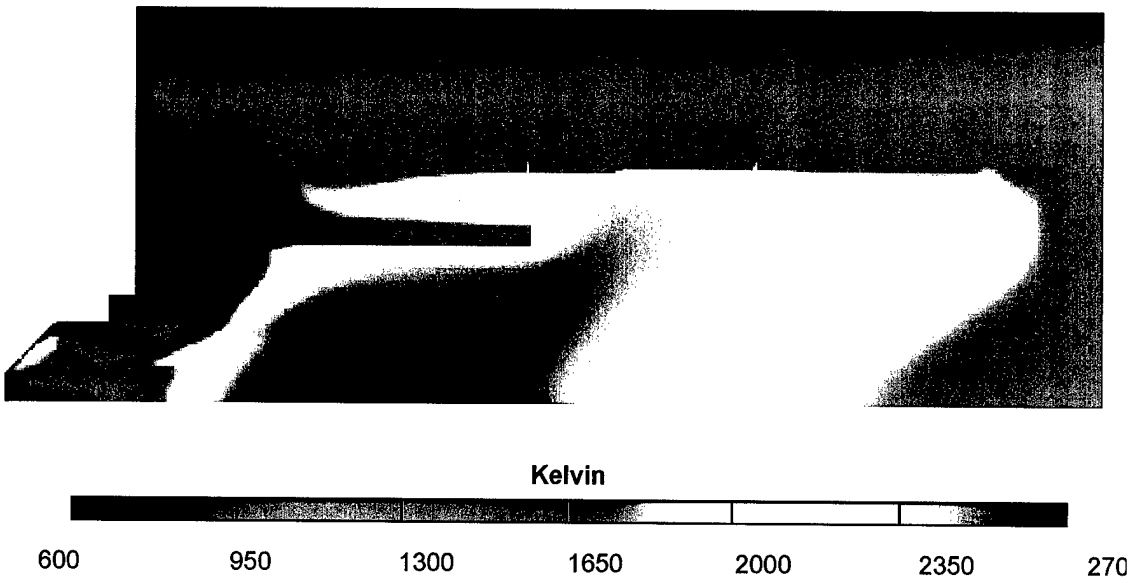

Figure 5-3 Combustion Chamber CFD Modeling - Contours of Temperature

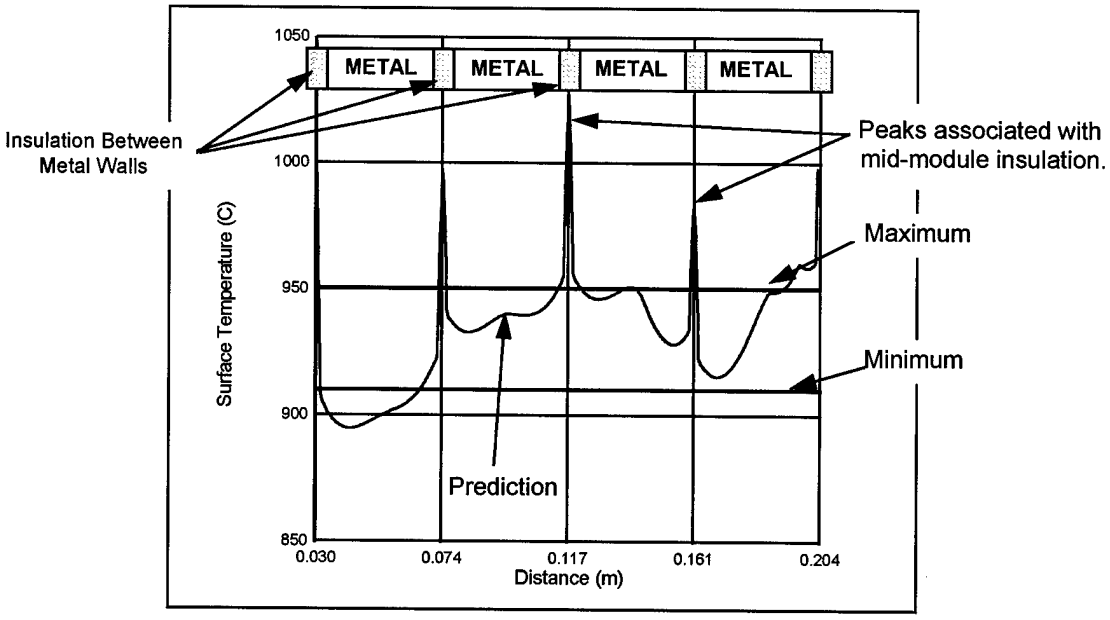

Figure 5-4 Combustion Chamber CFD Modeling - Predicted AMTEC Surface Temperature Distributions

5.2 Recuperator

Several recuperator options were analyzed early in the program. The preferred recuperator design is a laminar, counter-flow, stacked-plate heat exchanger (see Figure 5-5), which appears to offer the most compact and efficient approach for this application. This design represents the best compromise among the many competing design constraints on this component. Improved heat transfer can always be obtained by providing additional area (which adds mass) or additional flow velocity (which adds pressure drop, which entails higher parasitic power requirements and possibly again higher mass because of larger blowers). Thus the challenge is to minimize recuperator mass while achieving the maximum heat transfer at a reasonable blower power and pressure drop.

The stacked-plate recuperator is mounted on top of the stack of AMTEC cells at the combustor inlet end. Given the relatively low air flow rates the flow in the heat exchanger is laminar, which leads to very well-characterized convective heat transfer in the recuperator. Combustion air flows radially inward and is swirled as it enters the combustion chamber. The combustion products flow radially outward, heating the air as if flows inwards. Initial design analyses were supported by CFD analyses of the recuperator flowfield. Combustion air preheats of approximately 650°C are achievable at modest pressure drop.

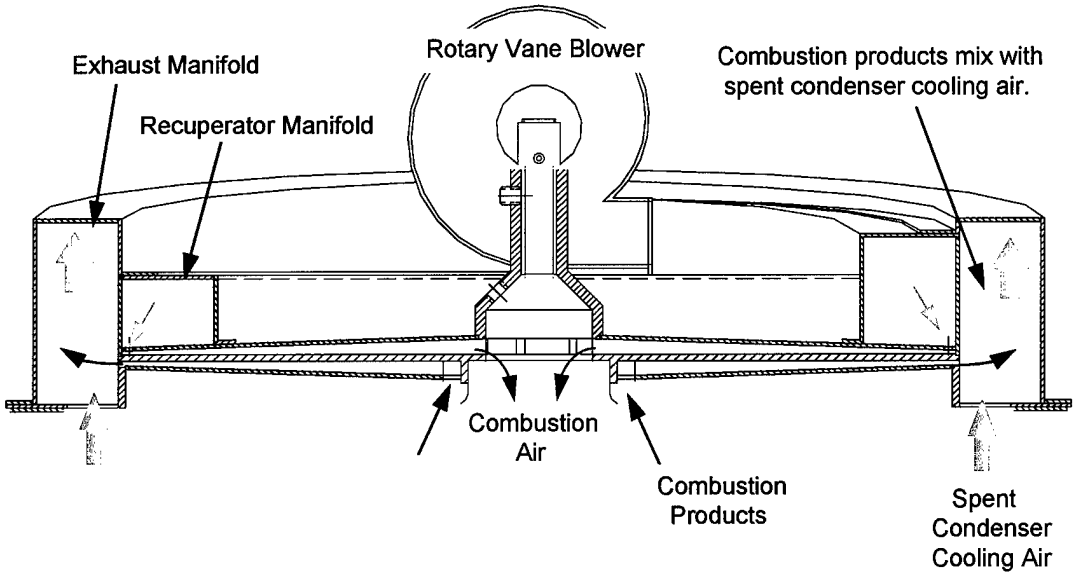

Figure 5-5 Arrangement of baseline MAPPS recuperator.

Thermal and structural finite element analyses were performed on the recuperator heat exchanger plate. The structural analysis of the original proposed design indicated that the greatest stresses were tensile stresses in the circumferential direction located at the outer edges of the plates. The stress magnitude was most severe in the upper plate, where the peak stress level was on the order of 90ksi (all reported stresses are for the worst case temperature profiles, which were computed without any allowance for in-plane or plate-to-plate thermal conduction.)

Two primary mechanisms were responsible for the predicted stress distribution. The first was an in-plane expansion mismatch due to the radial thermal gradient within each plate. This gradient produced a similar stress distribution in all three plates which was compressive at the center and tensile at the edge. The second source of thermal stress was an overall temperature difference between the three plates which gave rise to a tensile stress in the top plate, and a compressive stress in the bottom plate. In the top plate, these two effects worked cooperatively, resulting in a state of high tensile stress. In the lower plate, the two effects countered each other, which lowered the magnitude of the tensile stress generated in that plate.

Computational fluid dynamics (CFD) analyses of various proposed recuperator designs were run to better understand the temperature gradients likely to exist within the recuperator walls, and to provide more realistic temperature boundary conditions for structural analysis. The CFD models included thermal conduction within the recuperator walls, and the analyses were carried out for two different materials; 1) Haynes-230 Nickel superalloy, and 2) GlidCop copper alloy. The high conductivity of the copper alloy, (~320 W/m K versus the relatively low thermal conductivity of the nickel alloy, ~22 W/m K), resulted in a 50% reduction of the OD to ID radial temperature gradient for the configurations analyzed, as shown in Figure 5-6. This reduction in temperature gradients should lead to lower stresses, as will be determined through structural analysis.

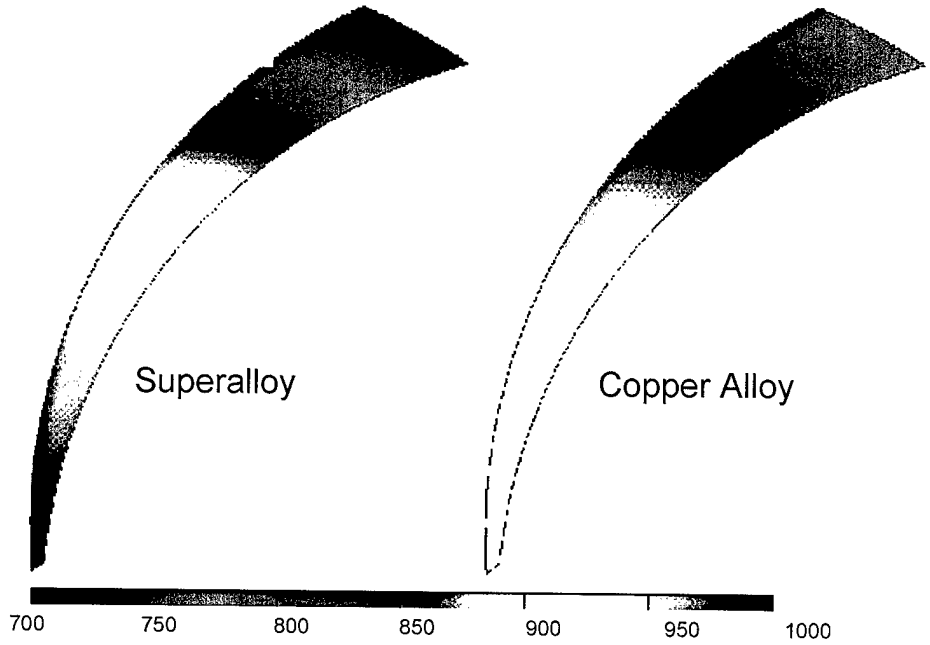

Figure 5-6 Comparison of Metal Temperatures for Two Recuperator Materials

The averaging of the recuperator wall temperatures due to their high thermal conductivity also resulted in a slightly reduced combustor inlet air temperature. In this radially configured system the hot and cold side flow gaps vary in height from 0.5 mm at the OD to 4.0 mm at the ID. Despite this variation the gap flow area steadily decreases from OD to ID, resulting in higher flow velocities and heat transfer coefficients at the ID. An averaging of the recuperator wall temperatures results in a lower heat transfer temperature difference at the ID where the heat transfer coefficient is highest. This, in turn, yields a lower overall heat transfer effectiveness for the recuperator. The predicted exit air temperature for this recuperator configuration is 615 °C at the expense of roughly 3.0" H_2O pressure loss, (the goal is 650 °C at less than 4.0" H_2O). We have pressure drop margin available to increase flow velocities and heat transfer.

5.3 Condenser Heat Transfer

An impingement system was also selected for the condenser heat transfer. A design model was developed based on correlations of impingement heat transfer data from the gas turbine literature. These correlations include the effects of spent cooling air on the performance of subsequent (or downstream) impingement arrays. Initial analyses indicated that the blower identified for this duty would barely be able to provide enough flow at the desired pressure to accomplish the required heat transfer. Several options for increasing the airflow and accomplishing the heat transfer required were assessed with respect to size, weight, power requirement, turndown operation and system start-up requirements. One of the options investigated makes use of two blowers which can be configured to operate independently. During start-up only one blower would be operated so as to reduce start-up battery power requirements, reduce the amount of heat rejection at the condenser and speed warm-up of the system. As the system reaches operating temperatures, the second blower would be activated to provide sufficient cooling for peak power operation.

Off-the shelf or readily modifiable auxiliary components have been identified for most system auxiliaries. These include the combustion air blower, the condenser air blower(s), the fuel pump, the igniter, and the three-way solenoid valve (for fuel nozzle purging). Power consumption estimates were made for all components, see Table 5-2. Only one vane-axial fan is operated on startup, which reduces parasitic power requirements to approximately 50 W. Approximately 80 W of parasitic power is required at full power.

Table 5-2 MAPPS parasitic power requirements.

Component	Power (W)
Vane-axial blowers (2)	52
Rotary vane blower	21
Diaphragm fuel pump	2.2
Electrostatic injector	0.1
Fuel system purge valve	1.4
Glow plug igniter	1.2
TOTAL	**78**

5.4 Logistics Fuel Delivery and Atomization

Logistics fuels such as DF-2 and JP-8 are difficult to burn cleanly (i.e. without production of soot, smoke, and carbon monoxide) without pre-vaporization and/or pre-mixing. Vaporization is a challenge at small scales: the high end-point temperature (up to 350°C) and high aromatic content (~20-30%) of the fuels makes it difficult to effectively complete vaporization without either gumming or coking in the very small fuel lines. In addition, the relatively higher surface-to-volume ratios at small scale lead to higher heat losses and greater difficulty in achieving effective heat transfer to the fuels.

Thus the key to achieving soot-free combustion of logistics fuels at these scales is efficient and effective atomization. A desire to minimize parasitic power mitigates against the use of pressure atomization; similarly a lack of a secondary fluid (air or steam) at sufficient pressure makes twin-fluid atomization difficult to engineer. After considering a wide variety of options, electrostatic atomization was selected as the preferred approach for the MAPPS application. Fuel injection and atomization will be accomplished using the SPRAY TRIODE™ atomizer, developed by the Charged Injection Corporation (CIC).

Electrostatic atomization has several major advantages over the competing methods, including:

- Electrostatic fuel injectors do not require high fuel pressures for good atomization. The SPRAY TRIODE™ atomizer will disperse logistics fuels independently of flow rate and viscosity with supply pressures as low as 5 psi. This eliminates the need for high power, high-pressure fuel pumps, and allows for consistent performance with different logistics fuels, and at low fuel temperatures.
- The power requirements of the electrostatic atomizer are very low (a few milliwatts).
- The droplet dispersion velocities are low and the droplet field is self-dispersing because the droplets possess like and repellent charges. Low dispersion velocities are advantageous because the droplets are more easily entrained by the flow field and less likely to impact the combustor walls and generate carbonaceous deposits.

CIC have developed and supplied two prototype MAPPS fuel injectors (see Figure 5-7) which have been successfully tested in the prototype combustion system.

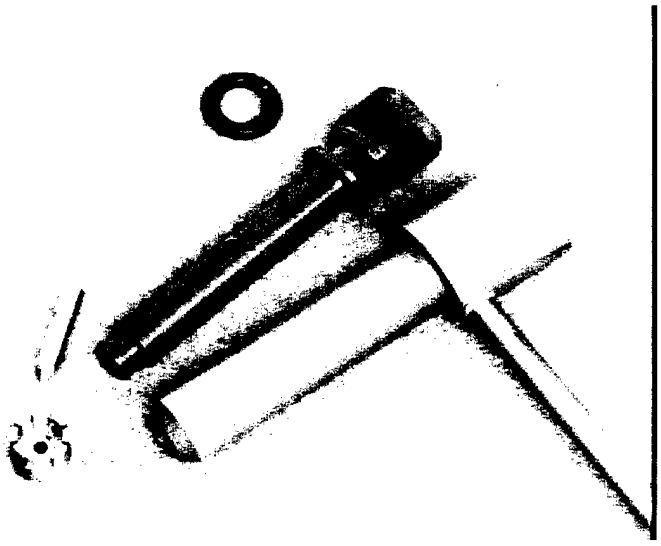

Figure 5-7 Prototype MAPPS electrostatic fuel injector components.

The smallest readily available fuel pump is a diaphragm pump which weighs only 70 g, consumes only 2.2 watts, but supplies 1.3 g/s of JP-8 at 15 psig. This is some 13 times the design fuel input rate, necessitating the use of a re-circulating fuel circuit. An advantage of this approach is that the by-pass fuel can be used to reject heat from the fuel injector stem, if necessary. The system is also configured with a three-way solenoid valve to allow entry of purge air from the rotary vane air blower during shutdown to flush fuel from the hot-end components and prevent fuel gumming due to heat soak-back.

5.5 Combustor Test System

The approach taken was to develop and test prototypes of the AMTEC cells and the combustion/heat transfer system in parallel. This means that the heat transfer characteristics of the AMTEC cells must be simulated in order to test the combustion system. The test environment must therefore simultaneously simulate the AMTEC cell hot-side temperatures and heat fluxes.

The details of the combustor test assembly are shown in Figure 5-8 and the overall experimental arrangement is illustrated in Figure 5-9. In place of the AMTEC cells are air-cooled annuli. The inner wall of these cooling modules is of the same material and design as the inner or hot wall of the AMTEC cells. This wall is instrumented with embedded thermocouples. The backside of this wall is impingement cooled using metered air. The impingement air is exhausted from each module separately. Each module contains a flow distribution ring upstream of the impingement ring to ensure uniform heat transfer. Air for each module is metered separately. Inlet and outlet air temperatures are monitored using multiple thermocouples per module. The test arrangement allows variation of individual module cooling rates to achieve the desired AMTEC cell hot wall temperature and measurement of the resulting heat flux.

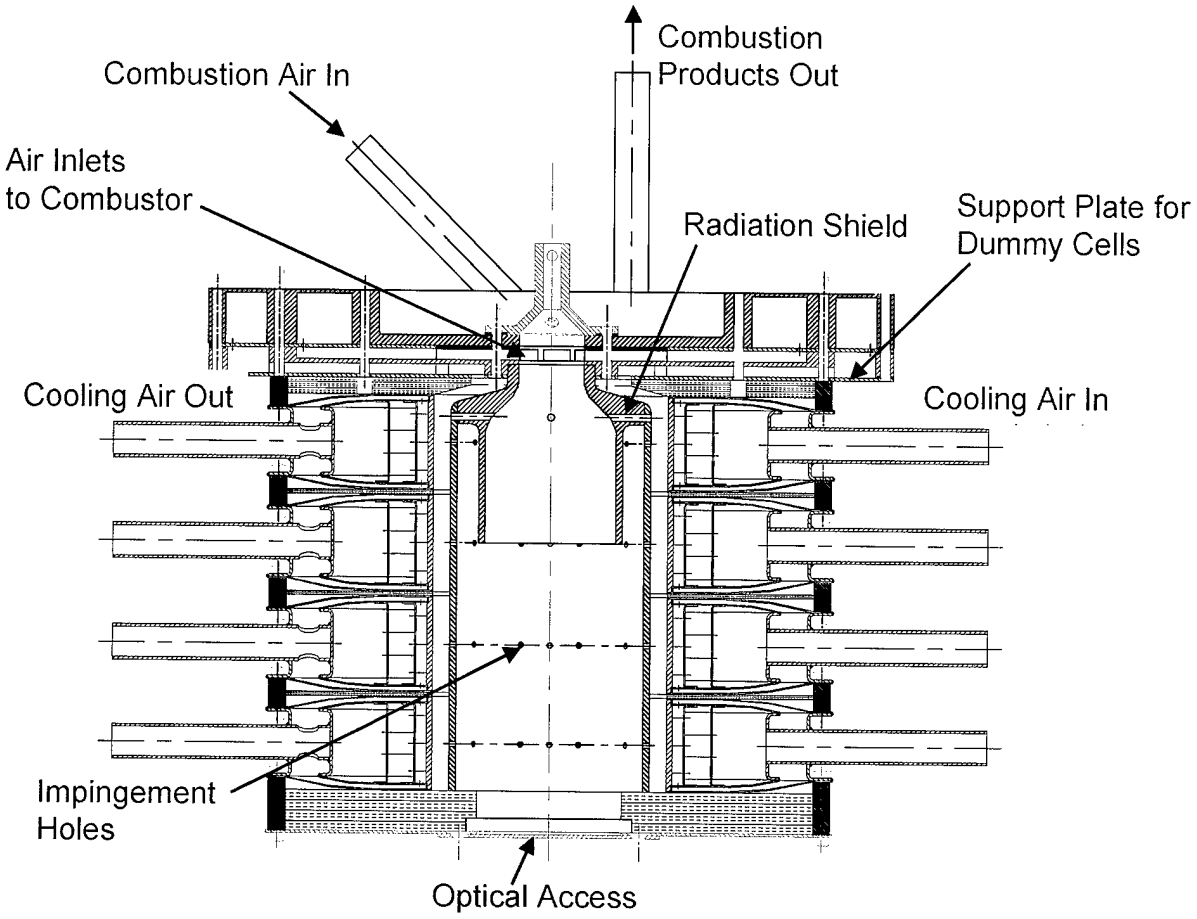

Figure 5-8 MAPPS Combustor Test Assembly

The combustion air is heated electrically rather than recuperatively, but is supplied to the combustor inlet via a geometrically similar flow path to that in the flat plate recuperator in order to generate the same combustion aerodynamics.

The combustor radiation shield will be fabricated from silicon carbide. However, to facilitate ease of modification and to reduce cost, the shield in the test combustor has been fabricated from a high temperature superalloy. Though this material will have a short life (due to high temperature oxidation), it will be more than adequate for test purposes. Use of a metal shield will facilitate changes of impingement hole patterns as the combustor heat transfer is optimized. Two shields were fabricated, one of which was left un-drilled.

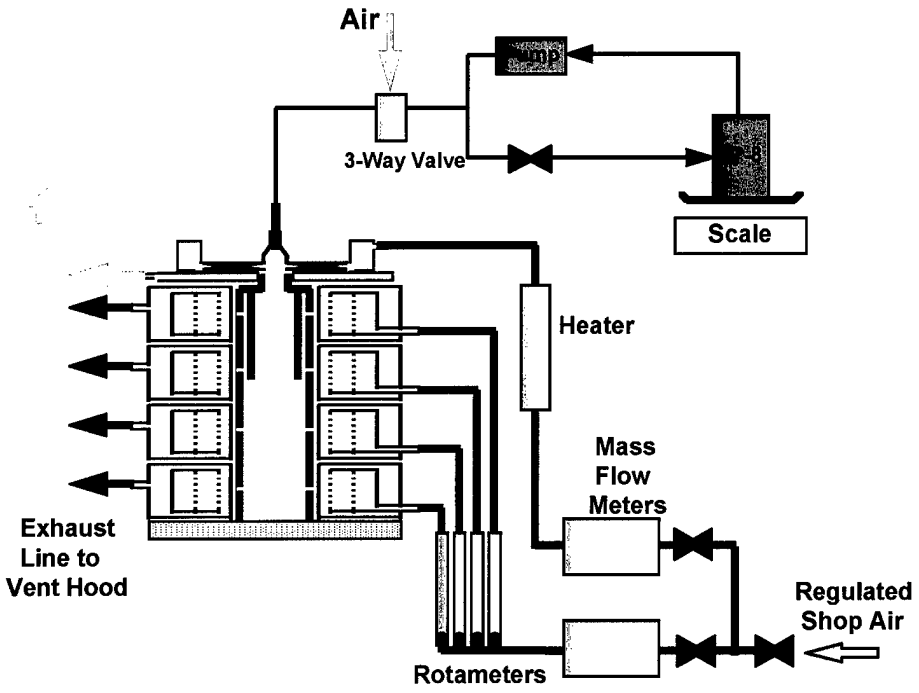

Figure 5-9 MAPPS Combustor Test System

Provisions for a quartz observation window at the opposite end of the combustion chamber from the atomizer have been made to facilitate simple flame diagnostics. An exhaust gas sample is drawn from the outlet manifold to allow measurement of typical flue properties (O_2, CO_2, CO, NO_x, smoke). Additional diagnostics include thermocouples to measure various air and combustion products temperatures, as well as surface temperatures, and a gravimetric fuel flow rate measurement. Figure 5-10 shows components of the test system prior to final assembly.

5.6 Combustor Testing

In initial testing, design flow rates of JP-8 were achieved at the design operating pressure with good atomization performance and stable JP-8 flames were achieved with both preheated and ambient temperature combustion air. Total power consumption of the injector system was very low, at approximately 1.5 W. No thermal soak-back problems (gumming, plugging) were experienced during the testing.

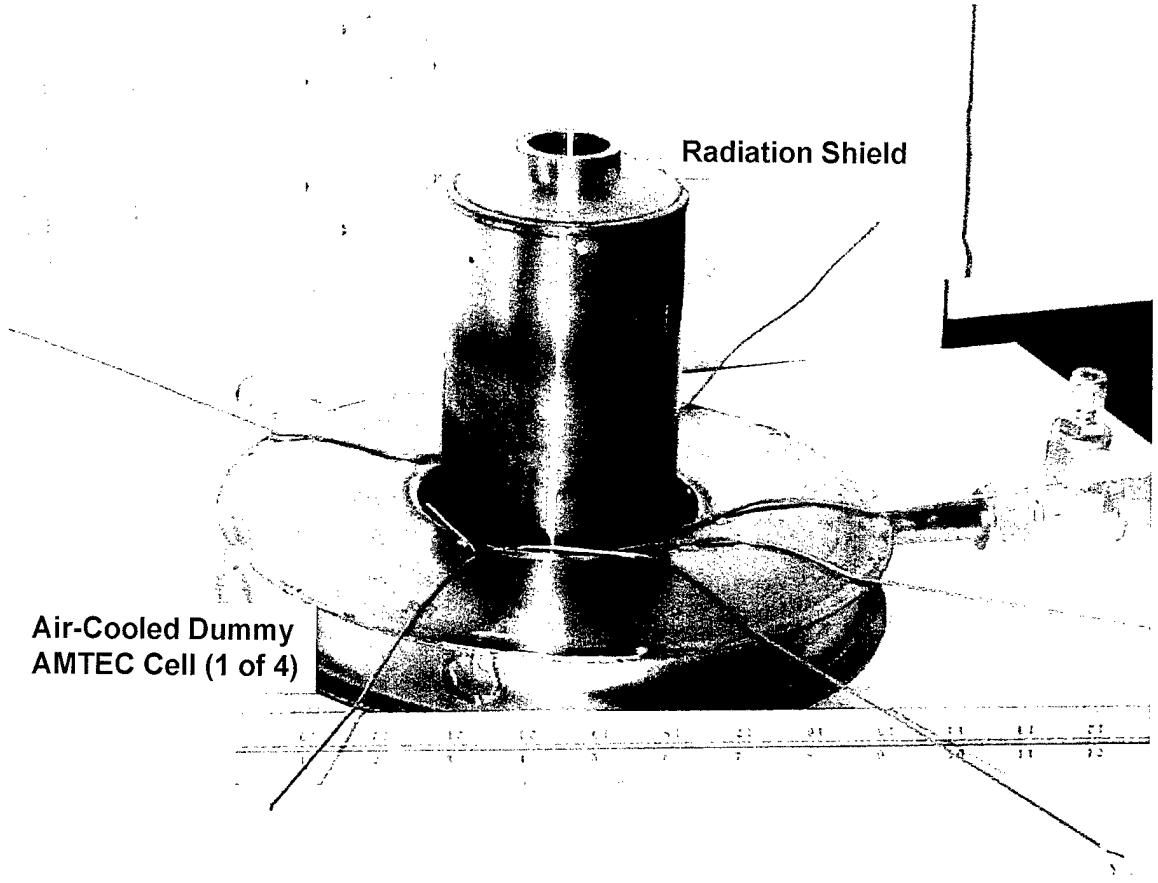

Figure 5-10 Combustor components: radiation shield inside one of four cooling modules.

Figure 5-11(a) shows a JP-8 flame at design thermal input ($4kW_t$) for optimum atomizer performance. The fine, self-dispersing spray produced by the electrostatic atomizer combined with the aerodynamic design of the burner leads to a very clean, compact and high-intensity flame.

Some inconsistency of spray pattern and droplet dispersion has been observed. Figure 5-11(b) shows a JP-8 flame, also at 4 kW_t , in which the atomizer is operating non-optimally. This flame is considerably longer than that in Figure 5-11(a) and generates visible soot emissions. With the assistance of Charged Injection Corp. staff these inconsistencies were traced to electrical breakdowns in the nozzle, possibly induced by fluctuations in fuel flow rate or pressure. In a separate ARO funded development, CIC are implementing a feedback control system to detect the onset of breakdown and modulate the applied voltage to avoid its occurrence.

Several backup fuel injection options were considered, including stock or modified pulse-width-modulated automotive fuel injectors and the design of a custom simplex pressure-swirl atomizer. Ultimately the former strategy was selected and the bulk of the combustion system testing was

accomplished with a standard automotive fuel injector. The data acquisition system was modified to permit simultaneous data collection and control of a pulse-width modulated automotive fuel injector.

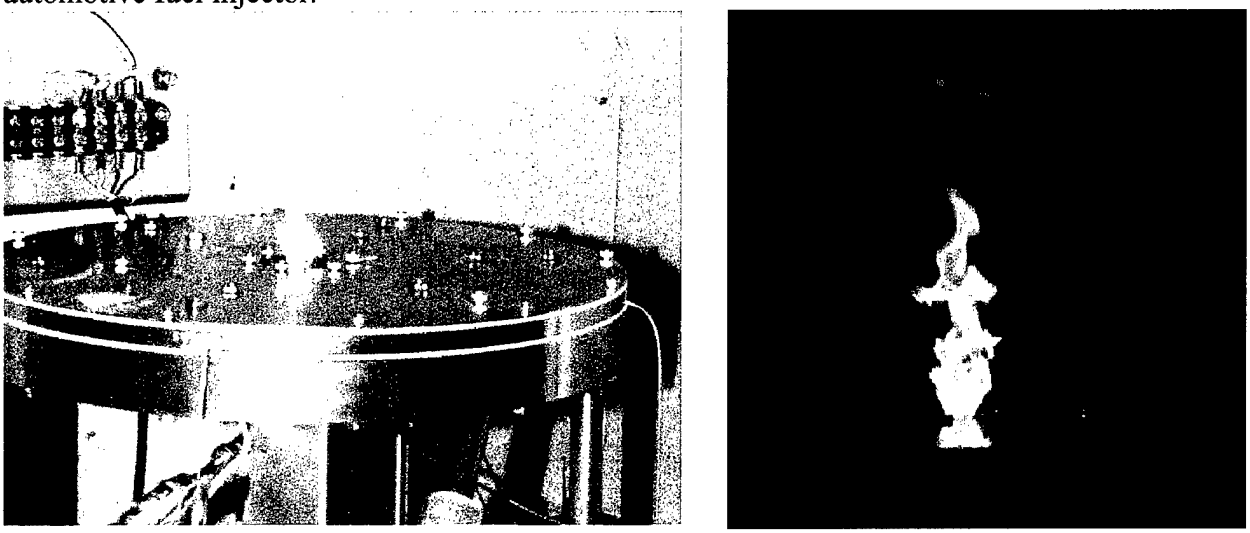

(a) (b)

Figure 5-11 (a) Compact 4 kWt JP-8 flame with optimum atomization; and (b) Long JP-8 flame with non-optimal atomization

Figure 5-12 shows the completed and instrumented combustor test stand. The fuel injector is located at the bottom center of the test assembly, and is not visible in this photograph. As a first step, hot-air shakedown tests were conducted for the combustion system. These tests were used to measure the performance of the inline heaters and also to measure radial and axial temperature distributions for the dummy cooling modules. Further, these tests were used to ensure data integrity for the DAQ system by comparing DAQ measurements with manual temperature measurements.

The flow temperature at the electric in-line heater exhaust is as high as 600°C. However, due to losses in the supply lines and heat capacity of the inlet chamber the flow temperature entering the combustion system drops to approximately 300°C. This temperature is sufficiently high to permit easy ignition for combustion tests and also to measure temperature profiles in the cooling modules. During combustion tests the inlet air will be further preheated by the exhaust products giving the desired combustor inlet temperature of ~600°C.

Uniform wall temperatures were achieved for each of the four modules during the combustion tests and a thermal balance for the test rig was closed to ~95%. The ~5% of the input energy unaccounted for was approximately equal to the uncertainty in the energy input caused by fluctuations in the fuel flow.

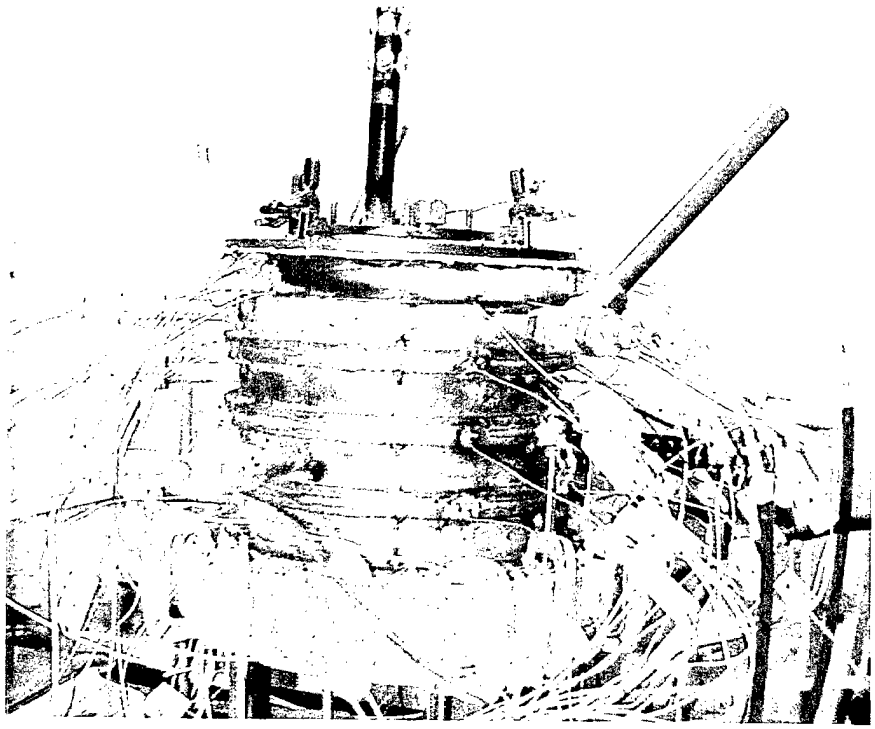

Figure 5-12 Instrumented combustor test assembly.

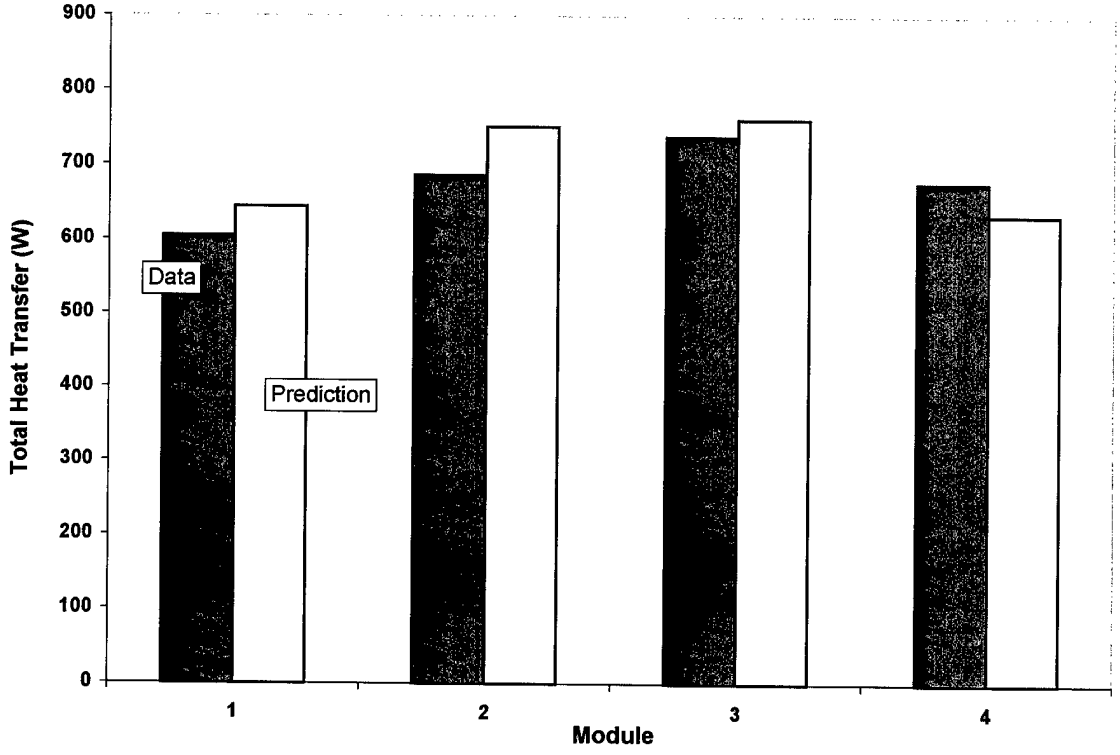

Figure 5-13 Measured and predicted heat transfer to cooling modules.

The measured heat fluxes to the four dummy AMTEC modules closely matched the predicted values from the combustor CFD analysis, see Figure 5-13, and the required ±10% heat flux variation across the entire hot side of the cells was achieved. The temperature variation from the median was somewhat greater than required.

Though the bulk of the testing was conducted with an automotive fuel injector, some combustion tests were also conducted with the electrostatic atomizer. In particular, cold-start tests were conducted to verify ambient light-off capability. The fuel droplet sizes generated by the automotive injector were too large to permit ignition with ambient combustion air. The electrostatic atomizer, on the other hand, can generate fine enough droplets to permit ignition using a standard residential appliance hot-surface igniter. The igniter power consumption was approximately 40W for a few seconds.

6 Improved AMTEC Converter Concepts

Significant progress has been made towards development of a JP-8 fueled power supply, but the embodiment of AMTEC pursued in 1997-8 is not very well suited to Army applications. A number of lessons were learned from the fabrication and testing of the AMTEC cell and the combustion system:

- BASE assemblies based on AMPS previous designs and developed through sophisticated modeling can be configured in an annular cell design.
- The current AMPS technology performs at close to predicted power and efficiencies with minor performance problems.
- Combustion of JP-8 (including cold-start) can be accomplished efficiently and cleanly at small scale with appropriate choice of atomizer technology.
- Challenging heat transfer and surface temperature goals on the AMTEC cell hot sides can be met.
- CIC's electrostatic atomization system is the most appropriate for these systems, but the development of a proprietary controller is required to achieve long-term performance goals.
- Fabrication of current AMPS designs is expensive and time-consuming and has paced the overall development program.

The current AMTEC cell designs are complex and raise questions regarding achievement of DARPA and the Army's ultimate cost and reliability targets. Given that the designs contain many components, many manufacturing operations per tube, many complex metal to ceramic and ceramic to ceramic joints, and high-temperature braze seals, they are not amenable to cost-effective mass production.

This provoked both Arthur D. Little and AMPS staff to independently re-think AMTEC implementation and design for these terrestrial applications, focusing on improving the manufacturability of the technology. It was recognized that at least one order of magnitude reduction in part count was necessary to achieve the desired cost targets.

An improved system architecture which was compatible with two improved AMTEC converter concepts was developed and is illustrated in Figure 6-1. The system design draws on lessons learned from the MAPPS combustor development at Arthur D. Little. In particular, the combustor geometric volume is more compatible with the flame envelope volume for the design heat release and the recuperator configuration is much more desirable from a thermal stress management perspective.

Features:

- Monolithic or tubular AMTEC.
- Tangentially-fired, high-swirl logistics fuel burner.
- Combustion chamber volume consistent with heat release rate.
- Integrated mixed flow recuperator.
- Nested-can recuperator geometry accommodates thermal expansion well - lower thermal stresses.
- Electrostatic atomizer.
- Compact, highly-integrated configuration - smaller & lighter than current MAPPS design.

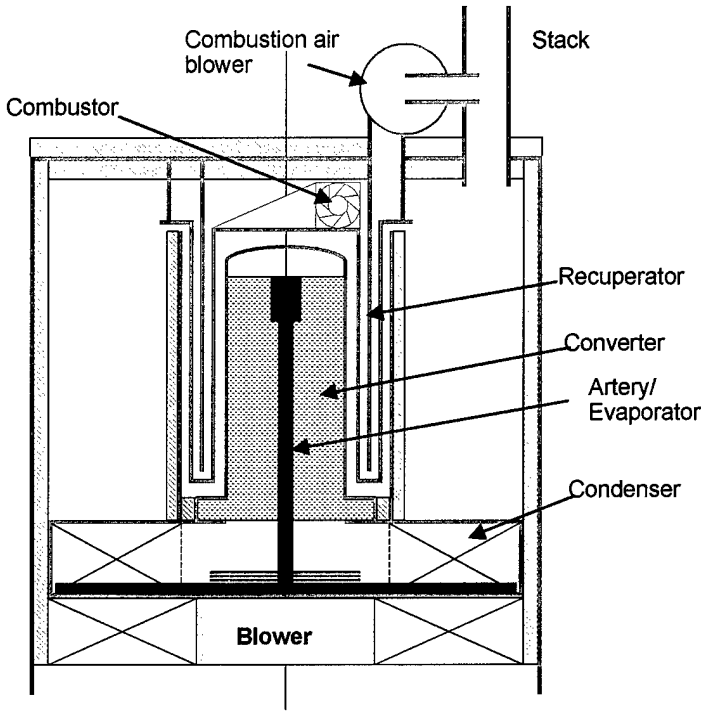

Figure 6-1 Schematic and Features of An Improved MAPPS System Concept

The two improved AMTEC converter concepts are shown schematically in Figures 6-2 and 6-3, along with a summary of their features and benefits. Both incorporate a remote condenser, for reduced heat losses and improved efficiency. The improved tubular concept (Figure 4-11) makes use of fewer, larger BASE tube assemblies, each re-designed with fewer components. In addition, the hot side of the BASE tube operates with a liquid sodium anode (the internal, self-heat pipe, ISHP) design that isothermalizes the BASE tube and improves performance.

The monolithic AMTEC converter (Figure 6-3) has the highest power density and efficiency potential, but represents a much greater departure from AMPS design history. The concept is to fabricate the converter from a monolithic extrusion of beta alumina and avoid the manufacturing overhead of assembling multiple tubes. Efficiency improvements can be obtained from use of thinner solid electrolytes (in the monolith webs) and because much of the active area radiates to itself. The performance penalty for this design comes in the form of increased pressure drop in the monolith channels on the low-pressure side of the converter. The simple design tradeoff analyses performed to date indicate that the benefits of the reduced radiative and conductive heat losses more than outweigh the pressure drop penalty.

Features:

- Fewer, larger, longer BASE tubes
- Much reduced part count
- ISHP
- Remote condenser

Benefits:

- Reduced radiative losses
- Reduced conduction losses (less cell wall per watt)
- Higher power density (isothermal BASE, more surface area per cm^3, more surface area per kg)

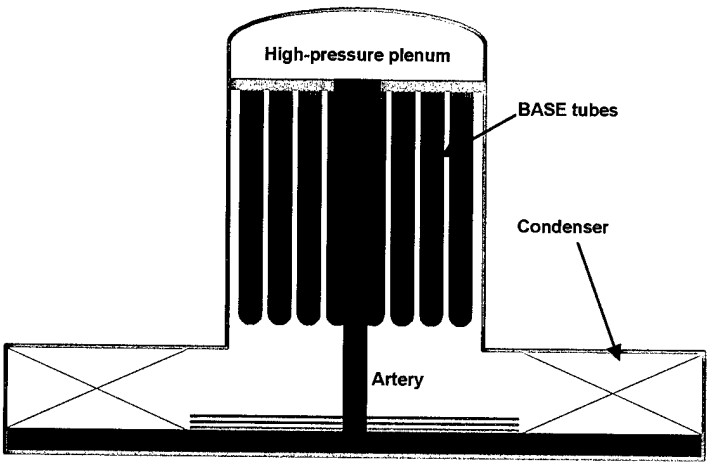

Figure 6-2 Improved Tubular AMTEC Converter Concept.

Features:

- Single β"-alumina monolith
- Much reduced part count
- Single simple compression seal
- Remote condenser
- Remote evaporator

Benefits:

- Reduced radiative losses (most of active BASE radiates to itself)
- Reduced conduction losses (less cell wall per watt)
- Higher power density (thinner BASE, isothermal BASE, more surface area per cm^3, more surface area per kg)
- Highly robust architecture

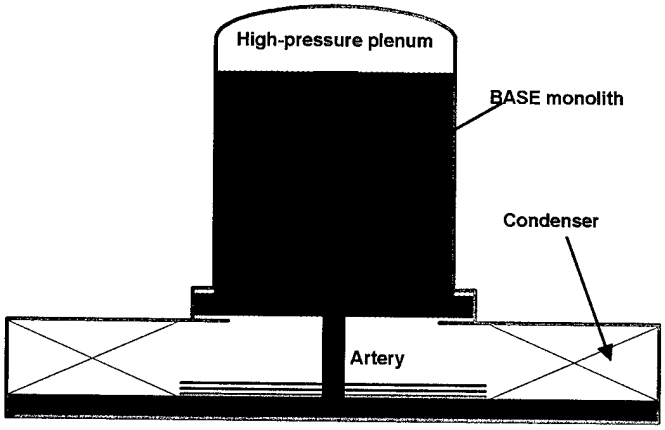

Figure 6-3 Improved monolithic AMTEC converter concept.

7 Monolithic AMTEC Cell

7.1 Monolithic Cell Concept Evolution

As originally conceived, the monolith concept was as illustrated schematically in Figure 7-1. Features and advantages of this approach were identified as:

- ***Reduced part count*** - Easier fabrication and higher reliability.
- ***β''-alumina in compression*** - Allows for thinner β''-Alumina, yielding higher output and efficiency at equivalent operating temperatures.
- ***Isothermal β''-alumina*** - Relieves design of thermal constraints.
- ***Remote evaporation/condensation*** - Fosters geometric freedom and reduces heat losses.

Starting from the early configuration presented at the end of Phase I, a series of conceptual arrangements were developed and assessed for manufacturability and functionality/performance. Performance considerations as well as design innovations have caused the monolithic AMTEC cell design to evolve from its initial concept. One of the principal drivers leading to changes in the monolith configuration has become the electrical interconnections required to build a reasonable working voltage and minimize ohmic losses in current collectors and leads. This and other requirements has led to an evolution of the monolith cell configuration, as illustrated in Figure 7-2. Figure 7-3 shows one concept for a molded monolithic converter.

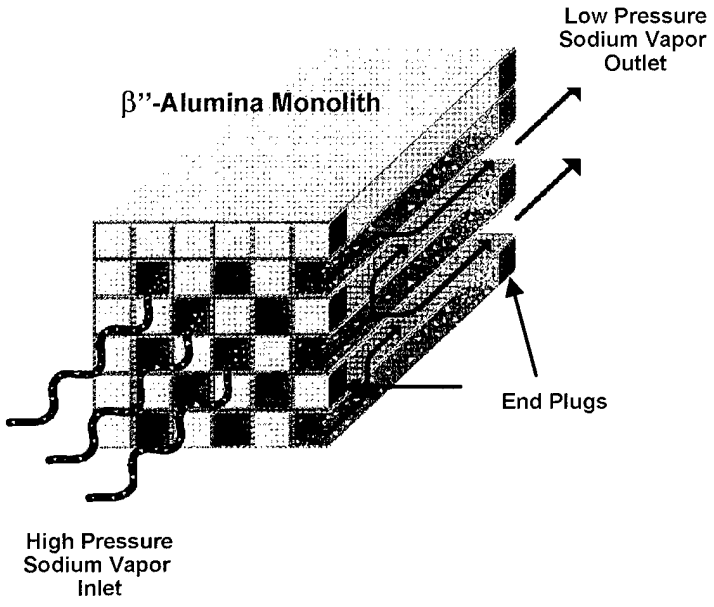

Figure 7-1 Original Monolith Concept – Conceptual Drawing

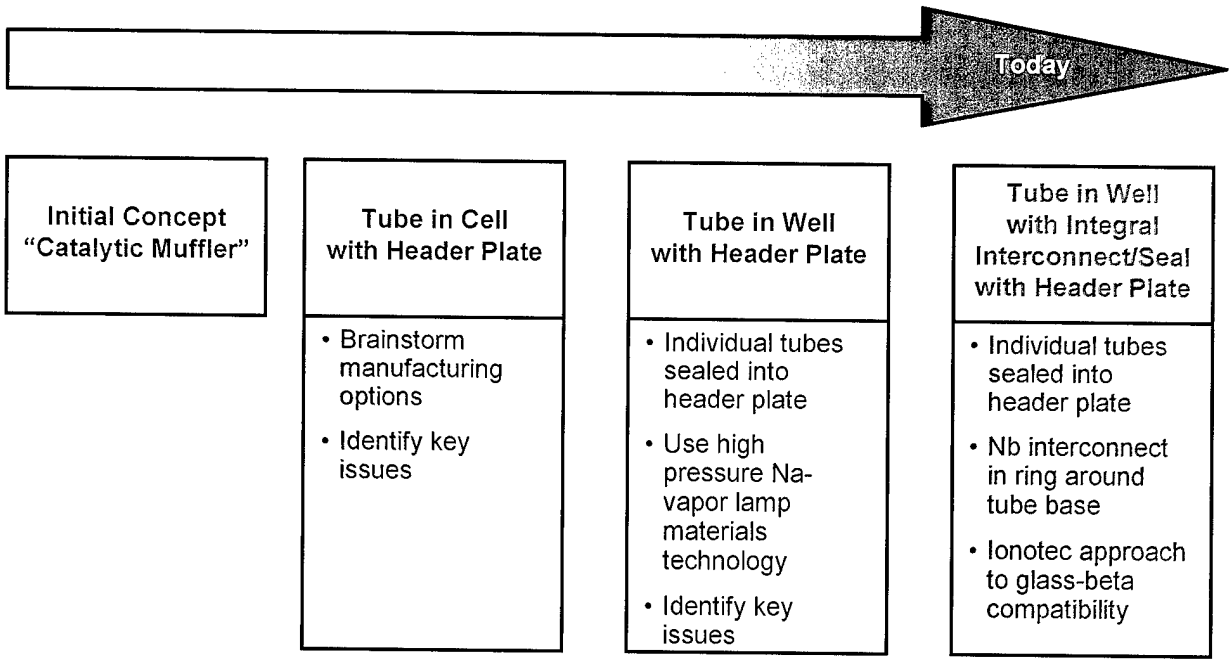

Figure 7-2 Evolution of Monolith Design Concept

Concepts have been developed for both extruded and molded or cast monolithic structures. As the concepts have been developed and evaluated, the following design and process issues have been considered.

- Interplay of design and manufacturability
  - Tolerances, gaps, web thicknesses, complexity, shrinkage
- Compatibility of process steps
  - Material stability versus temperature
  - Material interactions
  - Green strength of structures
- Reliability and reproducibility
  - QC of individual steps and integrated structures
- Specific issues
  - Interconnects between series cells
    - Method of fabrication (material, metal to ceramic seal, ...)
    - Connection to electrodes (mechanical or "joined")
    - Resistance drop
  - Impact of L/D ratio of cavities on coating processes
  - Approach for sealing monolith ends
  - Liquid Na anode (Heat Pipe) versus vapor electrode

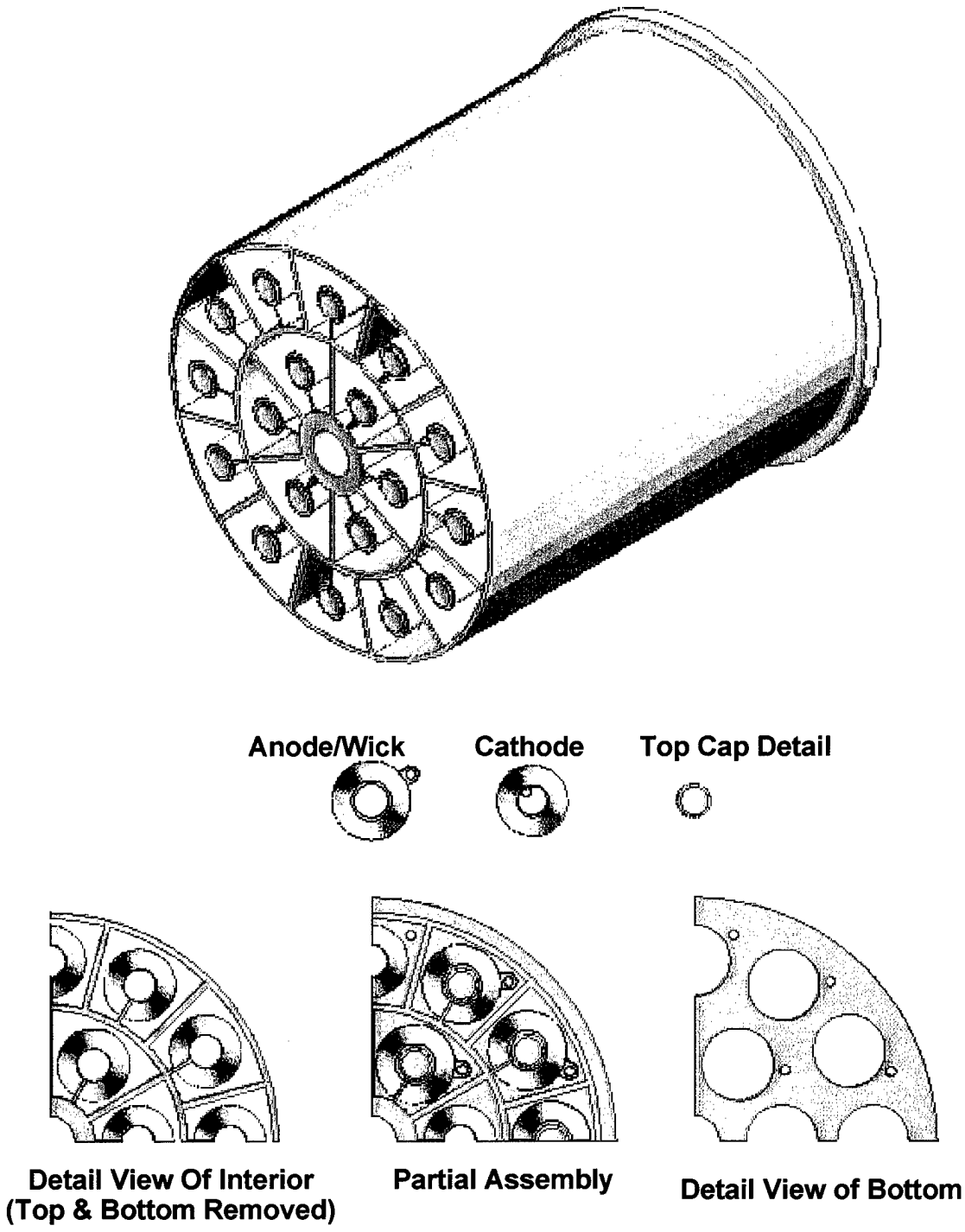

Figure 7-3 Concept for a molded monolith.

Figure 7-4 illustrates the major process steps envisioned in the monolith manufacture. A variety of processes for the production of the monolith have been identified and characterized. A preliminary list is shown in Figure 7-5.

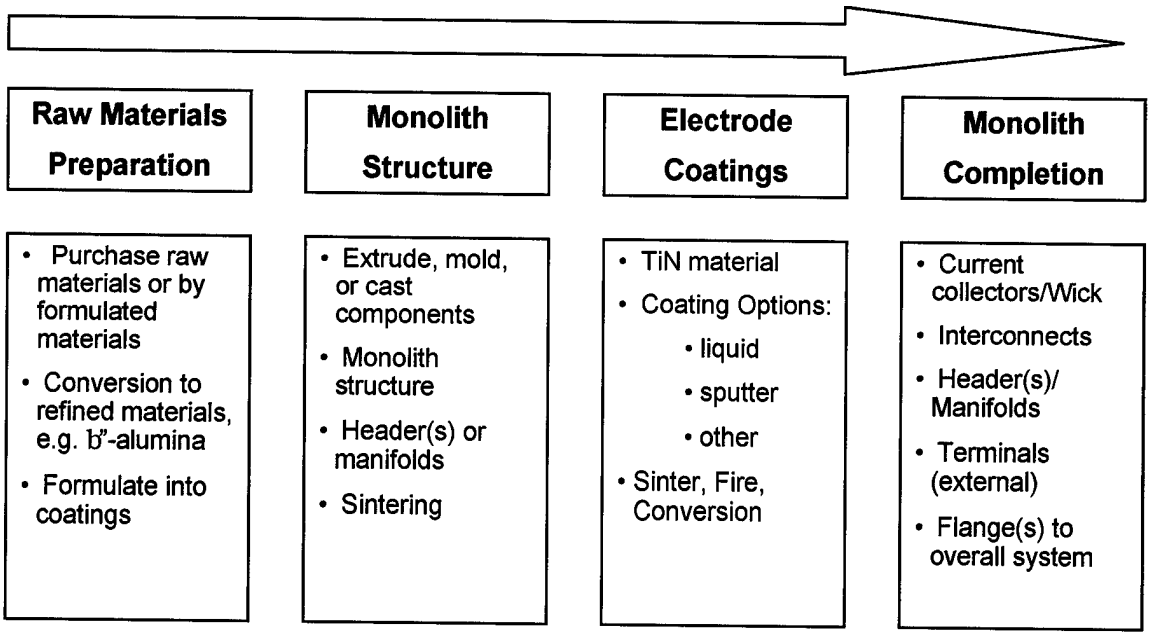

Figure 7-4 Overview of major process steps in monolith fabrication.

Process Technology	% Solids Mold Mat'l	Green Part Density	Part Complexity
Electrophoretic	Colloid	?	Low
Extrusion	Medium	?	Hi - 2D None - 3-D
Deposition (coating) Spray Dip CVD (Adv.Mat'ls, CA)	Low	Can use for densification!!	Low - Medium (graded thickness by dipping)
Investment Casting (lost wax)	Low	85%	High
Injection Molding	Low	85%	Medium - High (with cores)
Molding and Isostatic Pressing	High (powder + binder)	> 90%	Medium (bag with internal features)
Drain/Slip Casting plus Core (e.g. lost wax)	Low	?	High

Figure 7-5 Preliminary characterization of monolith production methods.

Our assessment was that casting or molding processes would be more attractive than extrusion processes, primarily because 3-D shapes can be produced near the final desired form. We believed that fabrication of monolith as originally configured would be feasible and we approached ceramics companies with the design and let them recommend a preferred process from the candidate processes identified. Sealing of metallic feed-throughs to the "headers" is doable, but the details must be addressed in near final design discussions with vendors. Presently the bonding of the headers to the ends is an open issue. In order to facilitate discussions with potential vendors, a mockup of the monolith concept was fabricated and is illustrated in Figure 7-6. Initial discussions were held with Ionotec and Beta R&D concerning the monolith fabrication.

Following these discussions, as well as discussions with AMPS staff, a preferred final concept was selected, as illustrated in Figure 7-7. A tube bundle design which retains the performance attributes of the original monolithic concept has been selected for the following reasons:

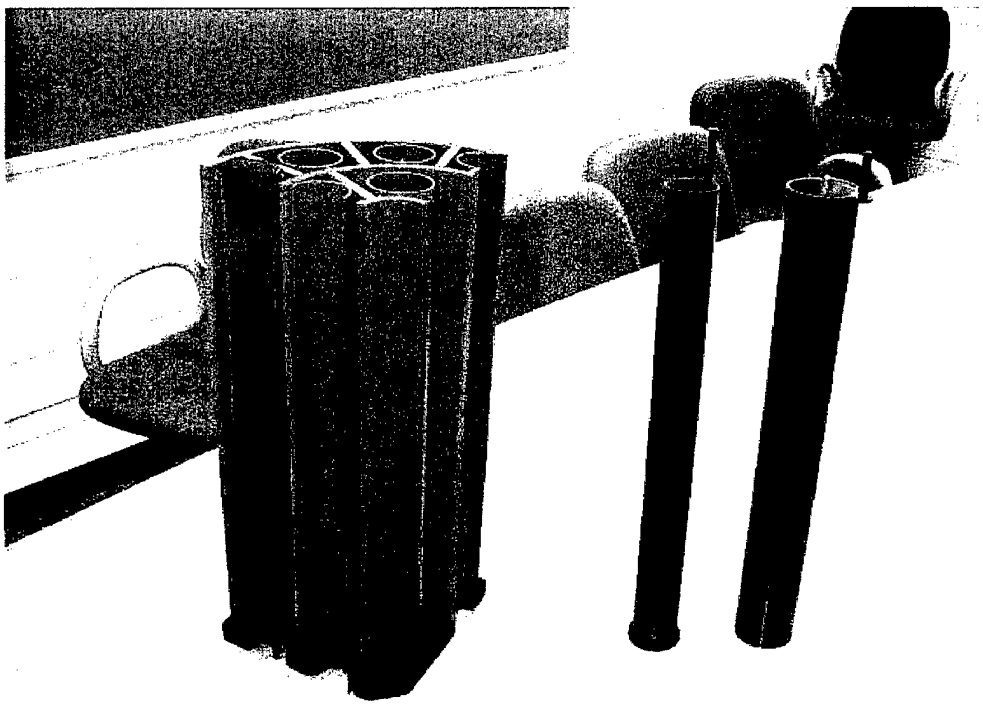

Figure 7-6 Mock-up Used to Illustrate Design Concept in Discussions with Vendors

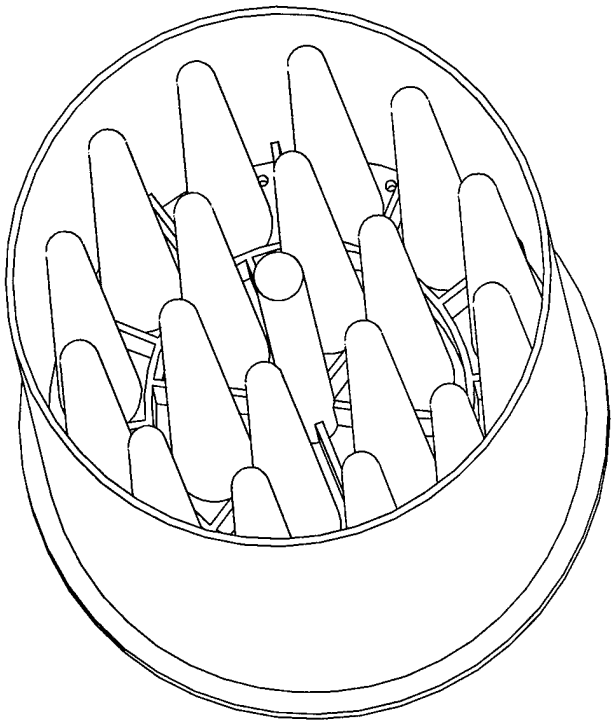

Figure 7-7 Isometric View of Preferred Monolith Structure

- The custom extrusions necessary for low-ohmic and -ionic loss cell configurations also require complex end cap shapes and joints and raise production yield issues.
- Extensive wire feedthroughs and seals are required for series connection of unit cells.
- Current β"-alumina manufacturers are geared up to produce tubular shapes quickly.
- Innovative wet seal/return artery/evaporator and radial heat input design concept lends itself to open tube bundle geometry.
- Proposed ceramic glass joining technology make tube assemblies an attractive alternative to a true monolith.

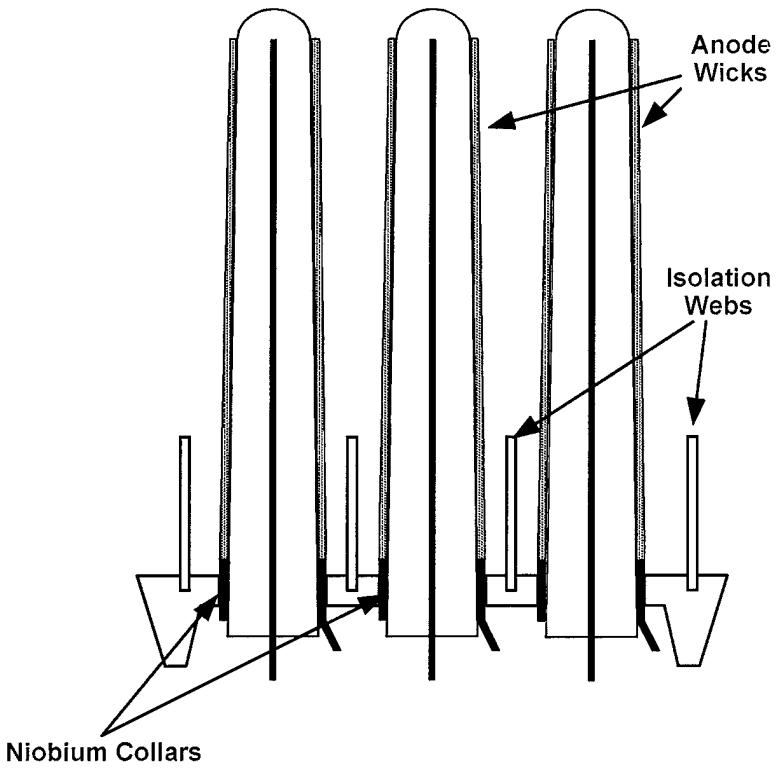

Figure 7-8 Details of Monolith Ceramic Structure

The current AMTEC core configuration (see Figure 7-8) consists of individual β"-alumina tubes "glassed" into an α-alumina header through niobium collars. The design makes use of AMPS' Internal Self Heat Pipe (ISHP) technology to isothermalize the structure and generate a liquid sodium anode. Recent tests at AMPS using large diameter tubes (15 mm OD) and multiple small-diameter tubes have demonstrated the feasibility of this concept. The niobium collars serve as anode current feed-throughs and include mechanical features that grip the anode wick material. Solid electrical connections are made by liquid sodium. Tapered tube geometry and α-alumina webs electrically isolate the anodes. Paintable Weber electrodes and Chinese-finger-puzzle-like current collectors are planned on the cathode side. The monolith cell concept also includes some innovative system-level features, as illustrated in Figure 7-9.

- The cell makes use of wet-seal and annular return artery/evaporator design which has precedent in the fuel cell world.
- The cell pressure differential forces the conic monolith geometry down onto the liquid sodium return artery wick forming the system seal.
- Greater freedom in the design of the return artery/evaporator system.
- The necked-down conic and radiation shielding reduce heat losses to the condenser section.

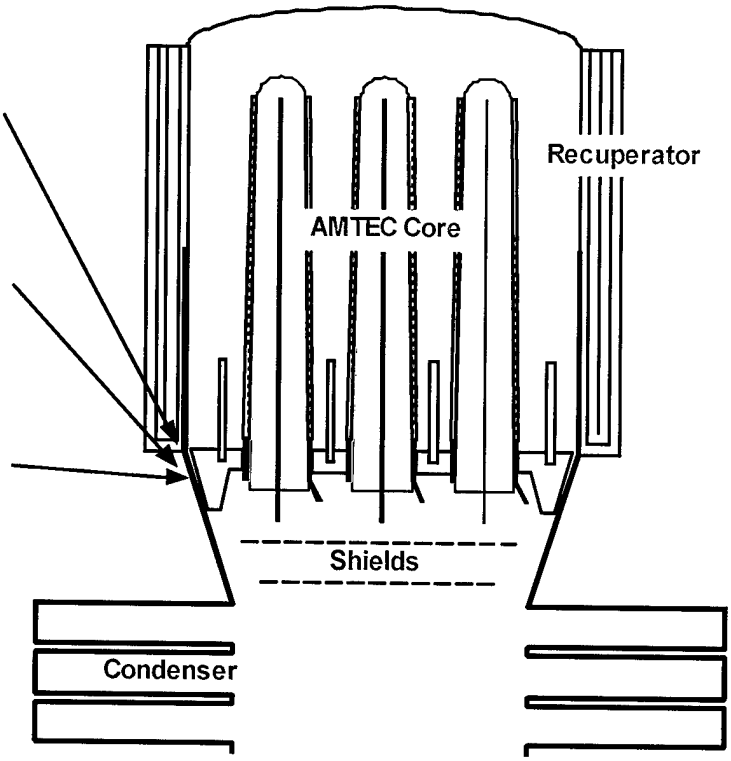

Figure 7-9 System Concept Including Monolith Cell

7.2 Process and Materials Selection

As alluded to above, a combination of performance, materials and manufacturing considerations led to the preferred monolith concept. The original concept was an extruded monolith and an early variant of that was a structure with molded tubes & wells with an integral header plate. Both of these structures are complex, require separate interconnect feedthroughs through the header plate and have the potential for low yields in manufacture.

Moving to formed tubes allows for QA/QC on individual tubes, thereby increasing yields significantly. However the sealing of beta tubes into an alpha header was an issue – there are known incompatibilities between standard glasses and beta-alumina. The concept for integrating the electrical interconnect into the tube joint/seal avoids the complexity of separate electrical feedthroughs and seals and allows us to take advantage of a glassing technology developed by Ionotec. Thus the preferred process and materials.

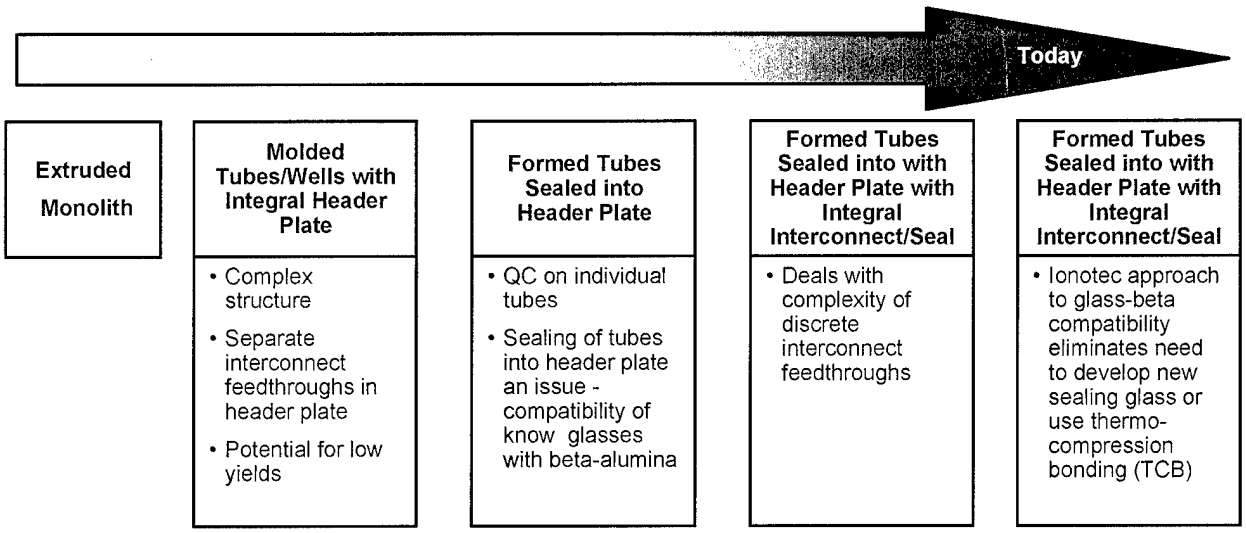

Figure 7-10 Reduction of Fabrication Complexity and Risk.

7.3 Fabrication Strategy

A fabrication strategy has been adopted that will lead to the fastest proof of concept. As illustrated in Figure 7-10, the fabrication complexity and technical risk has been reduced considerably since the beginning of the project. The currently envisioned approach includes:

Ceramic-to-Metal and Ceramic-to-Ceramic Joining

High pressure sodium vapor lamp manufacturers long-ago solved the problems of sealing and joining α-alumina to metal conductors (niobium) using a glass. The temperatures, pressures and sodium environments are directly relevant to AMTEC. However, the glass materials used by that industry will not work directly with β"-alumina due to ion exchange issues. Ionotec has demonstrated a proprietary barrier coating approach which permits glassing of the β" tubes to the niobium collar. In the same operation, using the same glassing material, α-alumina tube sections will be joined to the header to serve as electrical isolation webs.

β"-Alumina Tube Fabrication

Thin walled (0.5 mm), fine grained β"-alumina tubes will be fabricated using the electrophoretic deposition technique (which meets AMPS current tube quality specifications).

Cathode Electrodes & Current Collection

Paintable Weber electrodes and Chinese-finger-puzzle-like current collectors are planned on the cathode side. On the anode side we plan to take advantage of AMPS ISHP technology.

7.4 Prototype Hardware Vendors

We approached two companies with extensive experience in the development and the manufacture of beta" alumina sodium battery technologies for proposals on development of prototype monoliths.

Beta Research and Development Ltd.
Beta is a research group within the Swiss company MES-DEA SA. Beta developed the β"-alumina technology for the high temperature Zebra sodium nickel chloride battery. MES purchased the rights to Zebra and is continuing to commercialize the technology for targeted markets. Beta is currently contracted to produce Zebra batteries for a fleet of roughly 30 electric hybrid buses. Based in the U.K., Beta has a staff of ~12 professionals and a brand new pilot fabrication facility. Beta uses iso-static pressing methods to form components.

Ionotec Ltd.
Ionotec was formed from the sodium-sulfur battery R&D group of Chloride Silent Power. Based in the U.K. with a staff of ~6 professionals, Ionotec is the current supplier of β"-alumina tubes to AMPS. Ionotec manufactures sodium-, potassium-, lithium-, strontium- and proton-conductive ceramics for a range of applications, including energy conversion/storage, metallurgical refining and sensor technologies. Ionotec uses electrophoretic deposition to obtain high quality dense grained ceramic tube structures. Ionotec has developed proprietary ceramic/metal ceramic/ceramic joining techniques.

Both companies considered glassing and thermal-compression (diffusion) bonding (TCB) approaches for joining the beta tubes to the alpha header. Both companies were interested in working with us and were highly responsive. Each company has comparable experience with beta-alumina processing & manufacture. Ionotec has a proven technical approach for dealing with the glass seal/β" compatibility issues and had resources more readily available for our project. Beta's ability to shape the β" tubes was preferred for the TCB route. Overall, however, we felt Ionotec's technical approach had a greater likelihood of success for the preferred approach (glassing).

7.5 Feasibility Demonstration Plan

In developing a feasibility demonstration plan, we have simplified the prototype design to demonstrate the most critical aspects of the proposed approach. Critical aspects to be demonstrated will include:

- tube to header-plate bond/seal
- interconnect feedthroughs and connections to electrode current collectors
- integration of AMPS ISHP technology into the monolith
- sodium wick/current collectors
- sodium wells and unit cell isolation
- interconnect connection
- Weber electrode for cathode

Several non-critical design aspects were excluded from prototype designs to be fabricated. These include:

- sodium return wick (to be developed separately)
- monolith seal to test fixture will be a mechanical clamp around perimeter
- test monolith will be seven tubes rather than sixty-one, but the tubes will be full-height
- in addition, we will work with robust wall thickness rather than the lowest possible thickness

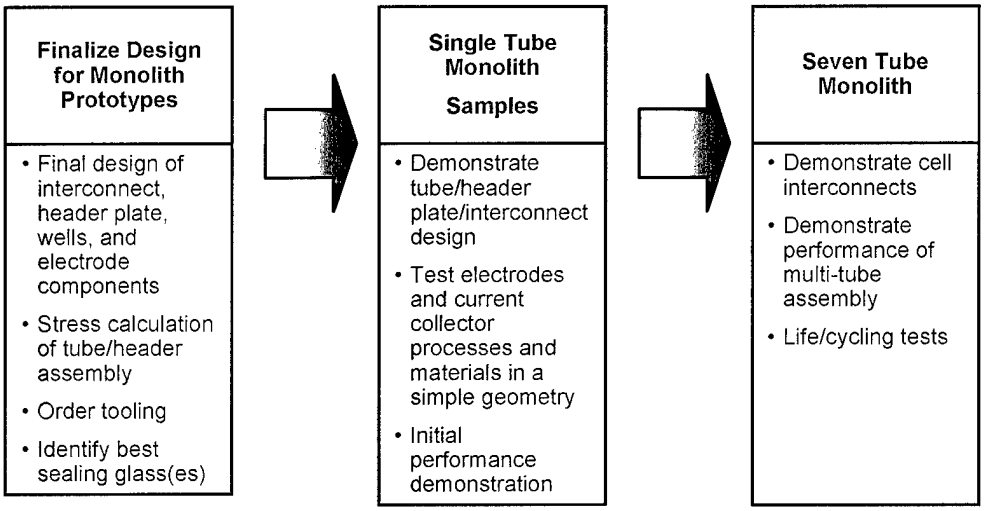

Figure 7-11 Planned Prototype Demonstration Plan.

Task	Description	Ionotec	ADL	AMPS
1	Finalize Design for Monolith Prototypes	• Glass formulations • Shape of seal design • Test glazing runs • Specifications	• Stress analysis of joint design • Specification of web design • Nb interconnect design	• Design input
2	Fabricate Single Tube Monoliths	• Procure parts • Manuf/ass'y trials • Single tube manufacture	• Review & progress monitoring • Coordination between Ionotec & AMPS	• Exposure tests • Electrode & current collector application • METC testing
3	Prototype Seven-Tube Monolith	• Design specification • Manuf/procure parts • Prototype monolith	• Review & progress monitoring • Coordination between Ionotec & AMPS	• Exposure tests • Electrode & current collector application
4	Additional Seven Tube Monoliths	• Manufacture/modify equipment • Manufacture/procure components	• Review & progress monitoring • Coordination between Ionotec & AMPS	• Electrode & current collector application • Once-through testing

Figure 7-12 Team Member Roles in Demonstration Activities.

The overall approach is illustrated in Figure 7-12 and the respective roles of the three team members is shown in Figure 7-13.

7.6 Glazed Joint Designs

Four initial joint designs were developed jointly by Ionotec and ADL. These are illustrated in Figure 7-14. The alpha-alumina disk dimensions in the single-tube assemblies was set at 44.4mm OD by 6.0mm thick. The BASE tube has been assumed to have a 19mm ID with a 0.5mm wall except in the area of the open end where the wall thickness will be increased to approximately 1.0/1.2mm to strengthen the tube in the vicinity of the glazed joint. In all these designs we try to use the rigidity and strength of the alpha disk to support the BASE to alpha disk joint.

DESIGN A represents the most conservative approach, closest to existing proven geometries. The alpha to BASE joint uses a recess in the alpha disk, similar to Ionotec standard glazing practice, while the current lead-thru uses a Nb pin in a hole, similar to high pressure sodium lamp practice. However, the use of calcium aluminate high temperature glass means that the BASE material cannot be in direct contact with the glass as degradation of the BASE and cracking of the glass will occur. Currently the ZrO_2 barrier layer has only been shown to work when applied to the green shape, which means that when the BASE tube is slit to length the cut face is left uncoated. Therefore, a ceramic cement layer is required in this option to prevent the glass contacting the exposed open end. The glass is then applied onto the top of the paste to produce a leak tight seal.

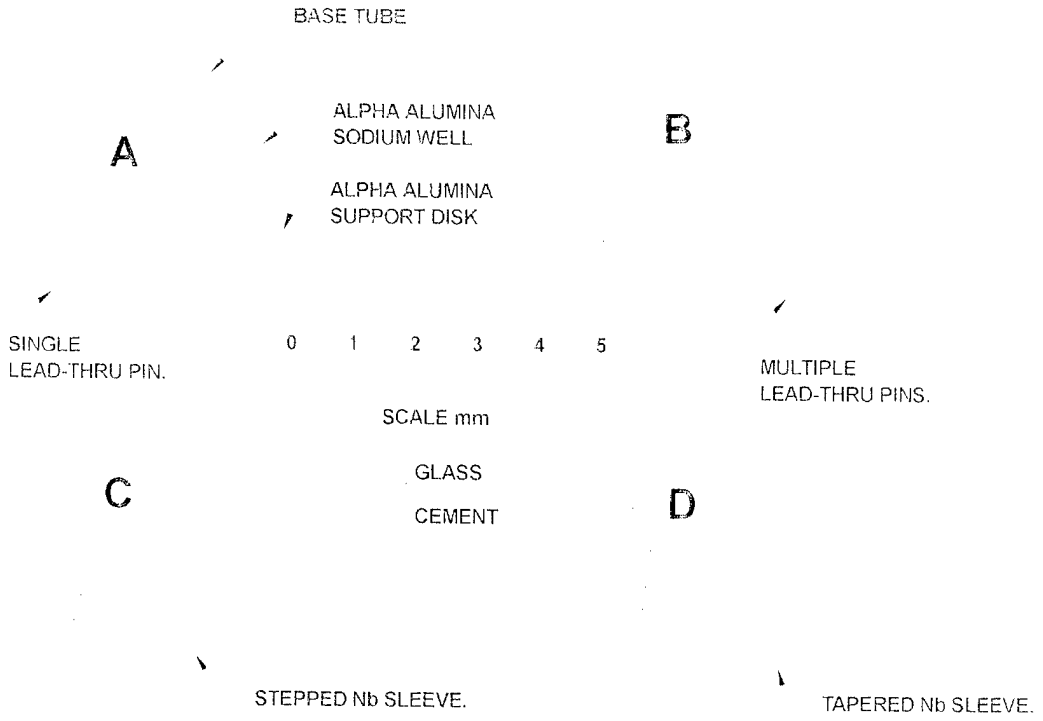

Figure 7-13 Four Proposed Joint/Seal Designs

DESIGN B uses a taper geometry between the BASE and alpha disk so that the unprotected BASE end face is removed from the area of the glazed joint. This means that it may be possible to eliminate the use of a cement and use glass only for the joint. However, the drawing shows that paste is still expected to form part of the joint for the following reasons. As the taper on the BASE tube is expected to be used in the as formed condition, ie. not ground, the clearance between the mating BASE and alpha tapers can be expected to vary. This may lead to problems with accurately locating the BASE tube and leave gaps between the BASE and alpha disk that allow the glass to drain from the joint area during glazing. A cement can be used to fill in excessive gaps and allow the BASE tube to be accurately positioned with respect to the alpha disk. The assembly is then fixed as the cement sets at room temperature, so eliminating the need for high temperature jigs, which is a big plus when large multi-tube assemblies are considered.

Designs A & B use lead through pins to provide a current path. For Design A, if a single, 3 mm diameter pin (7.1 mm^2) is used the ID of the Na well will be around 33 mm, while 4 off 1.5 mm diameter pins (equal in cross-sectional area to one 3mm pin) the Na well ID is approximately 30 mm, a 3 mm reduction but at the expense of more holes thru the alpha disk and more electrical connections. For Design B the use of a taper increases the Na well ID by 0.5 to 1 mm compared to Design A. The multiple lead-thru's could be used to locate the alpha Na well.

Designs C & D replace the Nb pin(s) with a Nb sleeve incorporated into the BASE tube to alpha disk joint. The information available on Nb indicates it is a very ductile material and can easily be pressed to shape for volume manufacture.

DESIGN C is evolved from Design A and retains a stepped recess geometry for the glazed joint. To maintain a 7.1 mm^2 area the Nb sleeve would be approximately 0.12 mm thick. The alpha Na well ID will be approx 26/27 mm and would use the Nb sleeve for location.

DESIGN D is evolved from design B and retains a tapered glazed joint geometry. The alpha Na well ID will be approx 26 mm and would use the Nb sleeve for location. This option has the simplest alpha disk design of all the options, requiring only one tapered hole per BASE tube assembly, and may also have an advantage over Design C in that the BASE tube passes thru the Nb sleeve and can help insulate the internal from the external electrical connections.

In all designs it has been assumed that the alpha Na well will be attached to the alpha disk using a glazed butt joint as it should not be under any significant loads. A number of other factors will need to be allowed for in selection of the finalized design:

- The Weber electrode will need applying to the inside of the BASE tube prior to the glazing operation at Ionotec. The nitrogen atmosphere required to convert the titanium hydride to titanium nitride cannot be applied in the presence of Nb as they will react. We intend to glaze using an Argon atmosphere, probably at around 1450°C, as this will not degrade the Nb and is the preferred method used by the lamp industries.

- The thickness of the glass will be important in obtaining a satisfactory operating life as there will be some slight attack by the Na on the glass.

- The means of application of the glass and cement will influence the tolerances of the gaps/clearances between mating components. Ionotec will need to carry out some trials to assess these factors.

- Material thermal properties. Information concerning strengths, expansion coefficients, etc and their change with temperature is being gathered and we will send it to you as soon as possible.

7.6.1 Design of Single Tube Assemblies

After discussions between ADL and Ionotec, option D was chosen as the preferred design for the experimental work, with option B as a fall back position if glazing with a niobium sleeve was found to be unsuccessful. Glazing of niobium pins to α-alumina with a high temperature matched expansion glass, as in design B, was already an established technology from the sodium vapour lamp and so the only unknown in this design was whether the same glass could be used to join β"-Al_2O_3 to both α and niobium without cracking.

The glazing temperatures of the glasses required to withstand AMTEC operating conditions are in excess of 1275°C and so it was highly probable during glazing that sodium oxide from the β"-Al_2O_3 would diffuse into the glass, thus modifying its expansion coefficient and causing cracking on cooling. To prevent this, it was planned to apply an inert coating of zirconia onto the surface of the β"-Al_2O_3 tube in the area required to make the seal, the idea being to prevent, or limit, the diffusion of sodium oxide.

It was envisaged that application of the glass prior to glazing would be fraught with practical problems due to the complex nature of the proposed designs. The β"-Al_2O_3 tube must be an as sintered component since any grinding to improve the fit of the various parts would mean removing the protective zirconia layer, therefore there was a likelihood that any ovality in the BASE tube could provide a gap which allowed the glass to run away. For this reason it was decided to incorporated a high temperature zirconia cement into the design which could be used to jig the components prior to application of the glass and would provide a support for the glass at the glazing temperature.

7.6.2 FEM Analysis

Finite element modelling was carried out by ADL, initially with the components as shown in design option D and then using a more detailed analysis with the α-alumina ring having radiussed edges and being undercut for incorporation of an external niobium flange (to which the external cell case will ultimately be attached).

The CTEs (coefficients of thermal expansion) of the materials are all similar, with the alpha alumina having the highest CTE and the beta alumina having the lowest CTE. The analysis

modeled the cool-down of the assembly from the curing temperature of the glass (1290°C) down to room temperature (20°C). It was determined that the heating process (heating the assembly form 20°C to 1290°C) would result in negligible stresses since the alpha alumina disk expands more than the niobium sleeve, which expands more than the beta alumina base tube. This results in the cement components being put in tension. Since the cement would likely fracture in this situation, then stresses are not transmitted through the cement and the parts are allowed to expand stress-free. Therefore, the cool-down process begins with the assembly in a stress-free state.

Figures 7-15 and 7-16 show the predicted hoop and radial stresses for the glazed joint, respectively. In both cases the maximum stresses for the assembly are located in a small region of the α-alumina ring and only amount to approximately half of the yield data level as quoted by the manufacturer.

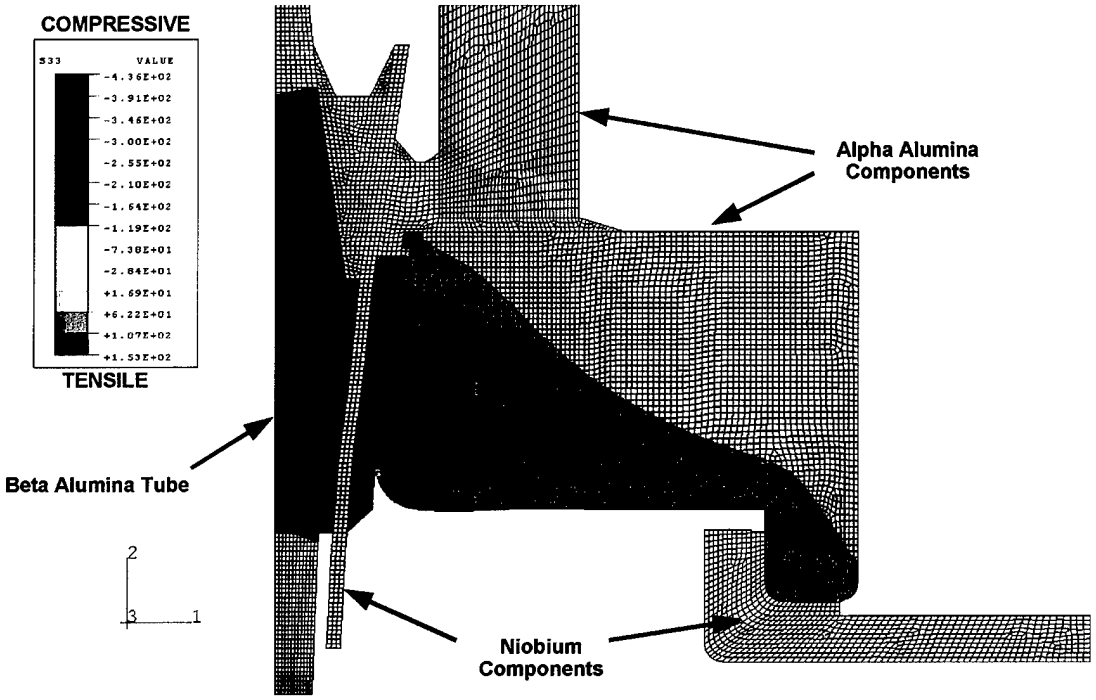

Figure 7-14 Predicted Hoop Stresses for Preferred Joint Design

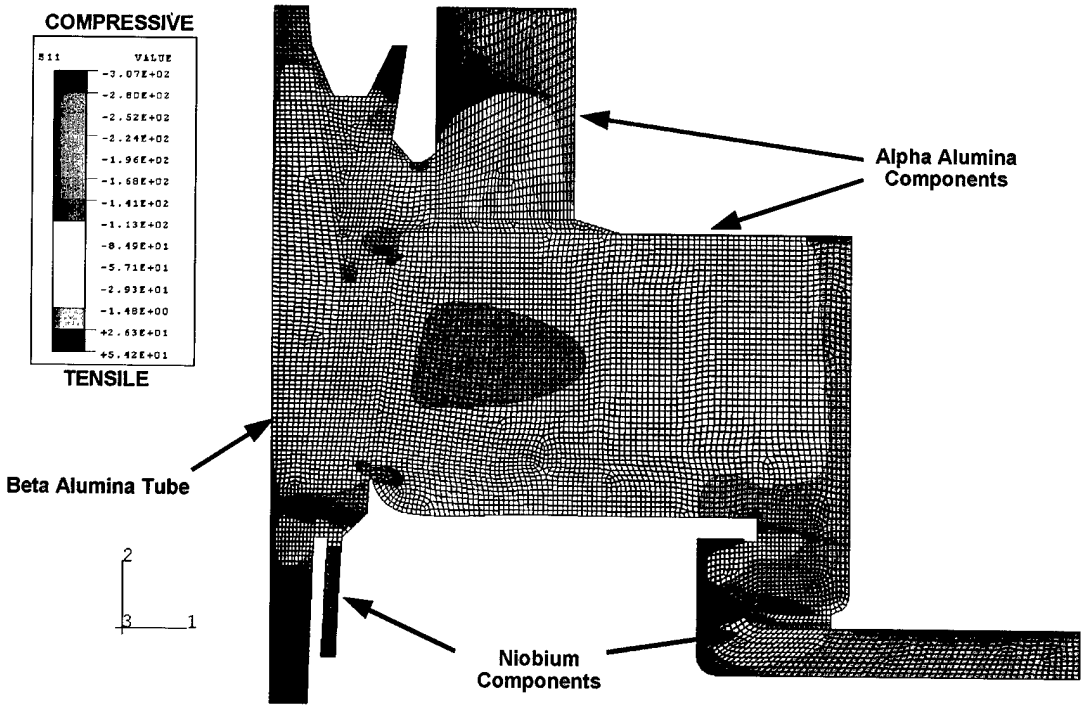

Figure 7-15 Predicted Radial Stresses for Preferred Joint Design

7.6.3 Selection of Glass and Cement

Before commencing the development work to select a glass matched to the requirements of the seal, advice was sought from people/companies with experience in sodium vapour lamp manufacture, where niobium is joined to α-alumina as part of the standard assembly process. Information was obtained with regard to heating/cooling rates, glazing atmosphere and glass composition, and 7 different sodium resistant glasses were selected for trials supplied by 3 companies. All were recommended for the glazing of α-alumina to niobium for sodium vapour lamps.

Initial tests at Ionotec centred on investigating if there was any reaction between the glasses and β"-Al_2O_3, using the temperature profiles recommended by the glass suppliers. β"-Al_2O_3 ceramic pieces were made to Ionotec's zirconia strengthened formulation which has a very controlled microstructure and then these ceramic pieces were partly coated with a thin zirconia layer to limit diffusion of sodium oxide into the glass during the glazing process.

Each glass was tested on both a coated and un-coated section of the ceramic to determine if there was any observable reaction. On the uncoated surface, all of the glasses were modified by the uptake of Na_2O, ranging from gross reaction to severe crazing but on the coated section the diffusion was drastically reduced.

The most successful glass was the lowest melting one and is used by Philips in their lamp. It has a melting point of 1309°C and wets the coated surface well with only slight cracking at the edges of the glass drop where it is very thin. All of the other glasses were significantly cracked, probably due to enhanced diffusion at their higher melting points. With the Philips glass, joints have been made which have no detectable leak to helium (10^{-9} torr l/s) for alpha to alpha, alpha to Nb (using Nb1Zr pins mounted in a 4mm hole), and alpha to BASE, all glazed in argon. The Nb appears to survive the glazing conditions without any significant corrosion and embrittlement providing the metal surface is clean, grease free and that there is no trace of oxygen in the glazing atmosphere.

Trials have also been conducted in a vacuum furnace but while the glass appears to perform well under these conditions, soda is lost from the β"-Al_2O_3 surface leading to a layer of non-conductive α-alumina, as determined by x-ray diffraction.

A preferred cement has also been selected for the joint from a group of 5 which have been tested. This cement is supplied by Cotronics and is zirconia based. It is specified as being usable up to 2200°C and is recommended for use with molten metals with an excellent resistance to alkali. It has no discernible reaction with the glass and has the advantage of being cured at 70°C which means atmosphere control is not required during the curing. Other cements require curing time at 370°C where argon or vacuum would be needed to protect the Nb from corrosion. With this cement/glass combination, joints of an alpha ring to a Nb collar to a zirconia dipped BASE tube have been made which are helium tight.

A number of sample tubes were received from Amps Inc. coated with the Weber electrode and were put through the proposed glazing regime. There was no weight loss and the resistance of the coating appeared to be unchanged. These tubes were returned to AMPS for their assessment of the quality of the electrode after this heat treatment.

7.7 Prototype Joint Fabrication

Several prototype joints were fabricated, sectioned and examined carefully. Figure 7-17 shows a glass seal which was made using the preferred Philip's glass to join alpha to beta alumina. (One picture is an enlarged section of the other.) The beta"-alumina is the ceramic piece with the rounded end and you can make out the zirconia layer on the surface which shows up as a white line. The fine grain microstructure of the bulk ceramic is a result of using the zirconia strengthened composition.

The pictures show that the glass has wicked very well into position, indicating that viscosity and surface tension characteristics are suitable. In the center of the join, there is a significant number of large pores due to the glass only having a very short time to flow since it is only taken up to its melting point and then cooled. In this geometry the glass would have had to flow horizontally to fill the pores but in our final seal it will be flowing under gravity and so the pore should fill more easily.

Higher magnifications of the joint shown in the photos show a thin modified layer in the glass adjacent to and of similar thickness to the zirconia coating. This indicates that while the coating

is very well bonded with no evidence of partial detachment, there is some slight sodium exchange into the glass. The expansion coefficient of the glass is modified in this layer and a few microcracks appear but they do not penetrate into the bulk of the glass. With the higher temperature glasses the diffusion is increased and without the coating the all glasses are completely modified.

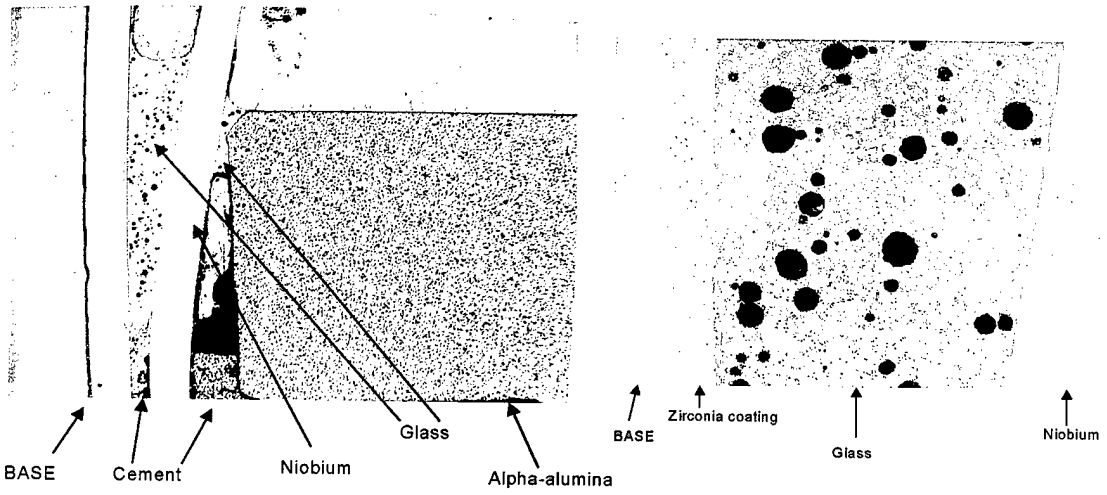

Figure 7-16 Micrographs of prototype glazed joint

7.8 Prototype Single-Tube Assemblies

Some modifications were required from the original design, due to the lead times and costs of manufacture of the original Nb1Zr components. For both the current collector and the flange seal, Nb1Zr sheet could only be obtained in minimum order quantities which were way beyond that which was required. It was agreed, therefore, that for this verification of concept it would be sufficient to use pure Nb in place of Nb1Zr. The designs were also simplified to assist fabrication, changing the Nb flange into a flat component to be sandwiched between the original upper α-alumina collar and a new additional lower ring. This extra ring also meant that the Nb connection tag no longer protruded from the complete assembly and so it did not require bending flat after glazing.

Thirty long BASE tubes were manufactured with the zirconia coating on the open end and were machined to length. These were then sent to AMPS for application of the Weber electrode to the inside surface. Around twenty shorter BASE tubes with the same open end geometry as the larger ones were also produced and were used during commissioning of the new kiln and for proving the assembly method.

Glazing trials were carried out using the shorter BASE tubes in order to optimise the method of assembling the components and of applying the Philips sealant. These trials were also used to examine the effects of peak temperature on the wetting and flowability of the sealant, and the effects of any reaction with the BASE. The preferred order of assembly was established as follows:

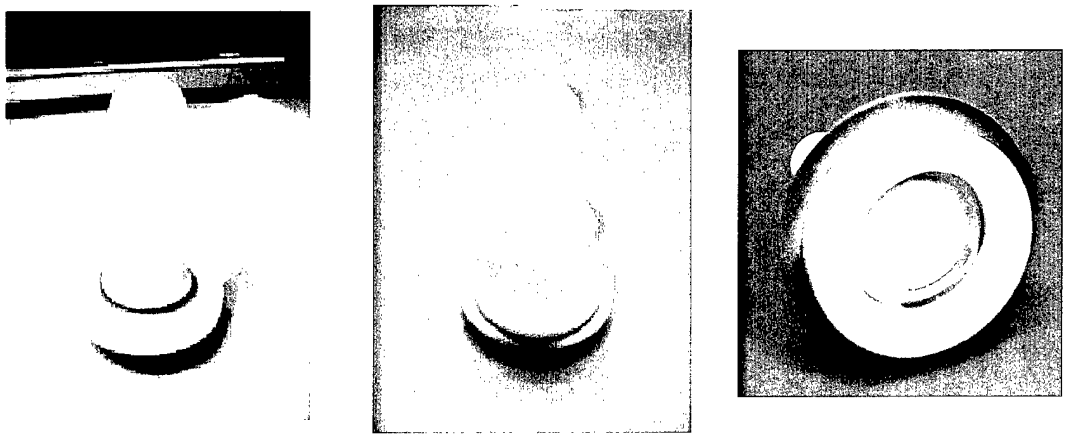

Figure 7-17 Prototype single-tube glazed assemblies:

(a) glazed sub-assembly showing BASE tube, Nb current collector and alpha-alumina header; (b) complete single-tube assembly; (c) view of bottom of assembly showing Nb connector and mounting flange.

- Apply bead of zirconia cement to tapered hole in upper α-alumina collar
- Position Nb current collector inside the ceramic collar, ensuring that there are no gaps in the bead of cement
- Cure the cement at 70°C for a minimum of 4 hours
- Apply another bead of cement to the BASE tube just below the point of maximum OD
- Assemble the BASE tube into the current collector, again ensuring there are no gaps in the cement
- Cure this new join as above
- Apply the Philips sealant, in the form of a paste with deionised water, to both sides of the current collector ensuring that the space between the Nb and the BASE tube is filled to the rim of the Nb
- Dry the paste at 70°C and then remove any excess sealant with a ceramic knife prior to glazing.

This part of the assembly required glazing before the other components were in place since the α-alumina well, when positioned, serves to shield the joint from the furnace elements and thus prevents it from reaching the peak temperature.

The sealant has a low bulk density as a powder and so it was applied as a paste to get more solid in the joint. Trials with pressed frits proved unsuccessful since the choice of binder is severely limited to those which can be burnt out in air below 200°C. Above this temperature an argon atmosphere must be used to prevent oxidation of the niobium components. Nevertheless the sealant still undergoes a dramatic volume reduction on melting and typically 3 or 4 glazing runs are required, topping up with extra paste each time, before a leak tight seal is obtained (better than 10^{-6} torr.l.s^{-1}). A glazed sub-assembly is shown in Figure 7-18(a).

The remaining parts are then assembled as follows:

- Apply Philips sealant as a paste around the top of the lower α-alumina ring
- Position the Nb flange on top, ensuring that it is centralised
- Apply another ring of paste to the upper surface of the Nb flange and locate the BASE sub-assembly in place to form the sandwich seal
- Apply a third ring of paste on the top surface of the upper α-alumina ring and locate the ceramic tube (the Na well) in place.
- Dry the paste at 70°C and then remove any excess sealant with a ceramic knife prior to glazing.

Figures 7-18 (b) and (c) show complete assemblies with a short BASE tube. Three of the smaller assemblies each with helium leak rates better than 10^{-6} torr.l.s^{-1} survived pressure testing using water at 2.8 bar, without any leaks. Subsequent helium leak test showed no deterioration.

A long BASE tube assembly (see Figure 7-19) was pressure tested at 900°C. A vacuum of 7.4 torr.l.s^{-1} was held on the assembly for 2 minutes without creating any leaks. This test has been used as a proof of concept rather than as a 100% quality test since the extra ceramic components used to form a seal at 900°C cannot be removed after cooling without damaging the assembly.

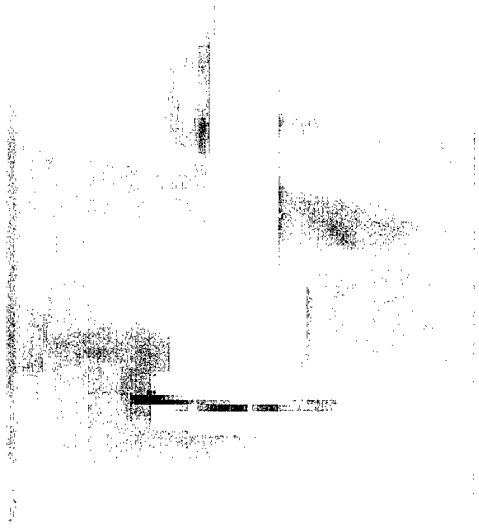

Figure 7-18 Prototype full-length glazed BASE tube assembly

7.9 Alternative Glazed AMTEC Assemblies

This concept replaced the multi-tube cell design which was originally planned to be fabricated by Ionotec. It is now based on a single tube design proposed by AMPS whereby a BASE tube is glazed to an α-alumina mounting collar at the open end and has a Nb1Zr pin glazed through a hole in the opposite end.

A slight modification to the pin joint has been proposed by Ionotec where the Nb1Zr pin and the BASE tube are separated by an α-alumina washer. This design gives the added benefit of an increased sealant path length and ought, therefore, to give longer resistance to sodium corrosion in cells.

As described above, pressings of sealant frit proved unsuccessful due to the problems of binder removal in a non-oxidising atmosphere and therefore the sealant was applied as a paste, prepared with deionised water.

Electrophoretic deposition (EPD) tooling was designed and manufactured for the production of BASE tubes to the geometry required. The tubes must be deposited with the hole (for the pin) present in the green state since the zirconia layer, which prevents diffusion of ions between the BASE and the sealant during glazing, must be applied at this stage. If the holes were to be drilled after the tubes had been sintered, then this would leave an uncoated surface free for diffusion to take place. To form the hole, an insulating plug is screwed into the flat end of the forming mandrel to prevent deposition in this area. Tubes of shorter lengths have also been manufactured for use during glazing trials.

Five prototype tubes were glazed with test Nb1Zr pins supplied by AMPS and were all measured as $<10^{-9}$ torr.l.s^{-1} on helium leak test. The test pins were made to a design which could be made quickly and at low cost but would be sufficient to determine the feasibility of the idea. Some further short tubes were used to make the alternative join with the α-alumina washer in place and these were also measured as $<10^{-9}$ torr.l.s^{-1}. Sample assemblies are shown in Figure 7-20. The 5 full size prototypes were shipped to AMPS for sodium corrosion and thermal cycling tests and the results of first tests, as reported by AMPS, are detailed below.

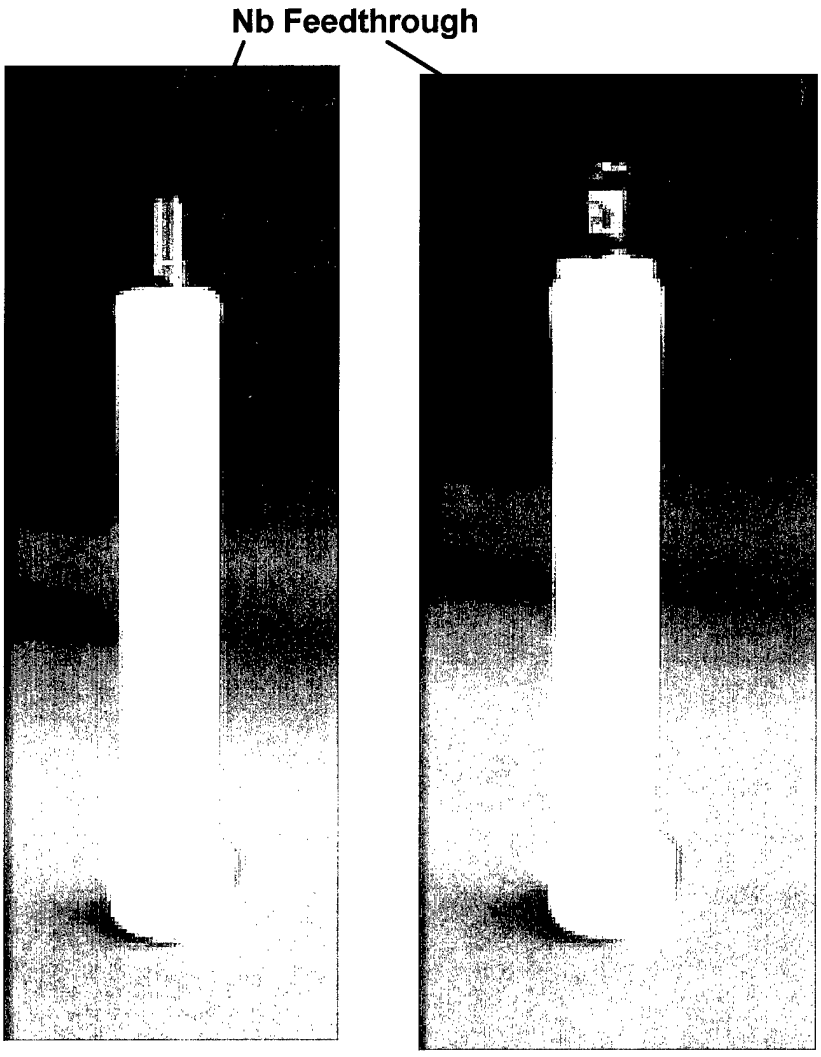

Figure 7-19 Glazed single-tube samples of AMPS alternative design

On thermal cycling the samples were heated up to 900°C in a vacuum at a rate of 25°C/minute and cooled to room temperature at about the same rate. After the first cycle, the leak rate had increased by about an order of magnitude to $<10^{-8}$ torr.l.s^{-1} but after nine additional cycles, the leak rates remained unchanged.

On sodium exposure test, the samples were tested at 900°C for 2 weeks with sodium on both sides of the seal. After removal, the seal was in tact but the leak rate had increased to 0.1 torr.l.s^{-1}. SEM analysis showed that the zirconia layer around the joint had crazed and EDS analysis indicated presence of a small amount of sodium on the zirconia surface in the same area. Since the sealant is essentially sodium free, this must have either diffused through the zirconia layer from the BASE, or more probably come from sodium vapour penetrating the seal.

The sodium corrosion test results indicated the need to increase the seal path length, from that achieved with the trial Nb1Zr pins, and this was achieved in a second the set of deliverables manufactured subsequently.

Five Nb1Zr pins to the final design were supplied by AMPS to Ionotec along with the six α-alumina collar for the open ends of the assemblies. This pin shape, by itself, will give an increased seal length but this is further enhanced by inclusion of the α-alumina separating washer.

All glazed joints without the washer have been helium leak tested to $<10^{-9}$ torr.l.s^{-1}. Those with the washer were measured at 10^{-6}torr.l.s^{-1} He, and so for subsequent runs it is planned to use ceramic weight on top of the components during glazing to improve the seal between the washer and the BASE tube. These deliverables were then returned to AMPS for cell testing. This cell testing was never performed, due to lack of resources at AMPS.

8 Advanced Tubular AMTEC Cell

8.1 AMTEC Cell and BASE Tube Design Evolution

A number of cell design configurations have been developed for various applications, including a small 8-tube cell for radioisotope-fueled space power, a 96-tube radial cell for solar and combustion systems (shown in Figure 4-1), and a scaled up version of both types with larger β"-alumina solid electrolyte (BASE) tubes. The small cells for space power systems have been built and tested for performance and durability. One of the first cells of this type logged over 6,000 continuous hours without degradation. While they will not be discussed here, performance models have been developed for all of these cell types. These models have been successfully validated against actual cell experimental data.

The radial cell shown in Figure 4-1 was developed for the Phase I version of the MAPPS power system. Results for this design approach were mixed. The first engineering cell demonstrated that the power output levels were predictable. The second cell, intended for fabrication development and prototype testing, encountered several difficulties. Cell fabrication processes used in this second cell were complex and one step in particular resulted in a serious degradation of the cell power by sputtering metal on the BASE tube insulators. Testing of this second cell produced only a few watts of power. There is every expectation that a build of a second prototype would be successful; however, a follow-up cell build has been suspended in order to evaluate BASE tube design.

The small (0.75 cm OD x 2.5 cm long) BASE tubes used first in early space power cell designs, as well as the MAPPS Phase I radial cell, were the product of early R&D level development work. These tubes had a high parts count and a very complex fabrication process. Minimal efforts had been focused on manufacturing improvements. This resulted in a low yield for tube assemblies during manufacturing and costly BASE tubes.

A new design, shown in Figure 8-1, was developed to reduce parts count and cost, increase ruggedness, and improve manufacturability. The new simplified design is scaleable for a variety of tube sizes and hence can be incorporated in any design configuration, whether small tubes or, as will be discussed, larger tube cells. Additional design innovations have been identified to further reduce parts and use less expensive materials.

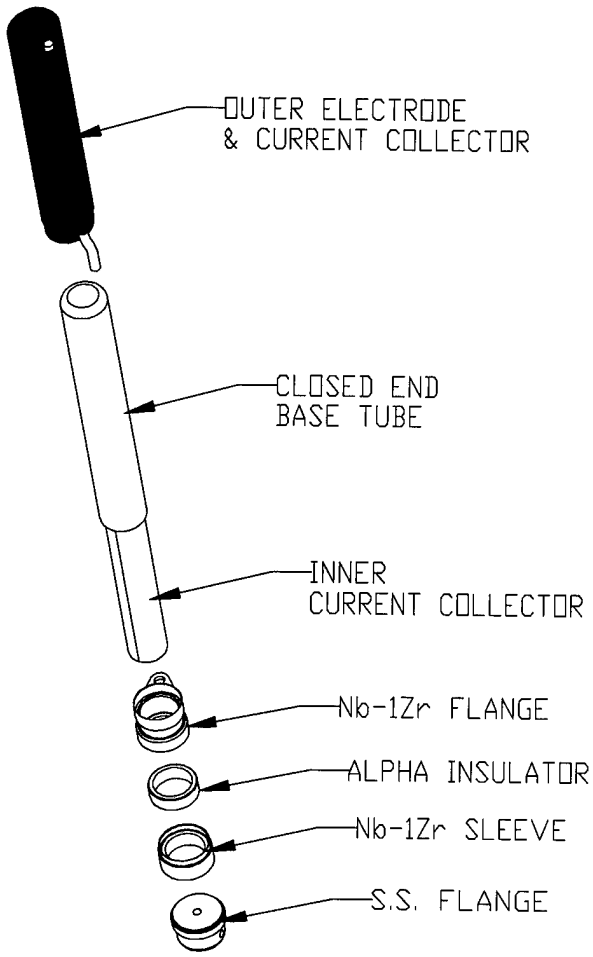

Figure 8-1 Closed end simplified tube design.

8.2 Internal Self-Heat Pipe Developments

One significant improvement in the new BASE tube design has been achieved by incorporating the Internal Self Heat Pipe (ISHP) mode of operation. In this mode the BASE tube inner current collector is filled with liquid sodium and uses two-phase flow, similar to a heat pipe, to transport heat inside the BASE tube. Earlier designs used a dry electrode and current collector on the inside of the BASE tube. Sodium was not allowed to condense. In this design, however, sodium is allowed to condense (by appropriate temperature control) and the BASE tube becomes isothermal resulting in increased power because of a higher average BASE tube temperature. The liquid sodium on the inside of the tube also eliminates the need for a separate inner electrode and provides much better current collection than a dry inner current collector. Finally, the ISHP mode allows the BASE tube to be much longer because the heat entering the hot end of

the BASE tube is easily transported to the cold end of the tube. This allows the total power of a BASE tube to increase without increasing the parts count.

8.2.1 Large Single BASE Tube ISHP

Test data for the tests of the large (1.5 cm OD x 10 cm long) single BASE tube ISHP (ISHP-3) showed that the cell was operating in ISHP mode, as seen before in small BASE tube cells (ISHP-1 and ISHP-4). The results were very encouraging. Figure 8-2 shows isothermal temperature profiles in the BASE tube at different operating conditions. The slope of the curve proves that the heat piping is taking place (with $dT/dx \sim 0$ in the isothermal zone).

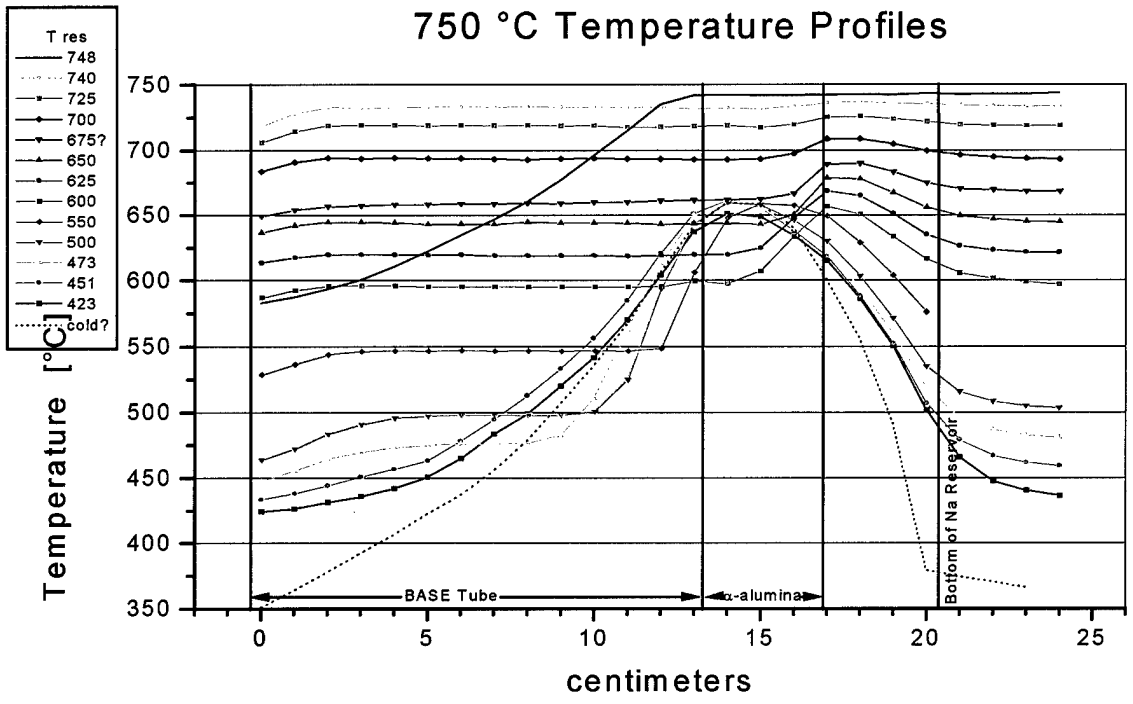

Figure 8-2 Thermal Performance of Large Tube ISHP Cell

Performance test results, shown in Figure 8-3, were very encouraging with over 8 watts at nominal operating temperatures. Historical test data and modeling results indicate that this tube will provide 5 watts in a multi-tube cell.

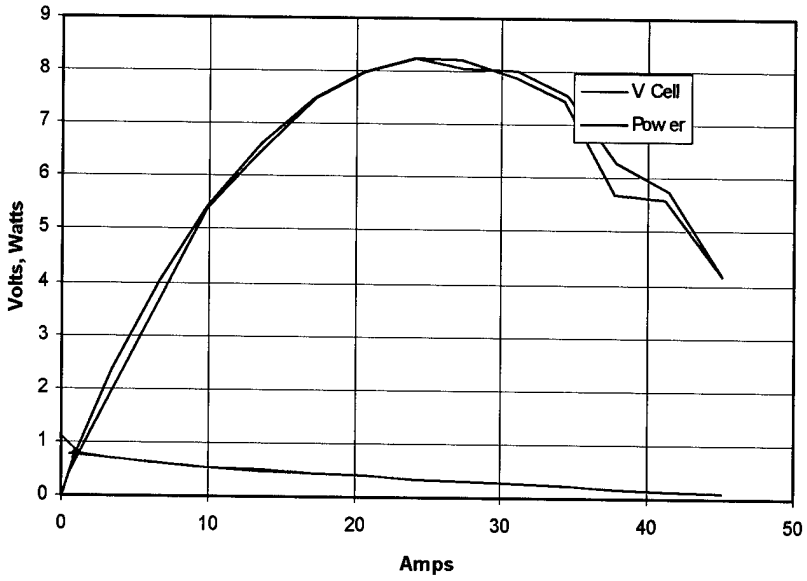

Figure 8-3 Single tube performance of simplified BASE tube design.

8.2.2 Multiple BASE Tube ISHP

The ISHP-4 test cell was designed to test ISHP operation in a multi-tube cell. The ISHP-4 cell contains three small BASE tube assemblies and a single artery/evaporator assembly, see Figure 8-4.

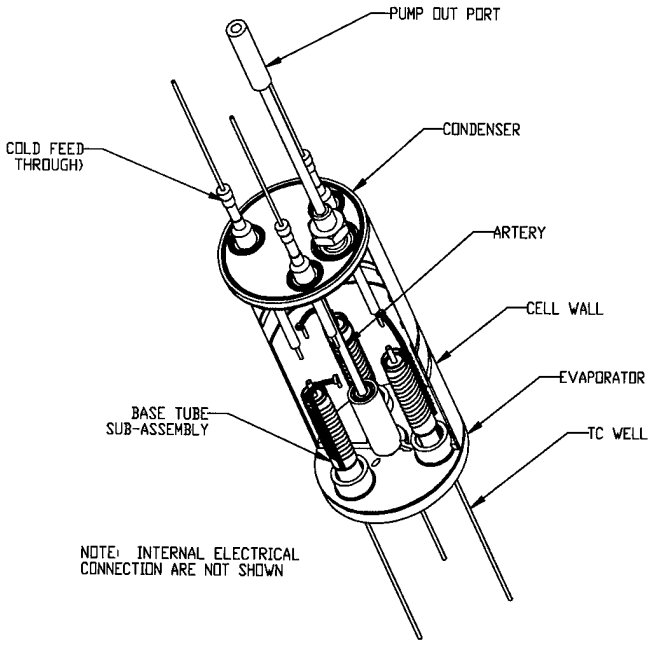

Figure 8-4 ISHP-4: Multi-tube ISHP demonstrator.

The ISHP-4 cell was set up for testing on the test fixture, which is equipped with moving thermocouples for taking temperature profiles (temperature as a function of position). Two computers are involved in the testing of ISHP-4: one that is dedicated to the moving fixture and one for monitoring and recording the cell's behavior.

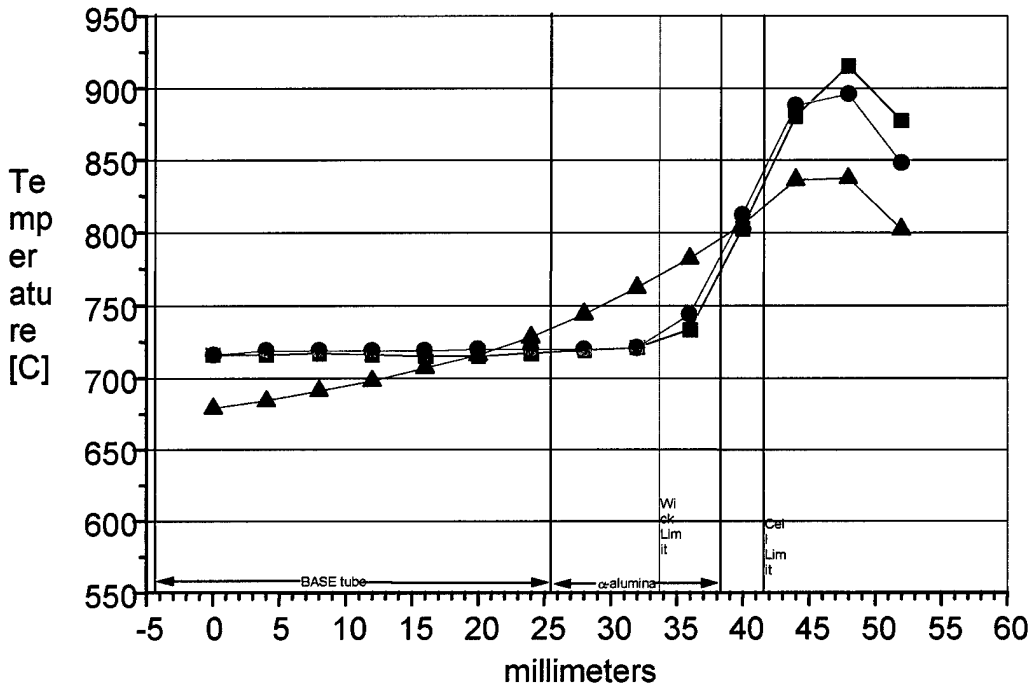

Figure 8-5 Temperature Data for Multi-tube ISHP Test.

Initial testing focussed more on the cell's thermal behavior and less on the cell's electrical performance (although for completeness, some electrical data was collected at every step of the way). The results were very encouraging. Figure 8-5 above shows simultaneous temperature profiles in the three BASE tubes. This trio of curves is typical of the many temperature profiles recorded so far. The similarity of two of the curves (circle and square) shows that the corresponding BASE tubes are locked onto the same temperature. Furthermore, the near-zero slope of the curves proves that heat-piping is taking place (with $dT/dx \approx 0$ despite there being a sizeable heat flow, the thermal conductivity is extremely large – a value which can only be achieved by heat-piping).

The third curve in Figure 8-5 (triangles) has more of a slope, and so is evidently not heat-piping. In fact, that particular BASE tube was completely sealed-off during the assembly of the cell. This serendipitous mistake provides us with a reference point: in most cases, the behavior of the other two BASE tubes can be compared to that of the third BASE tube. For example, in Figure 8-5, the third BASE tube has the temperature profile which our conventional BASE tube

assemblies would have had under the same conditions without the ISHP feature. The slope in that curve indicates that heat *conduction* is the primary means of heating the length of the BASE tube, the result being a drop in temperature as one moves away from the hot end of the cell.

The early electrical data shows that the performance of each of the two working BASE tubes is quite identical, and also is comparable with the performance of the lone BASE tube inside of AMPS's Single Tube Cell.

Figure 8-6 shows one of the IV graphs recorded for ISHP-4 thus far. The graph contains four curves, two for each BASE tube: the IV characteristic (diagonal line) and the power vs. current calculated from the IV curves (parabola). These particular curves were recorded with the BASE tubes at 766°C, the hottest setting so far. The curves show two things in particular. First, the curves for the two BASE tubes are quite similar, as we expected since they are under nearly identical conditions. Second, there is a lack of any hysteresis in the curves such as we find for all BASE tubes operating in the vapor anode or liquid anode mode (not shown) This benefit is due to the very high heat transfer afforded by the ISHP mode – the BASE tube temperature does not decrease as we start drawing power from the tube.

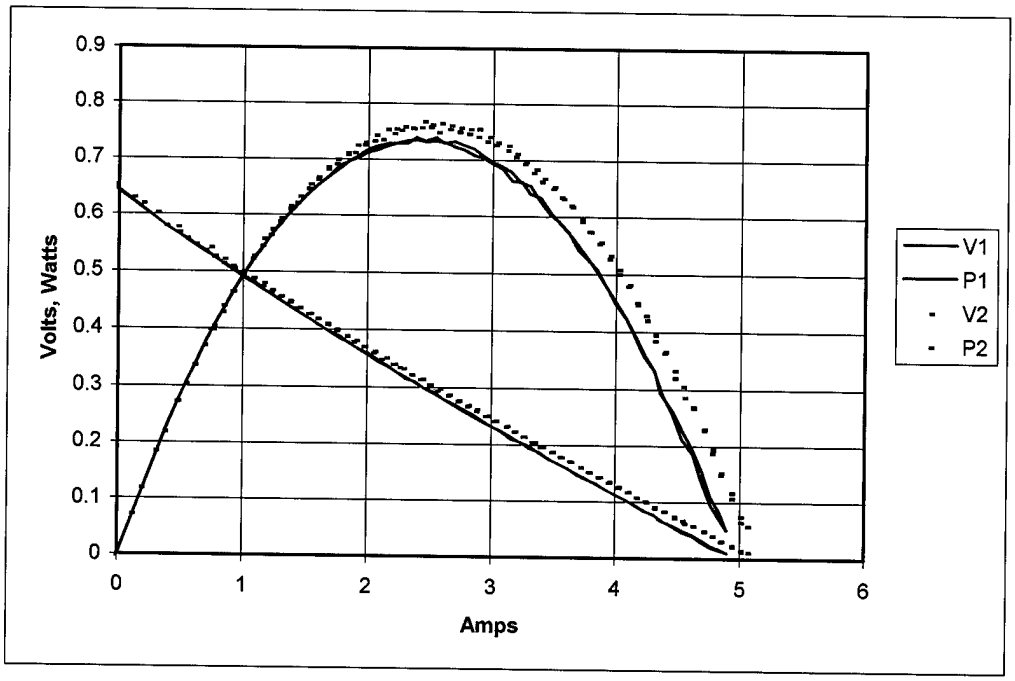

Figure 8-6 I-V and Power Curves for ISHP-3 Cell

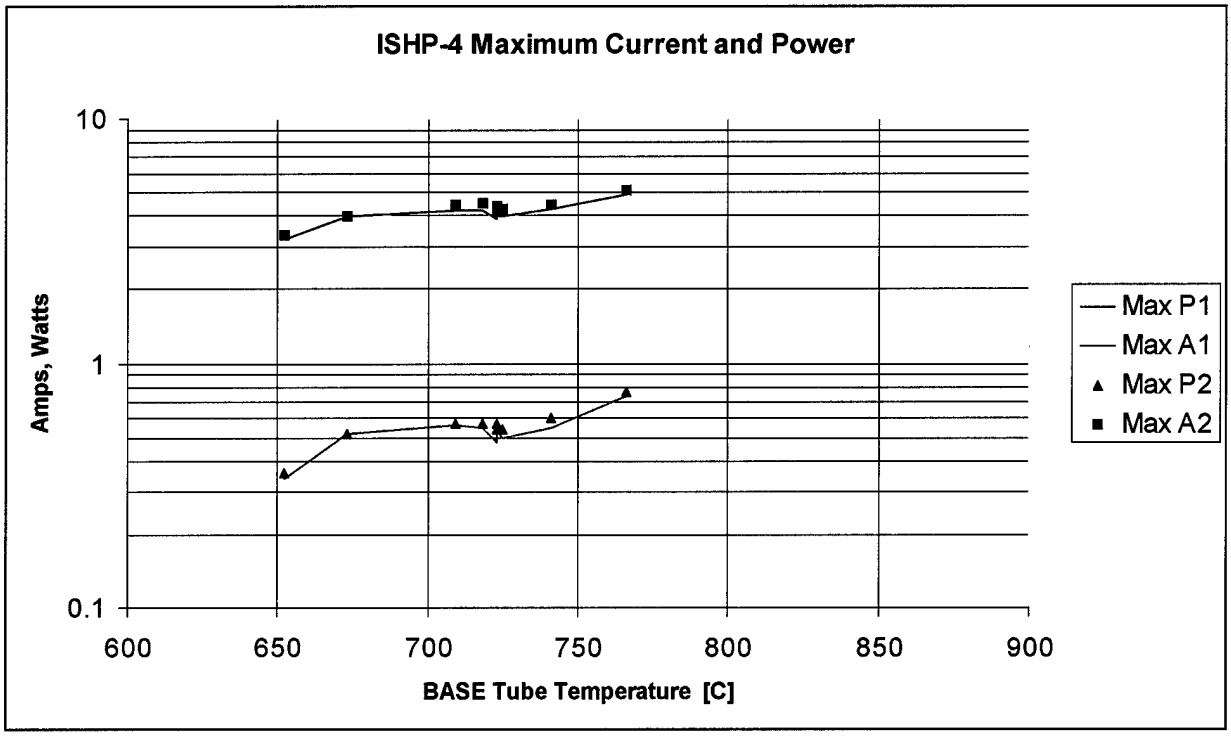

Figure 8-7 Power and Current Data for ISHP-3 Cell

The second graph, Figure 8-7, shows the maximum current and power found from many such IV curves. Both are expected to increase as the temperature increases, and it can be seen that they are. As we continue raising the temperature to 850°C, both the voltage and the current from the cell will increase; thus the power output could increase quadratically.

8.2.3 ISHP Cell Fabrication

The fabrication of an ISHP BASE Tube Assembly involves five major steps:

1. Inserting the inner wick.
2. Pressing together the BASE Tube and lower components.
3. Brazing the BASE Tube and lower components.
4. Sputtering the outer electrode on the BASE Tube.
5. Wrapping the outer current collector to the BASE Tube.

The picture in Figure 8-8 shows a pre-assembly layout of all the components used in a BASE Tube Assembly. Figure 8-9 shows the assembled ISHP Base tube.

1. The inner wick isothermalizes the BASE tube, thereby facilitating the ionization of sodium through the ceramic. The felt is rolled onto an insertion tool and then slipped into the BASE tube

2. The lower components of the BASE Tube Assembly electrically insulate the tube from the ground, provide the mating surface for connection to the evaporator plate and provide the surface to electrically link each BASE tube in series. The lower components and BASE tube are assembled and pressed together.

3. After the assembly is pressed together, the components are loaded into a high temperature furnace and brazed together using a band heater. Future improvement activities will focus on further automating this step or possibly eliminating it if the pressing operation can adequately seal the assembly.

4. The brazed assembly is loaded into a piece of equipment that sputters the outer electrode onto the outer surface of the BASE tube.

5. In the last assembly step, an interwoven mesh and a bus bar are "wire wrapped" to the exterior of the BASE Tube Assembly. The interwoven mesh assists with the axial conduction of the current while the wire that is used to affix both the mesh and the bus bar to the assembly serves to transfer the current to the bus bar. The bus bar serves to conduct the current along the length of the BASE Tube Assembly and transfer it to either the load or the next BASE Tube Assembly (hooked up in series).

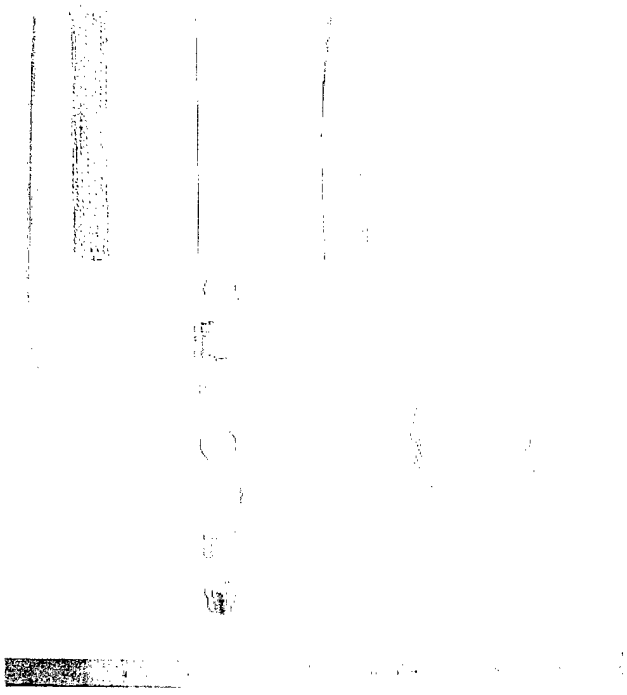

Figure 8-8 Components of ISHP BASE Tube Assembly

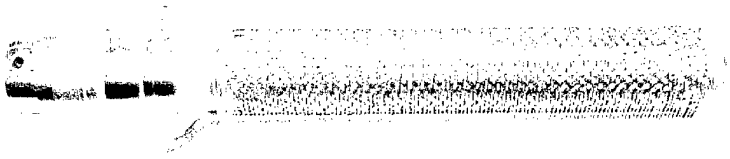

Figure 8-9 Assembled ISHP BASE Tube Assembly

8.3 500 Watt Cell Conceptual Design

A conceptual design has been prepared for a 500 W cell, based on the same BASE tube technology to be demonstrated in the engineering cell. This cell is illustrated schematically in Figure 8-10. Detailed thermal and performance models were developed using the SINDA-FLUINT code to support the advanced converter designs. The model layout is shown in Figure 8-11. The thermal models included all conduction and radiation heat transfer. No convection heat transfer was modeled except to assume a very high conductance along the length of the BASE tubes where the liquid filled wicks would produce a two-phase heat transport. The power output was based on detailed electrical and electrochemical models for the BASE tubes and current collectors. These models were integrated into the SINDA-FLUINT code to simultaneously solve the both the thermal and performance equations.

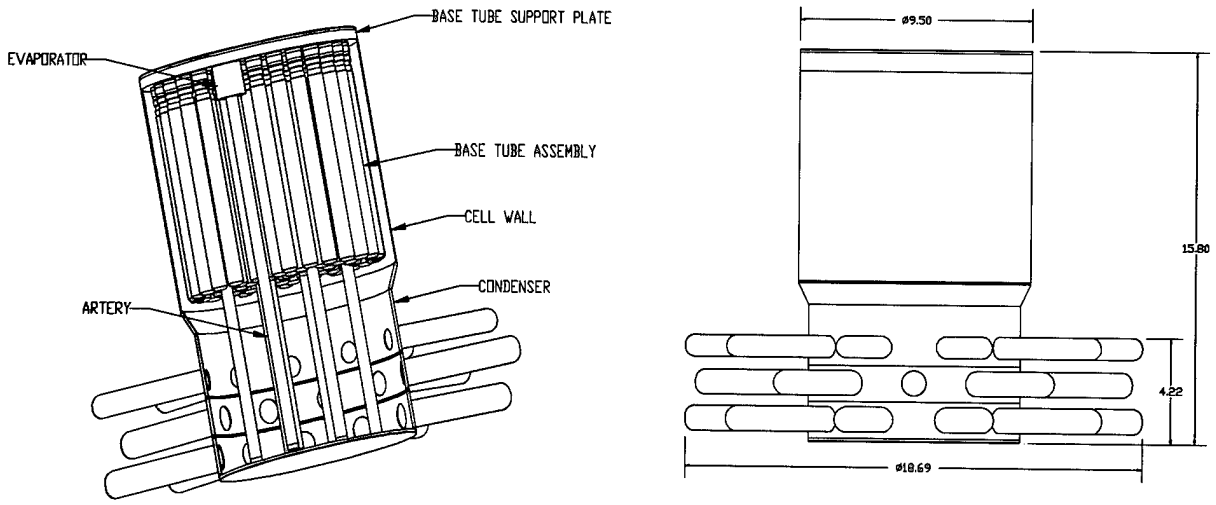

Figure 8-10 Conceptual Design for a 500W Cell

The radiation model and the heat transfer connections were calculated by RadCAD, with geometry input from AutoCAD. The actual geometries used is shown in Figure 8-12. The model was a $1/8^{th}$ section of the whole converter and the following assumptions were made:

- External containment surfaces shown in Figure 8-12.
- 1/8-scale model developed.
- The heat is entering only the top end of the converter. The walls are adiabatic, and are dry so the emissivity is that of stainless steel.
- No heat transfer from the wall to the BASE tubes due to sodium flow (vaporization and condensation) was considered. This is a small contribution to the overall heat transfer to the BASE tubes.
- No condenser tubes.
- No heat shields
- Internal component surfaces shown in Figure 8-12.

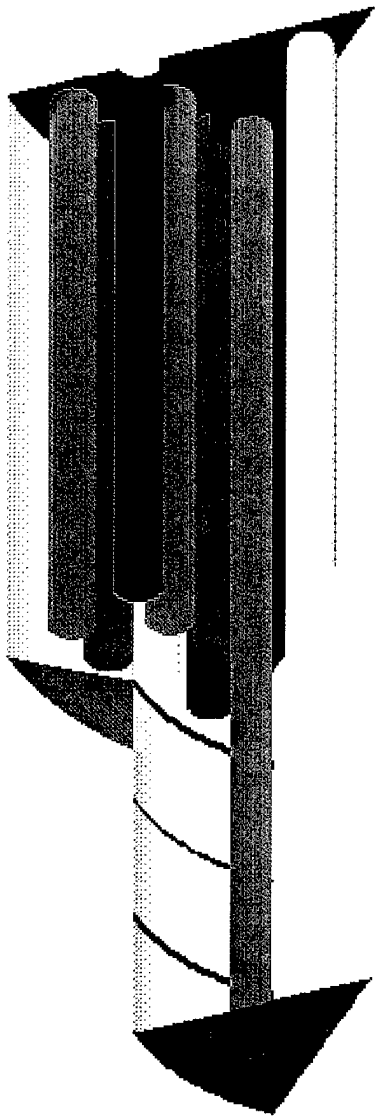

Figure 8-11 500W Converter Thermal/Performance Model Layout

Summary performance predictions for the 500 W cell were as follows:

- Hot end and cell wall temperature 900°C
- Cold end temperature 380 °C
- Evaporator temperature 779 °C
- BASE tube temperature 838 °C
- Cathode side pressure drop 30 Pa
- Total cell power 520 Watts

8.4 Engineering Cell

As indicated above, the ISHP results achieved in a large single tube cell and in a multi-tube demonstrator are promising. However, ISHP BASE tube designs still need to be tested in an operating multi-tube cell. This is the primary motivation for designing, building and testing an engineering cell. The engineering cell is designed to produce 35 watts and incorporates eight simplified BASE tubes and single artery system. The cell is shown schematically in Figure 8-12. This converter was substantially larger than any state of the art converters developed prior to this program. The scale-up is illustrated in Figure 8-13. The BASE tubes were 4 times longer than previous designs and twice the diameter.

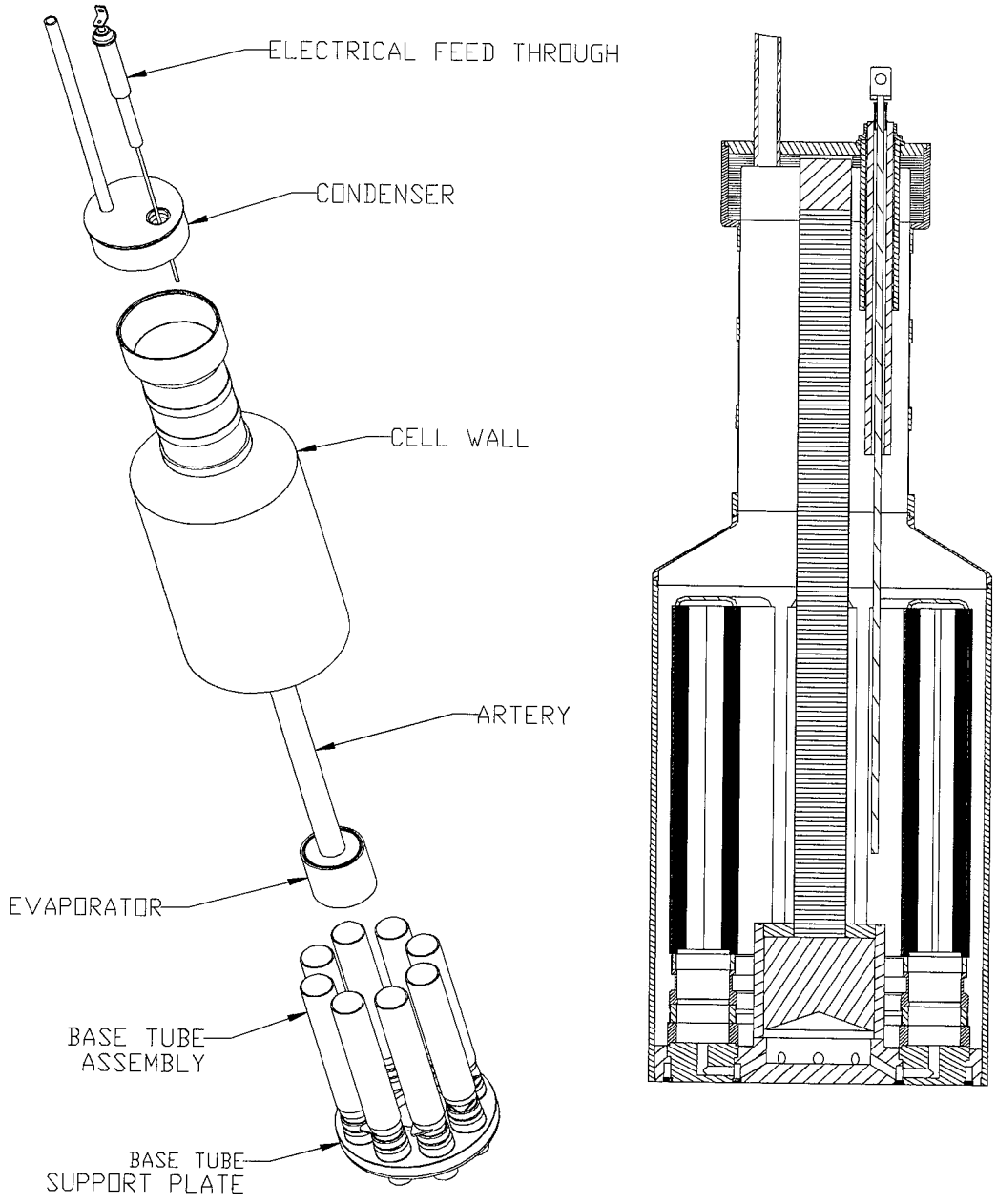

Figure 8-12 Engineering Converter Test Bed - Exploded View and Cross-Section

The primary issues that had to be addressed were:

1. Heat transport into the BASE tube – the longer tubes required that more heat be transported much farther up the BASE than any previous design,
2. Current collection from longer tubes – much higher currents required a more robust current collector design,
3. Sodium transport through the wick – sodium flow rates would be 8 times the flow rates in previous converter designs.

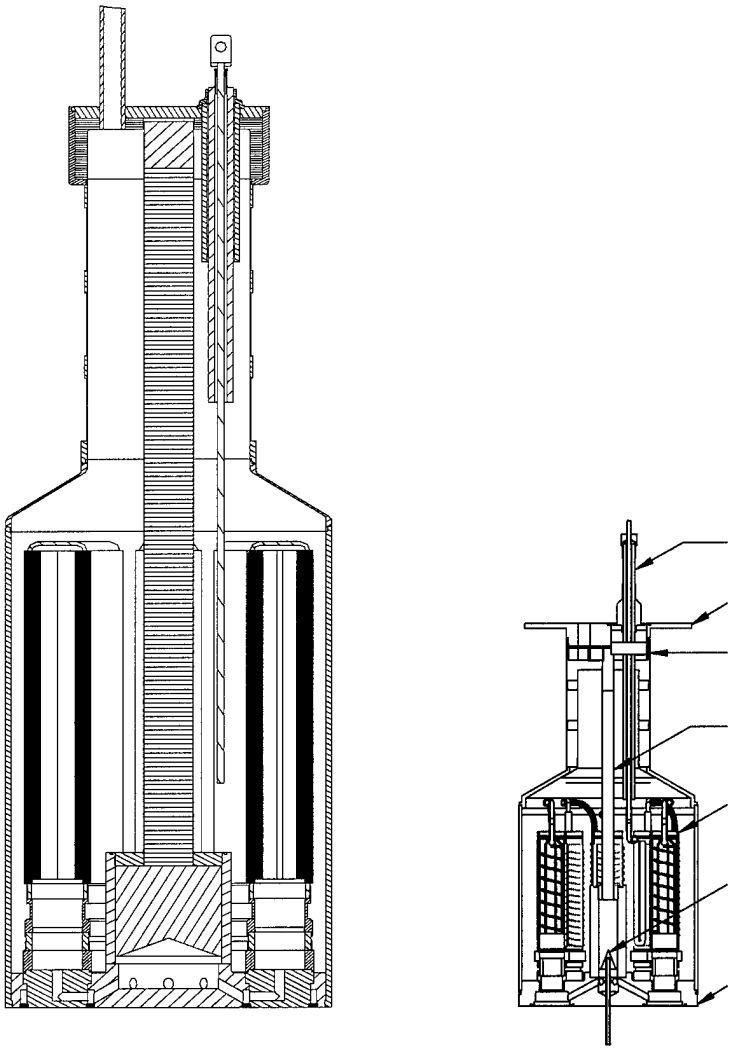

Figure 8-13 MAPPS Phase II Engineering Converter Compared to Previous Converter

8.4.1 Converter Design

The fundamental design configuration of this converter was much like the converters under development in other programs at AMPS. There were 8 BASE tubes connected in electrical series around a central artery-evaporator. The BASE tubes were much longer and larger in diameter, so heat transport from the hot to the cold end was enhanced with a sodium filled wick inside each BASE tube that would transport the heat entering the hot end to all points along the BASE tubes.

The stainless steel alloy 446 was evaluated in this converter. This alloy has higher thermal conductivity than standard 300 series SS and a lower thermal expansion coefficient. It also has better corrosion resistance.

A combined thermal, mass transport and electrochemical model was used to predict the performance of this converter. This model, described in detail in the literature,[1] has been used to predict the performance of a number of different converter designs. The physical model for the radiation heat transfer network is shown in Figure 8-14. The radiation network was used for input to the combined model. This model was used to predict the temperatures (Figure 8-15(a)), heat transfer (Figure 8-15(b)) and power output (Figure 8-16) of this converter for a hot and cold end temperature of 875°C and 350°C, respectively.

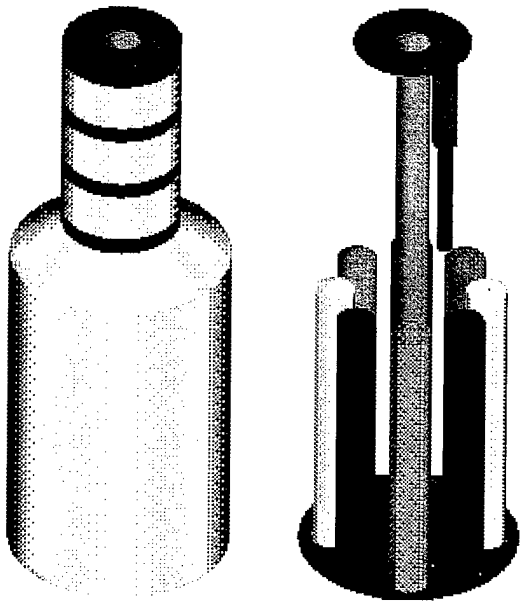

Figure 8-14 Outer Wall and Internal Component Map Used for Radiation Heat Transfer Network

[1] 'High-Performance Radial AMTEC Cell Design for Ultra-High-Power Solar AMTEC Systems', T.J. Hendricks and C. Huang, Journal of Solar Energy Engineering, V. 122, p 49-55, (May 2000).

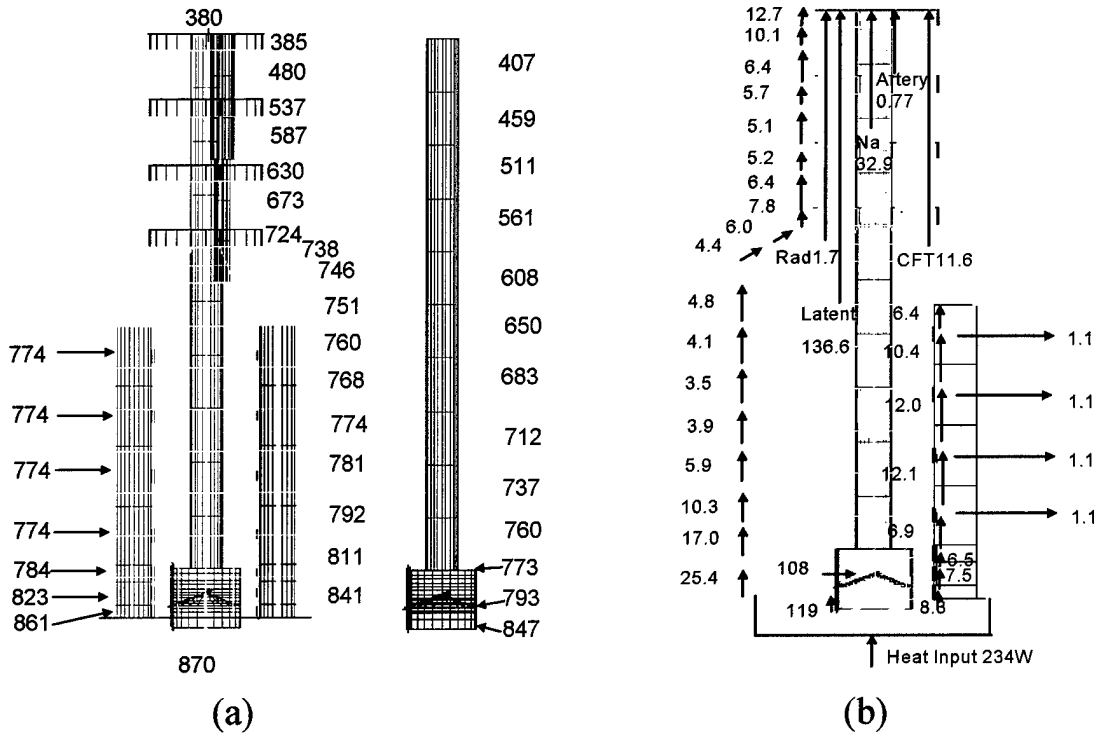

Figure 8-15 (a) Predicted Temperature Map and (b) Predicted Heat Flow Map for Engineering Converter

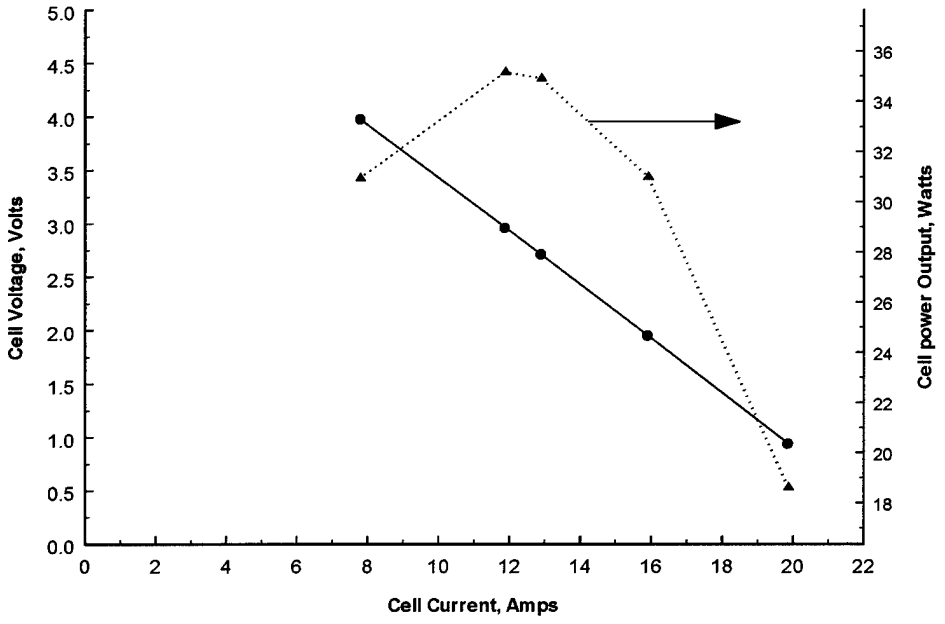

Figure 8-16 Predicted Performance of Engineering Converter at 875 deg C

8.4.2 BASE Tube Technology Development

The BASE tube, shown in Figure 8-17, represents the major breakthrough in the CC1 technology. The previous BASE tube design, shown in Figure 8-18, had 30 components and 4 brazing operations. This new design has 10 components and 2 brazing operations. This tube is substantially easier to fabricate with higher yields, more reliable, and much less expensive.

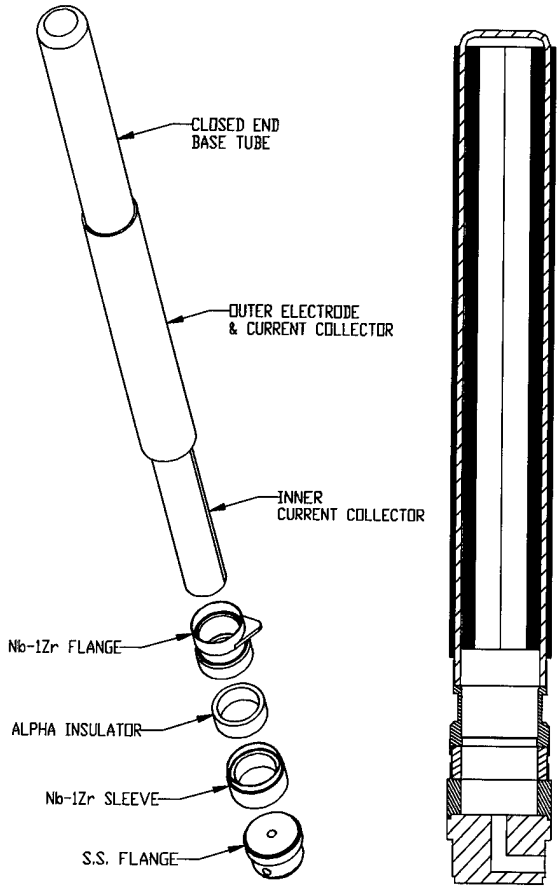

Figure 8-17 Large Diameter BASE Tube Exploded View and Cross-Section

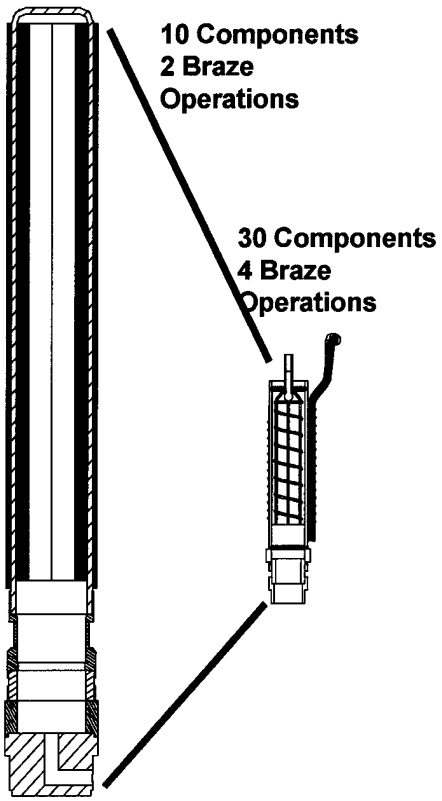

Figure 8-18 New Large Diameter BASE Tube Design Compared to Older Design

The development activity focused on:

1. Understanding how sodium fills the wick inside and makes electrical contact to the Nb-1Zr flange that provides the anode tab for electrical connection to the cathode bus on the adjacent BASE tube,
2. Sputtering of the TiN cathode on a larger BASE tube and an adequate current collection system and bus bar to minimize the cathode side electrical losses, and
3. Design and fabrication process that made the BASE tube easy to assemble, with reliable seals between the components.

The fabrication steps for the BASE tube are shown in Figure 8-19. The process steps are simple and each step lends itself well to further process improvements. For example, step 3 can be eliminated entirely by designing the joint to be self-sealing and mechanically locking. Recent tests have already demonstrated that this cab be done. Step 4 can be turned into a much larger scale batch process. These process improvements will be implemented at an appropriate point as manufacturing is scaled up.

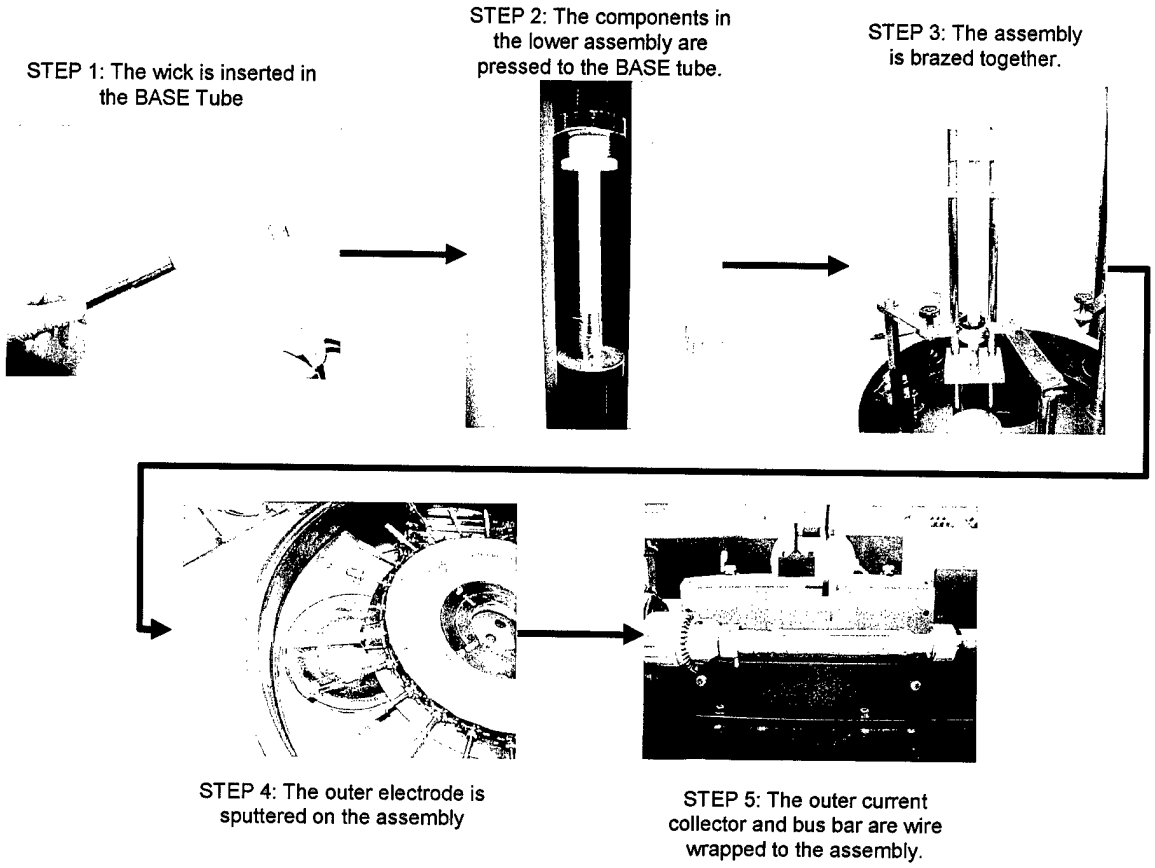

Figure 8-19 BASE Tube Assembly Steps

8.4.3 Wick System

The wick system for this converter was significantly larger in size than that in the previous converters. The overall arrangement and dimensions of the engineering cell artery/evaporator are shown in Figure 8-20. This led to some important investigations into wick scale up. Some new approaches were tried, some successful and some not so successful.

Before discussing the wick development efforts, it is important to understand the wick design. The wick pressure drop and pore size are very important to the ability of the system to move the desired amount of sodium from the condenser to the hot end. The pore sizes must always be small enough to generate a capillary pressure greater than the pressure difference between the saturated vapor pressure and the local liquid pressure. This limit ("the maximum pore size") is shown in Figure 8-21 for any axial location in the wick. (Figure 8-21 also shown the calculated local temperature of the wick.) Although the data is still limited because of the small number of converters for which we have made this performance prediction and then pushed the respective converter to the predicted (mostly on the molybdenum wicks in the space power converters), we expect that the wick will operate reliably, as long as the actual pore size is less than maximum pore size.

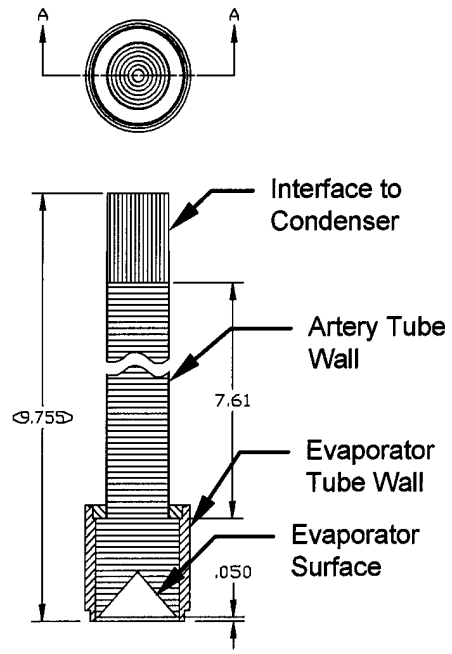

Figure 8-20 Overall Artery/Evaporator Arrangement & Dimensions

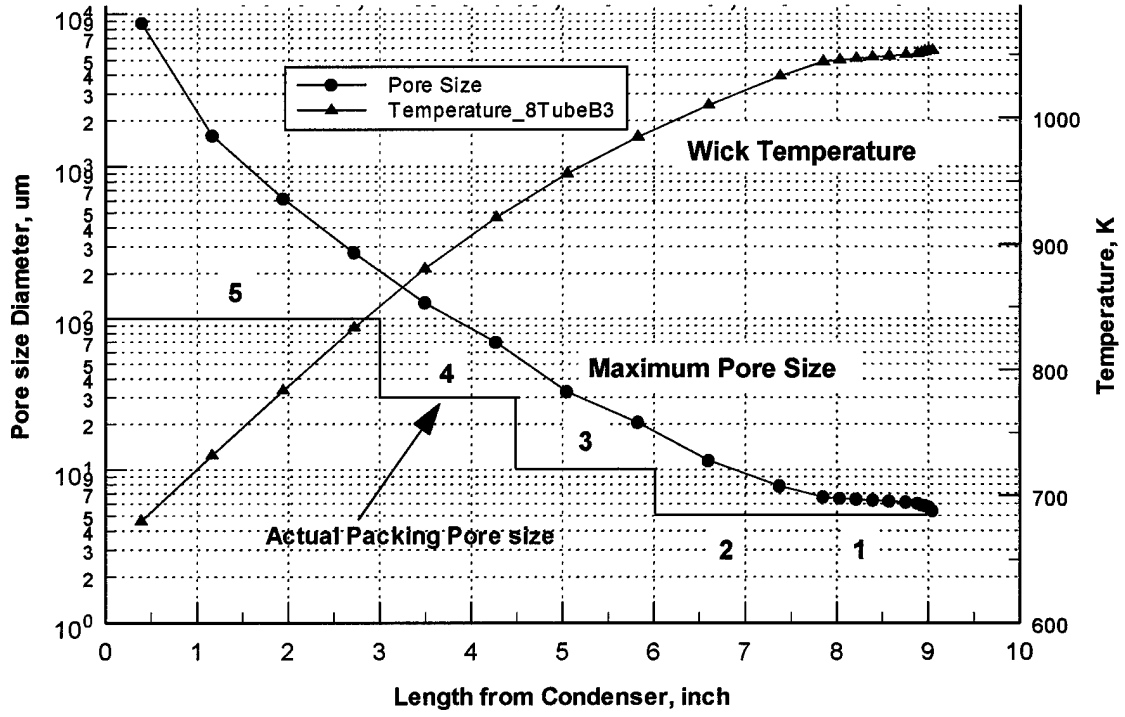

Figure 8-21 Calculated Engineering Cell Wick Conditions and Operating Limits

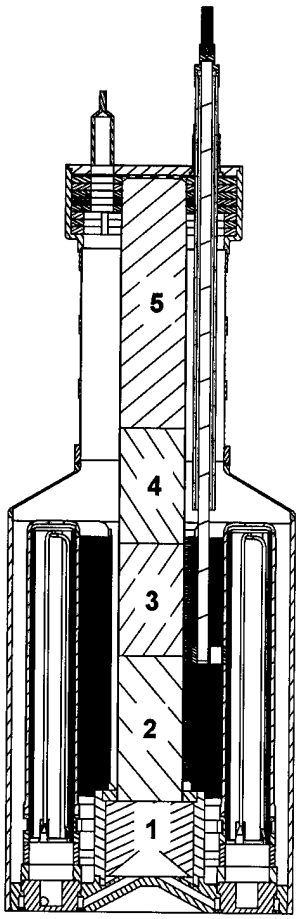

Figure 8-22 Engineering Converter Showing Wick Zones

In order to minimize the pressure drop the wick was designed to be fabricated in 5 zones, as shown in Figure 8-22. The actual pore size of these zones is shown in Figure 8-21. The zones in the low temperature region have large pores to minimize the pressure drop, while in the hot zone the pores are small to meet the capillary limit identified in the last paragraph. Figure 8-21 shows that this wick design can meet the target flow rates and temperatures.

Several new fabrication approaches were evaluated to produce the target pore size in this new, larger wick system.

1. Large disks for both the artery and evaporator were cut in a simple punching operation using felt material from a lower cost supplier (relative to our original supplier). The disks were later inserted a press to the target thickness and pore size.
2. The evaporator cone surface was machined after pressing and sintering. The machined surface was acid etched to remove the material smeared over the pores during machining.
3. The artery tube wall was initially machine slightly longer than the final length so as to be longer than the end of the wick at the interface to the condenser. The long tube (see Figure

8-20) was packed as disks to the design wick length, and then the thin tube wall was cut off to expose the wick for the interface to the condenser.

4. An evaporator sample was produced by Mott Metallurgy using their standard filter fabrication techniques.

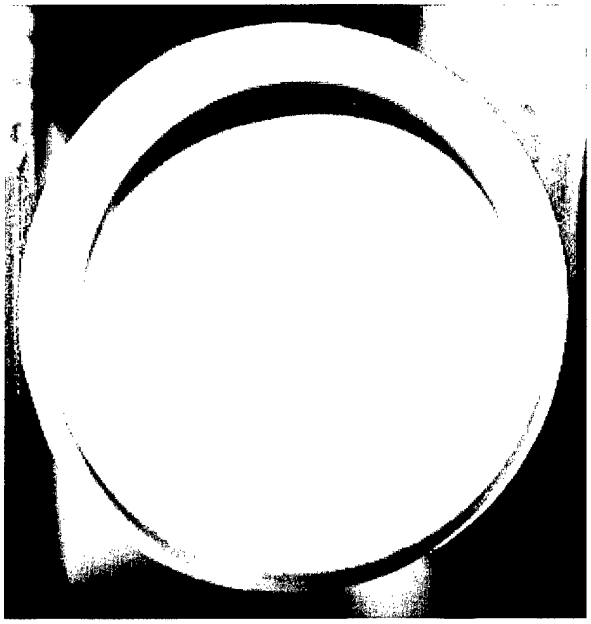

Figure 8-23 Engineering Cell Evaporator, Post Acid Etch

Initial evaluations led to the selection of all these new approaches except for #4. This latter step was not completed in time to be ready for the first engineering converter build, but should be considered as production volumes are increased at a later time.

Artery/Evaporator Assembly Process

The wick supporting components, as shown in Figure 8-20, were comprised of a short thick walled tube section for the evaporator wick and a long thin walled tube section for the artery wick. These sections had different diameters and were joined by welding each to a transition piece.

The welded assembly was placed in a wall support fixture while the wicking material is installed and pressed. The wick sections were made up of many stainless steel felt discs stacked up and compressed to a various forces to achieve the correct pore size as determined by the temperature of that section. A backing shaft was inserted from the artery end for the evaporator construction. A couple hundred felt discs at .010" thick were placed in this open end and compressed with 35k lbf. This produced pore sizes less than 5 μm in diameter. The cone was not formed at that time.

The assembly was then turned over and a backing shaft inserted from the evaporator end and hundreds of felt discs were placed in the artery tube and pressed. The felt discs closer to the evaporator were pressed with a higher force than the discs near the condenser. This assembly was sintered in a high temperature hydrogen atmosphere furnace. The next step was to machine the evaporator cone into the sintered wick material. To remove the smeared metal fibers, a warm acid solution was used to open up the pores in the machined evaporator surface. The finished evaporator cone is shown in Figure 8-23.

Pore size and flow rates were measured at several steps during the packing and assembly process. The actual pore size shown in Figure 8-21 was derived from some of this data.

To complete the artery, the top end of the tube was removed to reveal the felt disks inside. During the tube section removal process, it was observed that the felt disks were only lightly bonded together at the end, so a screw and retaining straps were installed, as shown in Figure 8-24.

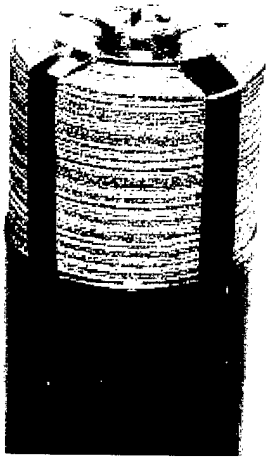

Figure 8-24 Artery Wick/Condenser Interface

8.4.4 Converter Fabrication

After BASE tubes and evaporators were fabricated, all the components were assembled into the converter. The BASE tube assemblies (BTA's) were inserted into the tube support plate, as shown in Figure 8-25. The cathode bus bars are aligned with the anode tab and the entire assembly is held in a fixture for welding.

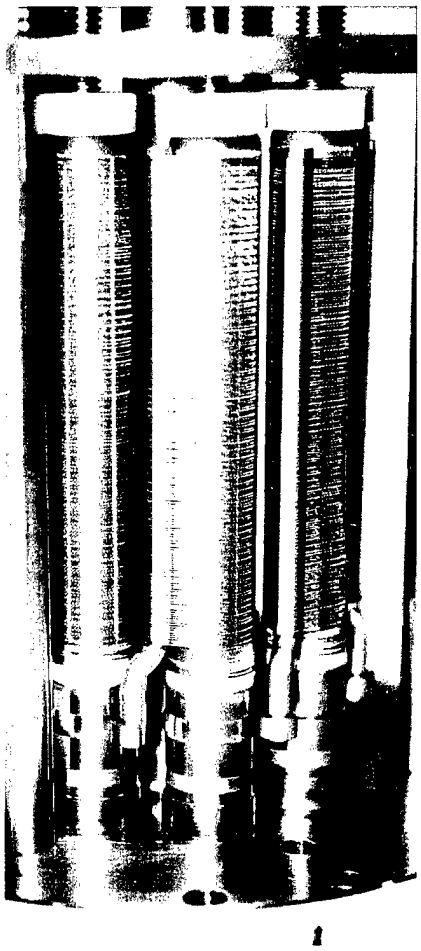

Figure 8-25 BASE Tube Bundle and Cathode-Anode Interconnect

A programmable electron beam welder was used to weld the BTA to the tube support plate and the cathode bus bar to the anode tab. During the welding of the SS446 BTA flanges to the SS316 tube support plate, cracks were found in the weld joint. These weld joints, shown in Figure 8-12, sealed the high pressure sodium inlet plenum from the low pressure region around the outside of the BASE tubes. Some leaking is allowable, but these leak were initially much greater than that. Several weld-patching operations were conducted, which reduced the leaks in all but one BTA flange weld joints to the point where they were acceptable. One BTA was completely removed, and a strap used to connect the anode and cathode from the tubes on either side of the removed BTA.

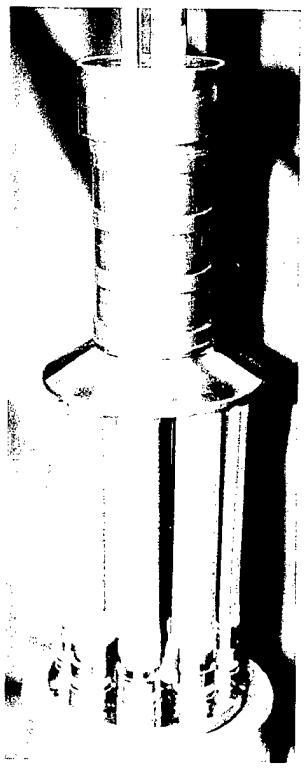

Figure 8-26 Engineering Converter Prior to Cell Wall Installation

Preliminary weld trials were conducted to evaluate the SS 446 to SS 316 welds prior to assembly of this hardware. Tube samples were TIG welded and were found to provide hermetic welds. It was expected that the actual welds would produce much the same results. The E-beam welder and the nested, non-tubular geometry, however, proved to be a significant departure from the TIG welded tubes. The physical constraints of the actual geometry and the very concentrated heating from the E-beam welder created stresses that led to the cracks. Although the weld joints, as designed, could be repaired in most cases, and with some additional development could possibly be perfected, it was recommended that future designs eliminate the SS 446 material.

It took a couple months to carefully understand the problem and institute the repairs, but after the BTA flange to tube support plate welds were repaired, the covers were ready to install. These were changed to SS 304 and were TIG welded into the assembly. These welds were successful.

Assembly then continued with the installation of the chimney, as shown in Figure 8-26. The last step was to install the converter wall and then complete the closure welds. The converter was baked out at 650°C under high vacuum for 2 days. Sodium was then loaded and the wicks were wet in at 400°C.

8.4.5 Experimental Results

The completed converter (see inset in Figure 8-27) was tested in the setup shown in Figure 8-27. The insert shows the converter location and orientation in the test facility. The control system on the right was used to set the heater power, monitor the temperatures and operate the power supplies to control the load (current) on the converter.

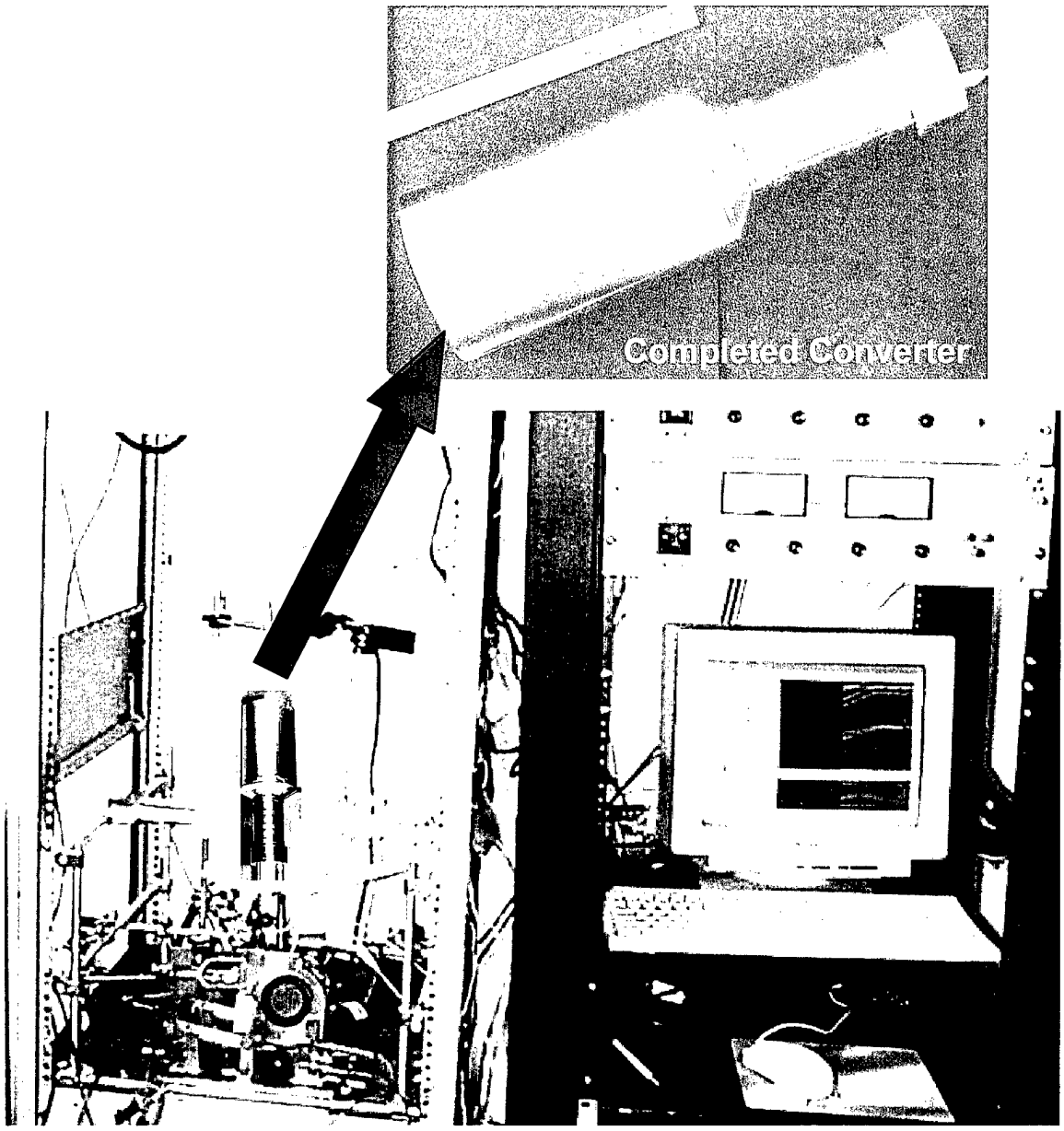

Figure 8-27 Engineering Converter Test Arrangement

Heaters were placed:

- On the hot end of the converter to simulate heat input,

- Around the portion of the converter containing the BASE tubes to simulate various levels of heat loss from the tube bundle in a real, flame heated environment,
- Around the chimney section of the converter to simulate various operating environments, and
- On the condenser to control the condenser temperature and investigate the effects of various heat rejection options.

This converter was tested for approximate 3 months over all possible thermal boundary conditions. Boundary conditions were varied over the following ranges.

- Hot End: 700 – 900°C
- Side Wall in BASE tube region: 600 – 850°C
- Condenser: 150 – 350°C

In general, the chimney section was allowed to float without direct heater control. This section was heated only for very specific investigations relating to the sensitivity of the BASE tube flooding.[2] Data was taken for the following.

- Converter voltage and power for any given current setting
- Temperature profile in the BASE tube

Voltage was measured at either a steady state point, where all the temperatures and the current were held constant, or during a "fast-sweep" of the current from zero current to the maximum current of the driving power supply and back to zero in about 10 seconds. These two approaches gave different results, with the fast sweep producing higher voltage for a given current. This was because the evaporator temperature was higher during the fast sweep since the current started at zero where no cooling sodium flow from the evaporator occurs. The sweep went too fast for the evaporator to reach a new thermal equilibrium with sodium cooling.

[2] Flooding refers to the conditions where the BASE tube wick is completely full and the liquid continues to collect in the BASE tube by filling up (flooding) the open vapor space at the end of the tube.

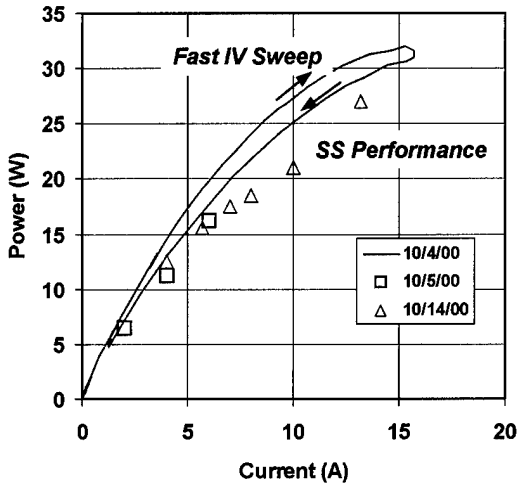

Figure 8-28 Typical Test Data for 800 - 876°C Hot End Temperature

Typical voltage and power data are shown in Figure 8-28. The steady state points are lower than the fast sweep data. The deviation is larger at higher currents because the difference in evaporator temperature is greater at the higher current. You can see from the fast sweep, however, that the power on the sweep back to zero current is lower, due to the cooling effects of current on the evaporator.

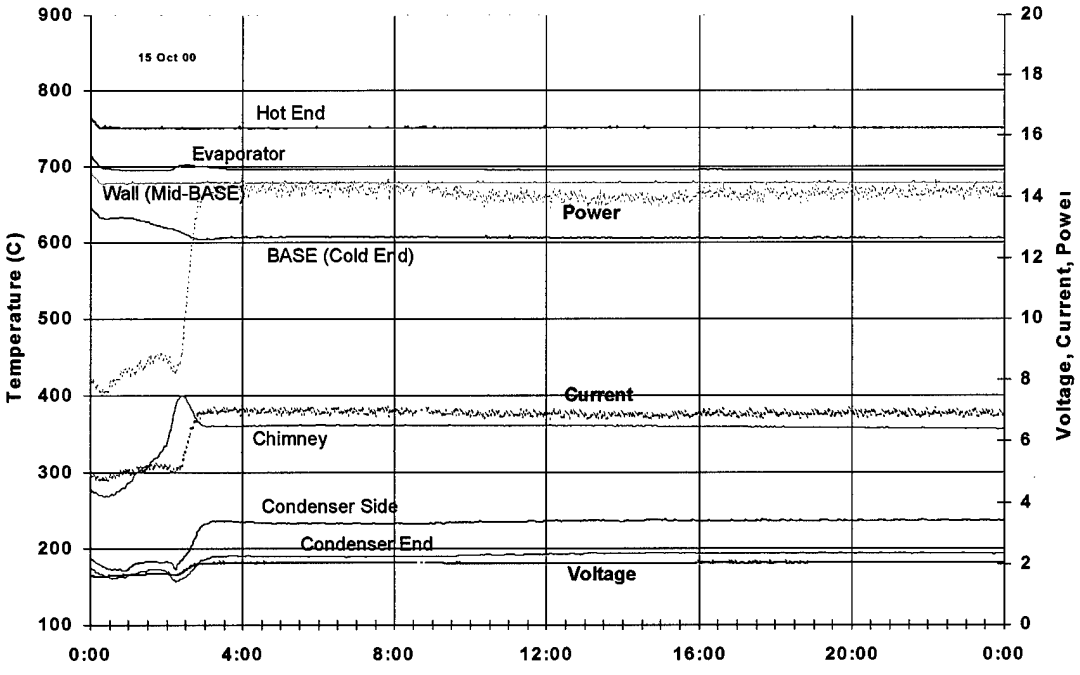

Figure 8-29 Converter Power and Temperature History Representing Stable Operation

The steady state points were data taken with the cell at a fixed load. Thermal equilibrium was generally reached in 5 – 10 minutes after a specific load was established. In cases where the converter was under 800°C, these steady state points were very stable. Data points from 10/5 in Figure 8-28 represent such data, as well as the history shown in Figure 8-29, where the converter operated for over 20 hours on a fixed load at a constant temperature. (The power and current in this figure were "noisy" because the millivolt signal used for the current measurement was picking up variations in ground loop leakage current from the ac heaters in the converter.) The steady state points above 800°C and high current (above 10 A) were not completely stable. The power and temperature history shown in Figure 8-30 illustrate the unstable operation. Starting from a low temperature where sodium had been allowed to accumulate in the BASE tube, the converter demonstrated excellent performance characteristics. The steady state data points in Figure 8-28 were recorded at a different time than the data in Figure 8-30, but also demonstrated the same high level of power out. Unfortunately the power could not be sustained and eventually dropped off to very poor performance. The power at time 20:40 in Figure 8-30 illustrates the start of this power drop.

The conditions that led to this unstable operation were duplicated many times. It was very repeatable. After carefully examining all the data, it was suspected that the artery-evaporator system could not supply sodium at an adequate rate to keep up with the sodium flow rate through the BASE tubes at the higher temperatures and current flow rates. Hydraulic testing and modeling, described in a previous section, did not indicate that these conditions should reach the limits of the wick system. This modeling has been found to be reliable in other converter designs, so it was difficult to suspect the wick when the models predicted adequate performance. However, the extensive examination of the data indicates that for any given thermal conditions, the power in the BASE tubes is very good, leaving only the wick system left as the source of the unstable performance. It would be left to the post-test examination to confirm or deny our suspicions about the wick system.

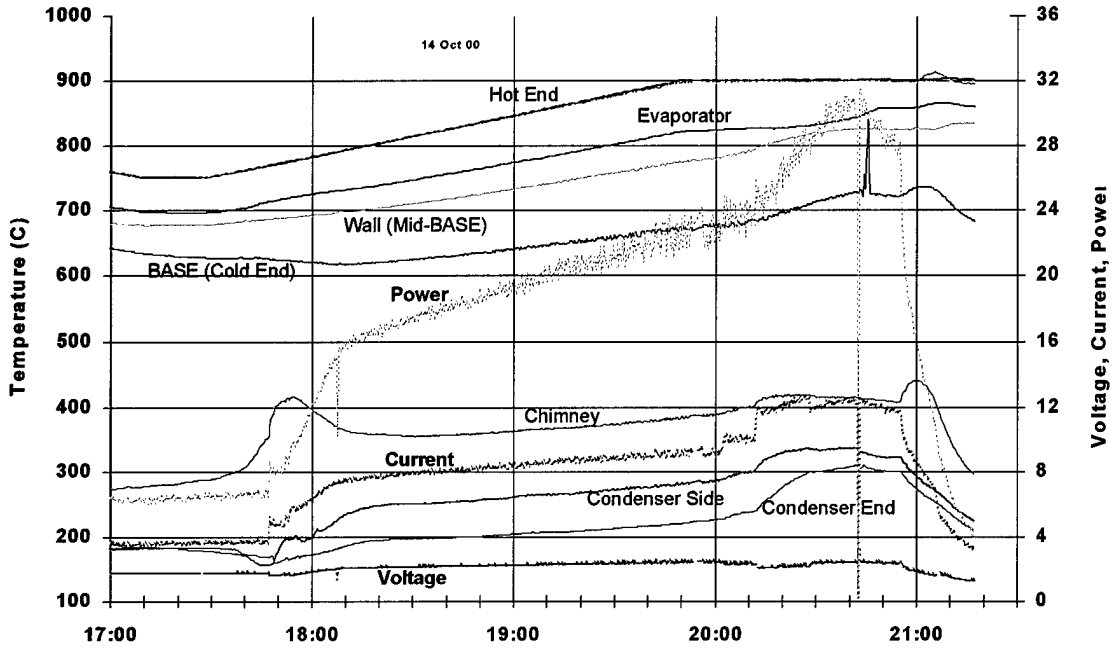

Figure 8-30 Converter Power and Temperature Showing Unstable Operation

8.4.6 Post Test Analysis

The converter was removed from the test station and disassembled to examine the state of the internal components. A view of the converter with the wall removed is shown in Figure 8-31. Sodium metal is coating the feedthrough wire and insulator as well as the artery. This typically occurs during shutdown when there is still sodium going through the BASE from the inside wick, but the temperature is too low to quickly move that sodium to the condenser. It coats the components on the hot end, just as it has done in this photograph. No anomalies were found at this stage of the examination. The current collectors, electrodes and inter-connections all looked in good condition.

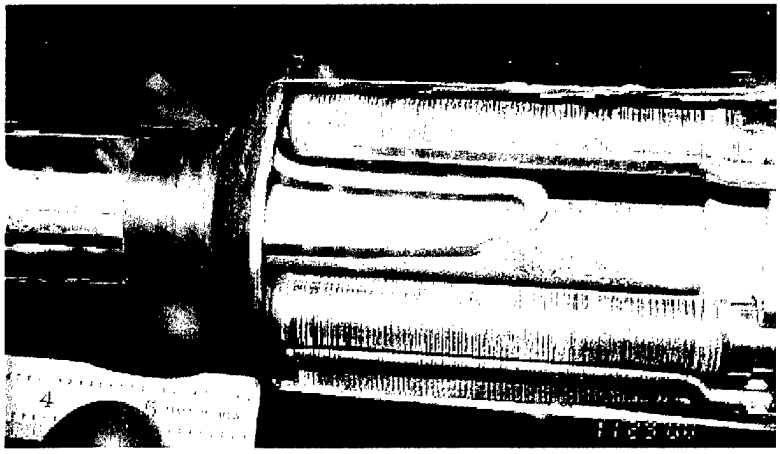

Figure 8-31 Post-Test Examination of the Converter - Converter Wall Removed

The condenser, shown in Figure 8-32, was removed and examined. It contained approximately 10 grams of sodium, but was not flooding the condenser area, as can be seen from this figure. The connection between the condenser reservoir and the artery, shown in Figure 8-32 as the hole in the center, appeared to be well wetted.

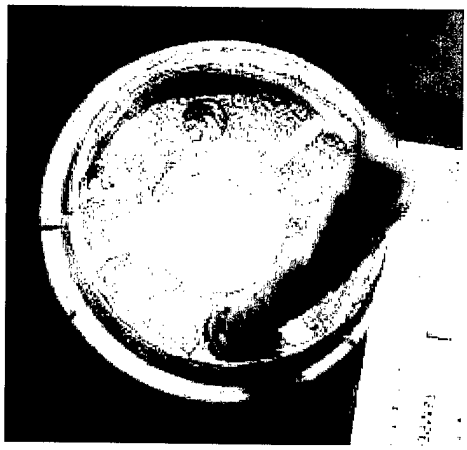

Figure 8-32 Condenser Wick as Viewed From Inside Converter

The evaporator, shown in Figure 8-33 looking into the evaporator from the high pressure BASE tube plenum, was a surprise. It was discolored with what looked like black oxidation products. A close examination of the surface revealed numerous "chunks" hanging from the surface as though something had been "flushed" into the area that is normally the sodium vapor space. Nothing of this nature has ever been observed.

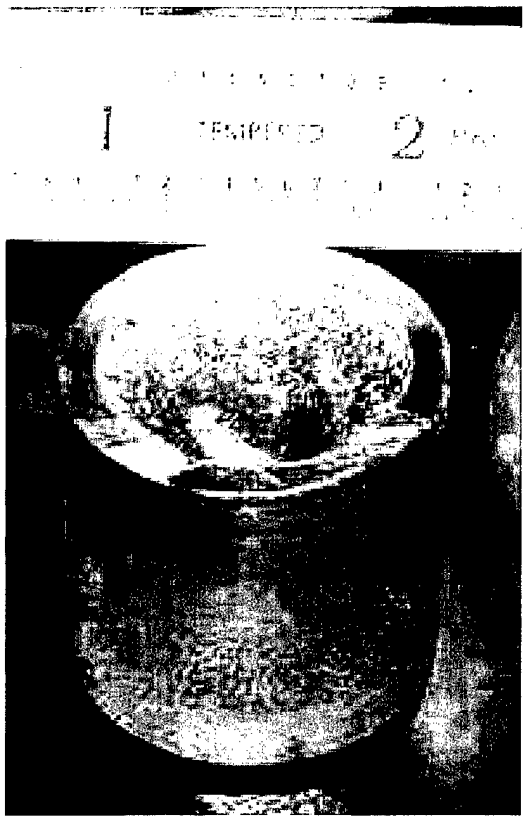

Figure 8-33 Post-Test Evaporator Surface

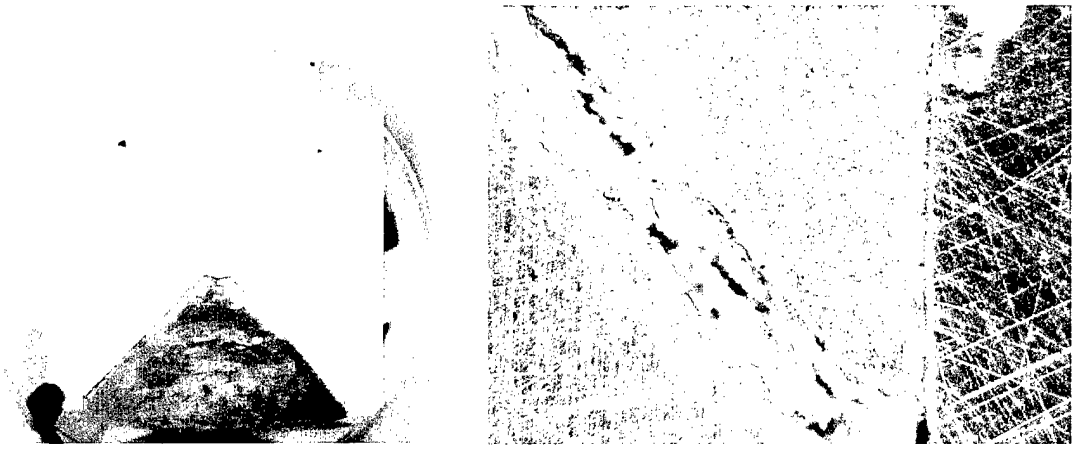

Figure 8-34 (a) Post-Test Evaporator Cross-Section and (b) Evaporator Cone-End

The evaporator was cross-sectioned, as shown in Figure 8-34. This section did not reveal any anomalies within the wick structure, but on the free evaporator surface and on the leading edge, shown in Figure 8-34 (b), there were two observable features that caused some concern. The first was the material on the surface. This material, which appeared to be black in Figure 8-32, was found to be surface oxidized copper as shown in Figure 8-35. SEM-EDS (Scanning Electron Microscope-Energy Dispersive Spectrometer) analysis confirmed the presence of copper, though the pore openings on the surface of the wick did not appear to be completely

closed off. The globs sit away from the wick surface leaving open areas around it for sodium vapor to escape. Analysis of the inner structure of the evaporator wick indicated no presence of copper. The supplier of the wick material claimed that no copper is present in the wick. It is unclear where the copper came from. It is possible that it was carried by vapor transport from the feedthrough lead in the hot zone to the condenser and then through the artery and deposited on the evaporator surface. The extent of the copper is more than has ever been observed on wick surfaces, and some converters with significantly more copper than this converter have been run for much longer times.

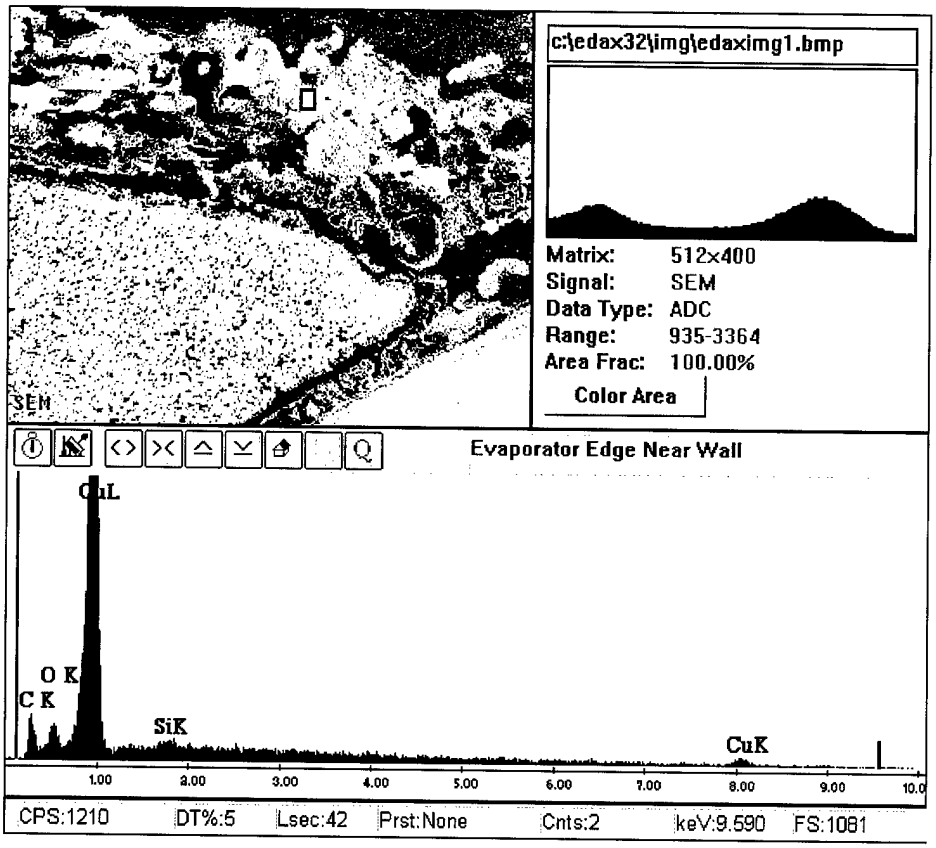

Figure 8-35 SEM Data on Material at Evaporator Surface

The second observation, clearly visible in Figure 8-34 (b), was the separation of the end of the wick cone from the vapor flow tube wall. It is the vapor flow tube that carries the heat from the hot end of the converter into the wick. It is very likely that this gap did not have sodium at the higher temperatures, possibly even the lower temperatures, and this could have caused some anomalous behavior, like a reduced power level capability, but it is unclear how it could have caused what appears to be a wick hydrodynamic limit, unless the gap was actually changing as temperature and flow conditions changed. And even if the gap was filled at lower temperatures, acting as expected, and then not filled with sodium at the higher temperatures, so that the heat had to travel a longer path to get to the evaporation surface, the phenomenon which resulted in starving the hot end of sodium is not understood. On thing is certain, however, is that this gap indicates that the sintering process, which normally bonds the wick to the vapor flow tube, was not successful.

While more investigation may reveal the specific phenomenon and ultimate cause of the observed converter performance, this post-test examination reveals this wick is not up to the standards of wicks used in other converters. The design and fabrication process needs to be addressed before the next converter is fabricated.

8.4.7 Recommendations

The evaporator design and fabrication process was a significant departure from previous converter designs. For example,

- The evaporator was pressed from flat disks with a flat surface on the pressing pin,
- The evaporator cone was then machined into the end of the evaporator,
- The entire wick was flushed with acid to etch and open the machined surfaces, and
- It appears that the sintering process, which was having repeatability problems at the time this converter was fabricated, was not adequate.

This program was taken as an opportunity to investigate other manufacturing options that might lead to lower cost wick systems. In retrospect, those approaches did not really lead to significant labor or material reductions. In addition, new uncertainties were introduced with the acid etching, especially in the dilution and removal of the acid from the wick after etching. Based on uncertainties about this new manufacturing process, it is recommended that the basic fabrication process used on previous converters be applied to this converter. Instead of the stack of felt discs, a strip of felt can rolled up to a diameter just smaller than the inner diameter of the evaporator tube section. It can then be inserted and pressed with a coned pushing tool, shown in Figure 8-36, to form the correct shape of the evaporator felt. Assembly trials have been successful and the correct permeability and pore size of the pressed assembly have be achieved. This is much more in line with the fabrication processes in the earlier converters, and is therefore expected to be more reliable than the design used in this first test.

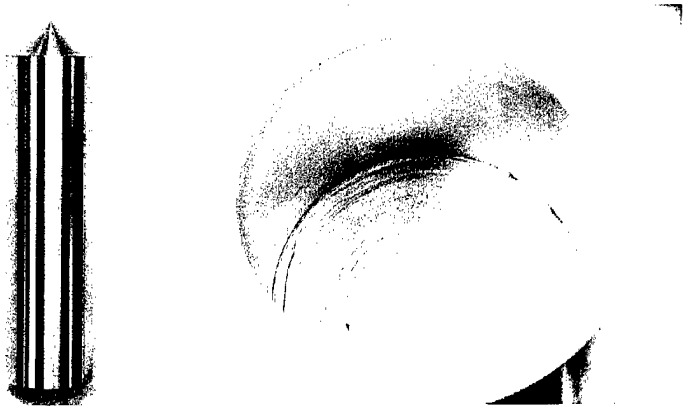

Figure 8-36 Coned Pushing Tool and Resulting Evaporator Felt Cone

The sintering process issues that prevented consistent sintering results has been addressed and sintered arteries now come out of the process well sintered and a bright metallic color. With this corrected and with the use of the coned pressing tool to eliminate the machining and etching

steps, this new (old) design needs to be taken through a number of fabrication trials on this size evaporator to verify that

- The cone ends are sintering to the vapor flow tube, and
- The wick has an acceptable permeability and pore size.

Once these have been verified, and a new artery-evaporator system is ready, a new converter should be fabricated and put on test to validate converter performance.

8.5 Advanced Seals

Two advanced BASE tube designs were evaluated at AMPS during the course of this program. Both designs were driven by the goal to reduce the cost of the BASE tube assembly. AMPS worked closely with Ionotec Limited to develop these designs.

1. The first design, shown in Figure 8-37, had an alumina insulator integrated on to the open end of the BASE tube. This alumina insulator would be tapered and serve as the mounting interface to the tube support plate. An anode lead was integrated into the closed end. This would provide the anode connection to the adjacent BASE tube cathode. Ionotec supplied the completed assembly shown in Figure 8-37.
2. The second design, shown in Figure 8-38 and 8-39, was based on the CC1 design concept. This concept had an Nb-1Zr mounting flange on the open end. An alumina insulator provided a mechanical bridge between the BASE and the metal mounting flange. An Nb-1Zr strip integrated into the joint also provides the anode lead to connect the anode outside of the BASE tube to the cathode on the inside of the adjacent BASE tube. (Note that this design has been configured with the anode-cathode layout opposite of the standard BASE tube.)

Both of these designs required interfaces to the BASE tube be integrated into the fabrication process at Ionotec, providing AMPS with a complete BASE tube assembly.

AMPS and Ionotec worked together to develop this low cost approach to BASE tube assembly seals based on calcium aluminate glass/ceramics. Calcium aluminate based glass/ceramics have used for many years to join alpha-alumina tubes to Nb-1Zr electrodes in sodium vapor lamps. These seals show excellent resistance to sodium attack and exhibit long lives. Because of this, these glasses have been considered for use as a means for sealing beta"-alumina to Nb-1Zr for AMTEC applications. The initial obstacle to using this glass has been the occurrence of ion exchange between the glass and beta"-alumina during the high temperature sealing operations. Calcium diffuses from the glass into the beta"-alumina replacing sodium which migrates into the glass. The presence of minor amounts of calcium in the beta"-alumina reduces the sodium ion conductivity.

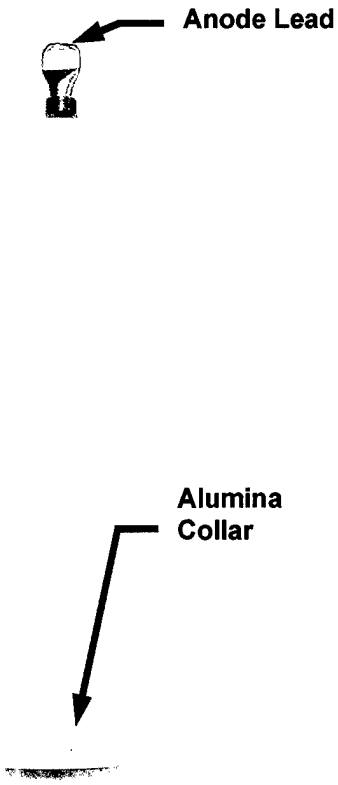

Figure 8-37 Advanced BASE Tube Assembly With Closed End Anode Lead

To eliminate the ion exchange reaction, Ionotec developed a process for applying a very thin layer of zirconia to the surfaces of the beta"-alumina which may be contacted by glass during sealing. The results of this effort have been very positive thus far. Nb-1Zr tubes have been sealed into the closed ends of tubes with alpha-alumina collars glassed to the other end. An example is shown in Figure 8-37. As produced, these seals have leak rates less than 10^{-9} std atm cc/sec. After ten thermal cycles between room temperature and 900°C, no change in leak rate is observed. Further, EDS analysis shows that the zirconia layer is effective in preventing any ion exchange between the glass and the beta"-alumina. Half a dozen BASE tube assemblies have been fabricated at Ionotec with Nb-1Zr tubes sealed into the closed end and a tapered alpha-alumina collar sealed to the open end.

The anode end of the BASE tube shown in Figure 8-37, has been tested in sodium exposure capsules to provide an initial assessment. Capsule testing is the easiest way to provide an initial evaluation, but it is also one of the most severe tests. The test results were promising and it is recommended that additional testing be performed in working cell with high and low pressure sodium chambers.

One completed CC1 assembly, shown in Figure 8-38, has been received at AMPS. This is currently in storage until such time as more testing can be funded. Some preliminary

evaluations have been performed to assess the fabrication process. The cathode on the inside of the BASE tube was of particular interest.

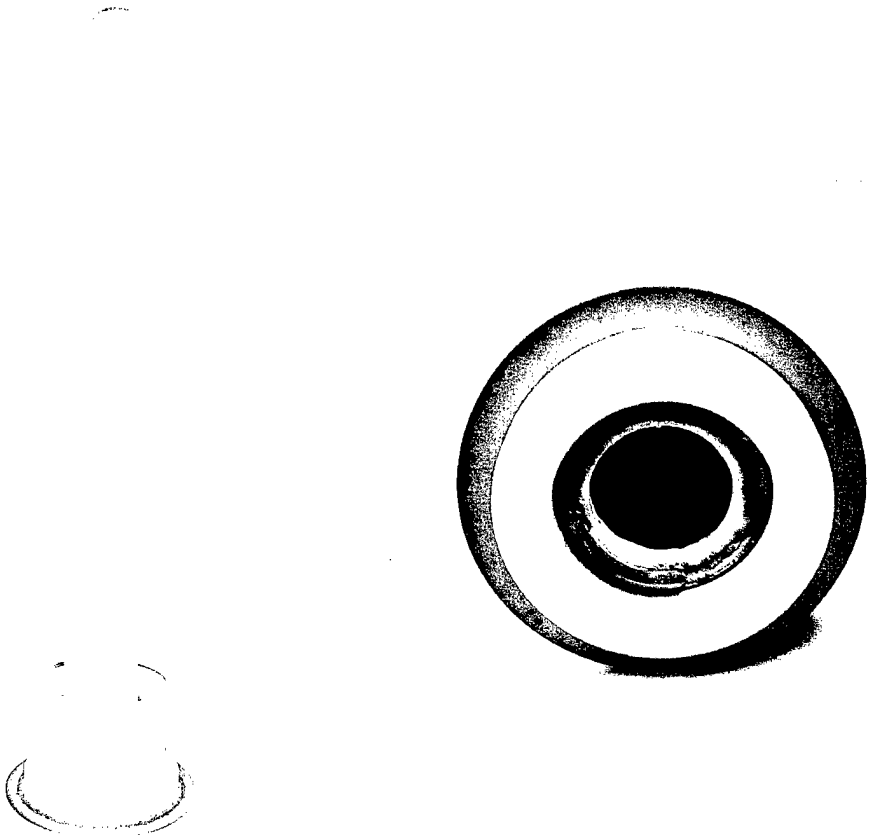

Figure 8-38 Glazed CC1 BASE Tube Assembly With Ceramic Header

Since this BASE tube has the cathode on the inside, a high quality electrode is needed on the inside of the BASE. There is only one possible electrode to use at this time, and that is the Weber electrode currently used at AMPS as an anode inside of vapor-anode converters in other programs. The Nb-1Zr mounting collar on this BASE tube assembly is not compatible with the Weber electrode fabrication process, so the electrode needs to be put on the BASE tube first. AMPS provided several BASE tube pieces, as well as a complete BASE tube, to Ionotec. The pieces were placed in the furnace and exposed to the same process as the BASE tube. The Weber electrodes on these pieces were examined after the processing and were found to adhere poorly to the BASE surface. It is unlikely that these electrodes, after processing to add the BASE tube mounting hardware, would make very good cathodes. More work would be necessary to make these electrodes suitable for this design.

8.5.1 Recommendations for Future Work

Development of low cost, reliable, long-lived seals remains a critical issue in the development of AMTEC for most applications. The work completed thus far is encouraging but additional development and testing is required to fully demonstrate the feasibility of the glass seal concepts described above. At present, two critical questions need to be addressed:

1) Has the ionic conductivity of the beta"-alumina been impaired as a result of the sealing process, and

2) Would the slight degradation of the beta"-alumina under the zirconia coating and seal occur when the assembly is subjected to more realistic AMTEC temperatures and sodium vapor pressure gradient conditions?

The ionic conductivity of the ceramic is of concern since the entire BASE tube assembly is heated to the glass sealing temperature during glazing. The melting temperature of the glass is over 1200°C, and because of the presence of the Nb-1Zr, sealing must be done at reduced oxygen partial pressures. These conditions may cause a loss of soda from the surface of the beta"-alumina resulting in lower ionic conductivity. The second question relates to the conditions to which the assembly is subjected during the capsule test which are far more severe those experienced in normal AMTEC operation. The degradation of the beta"-alumina ceramic, even though slight, has not been observed in electrolytes which have been removed from AMTEC cells, even after having been operated at normal AMTEC temperatures for thousands of hours.

To effectively answer these questions, AMPS recommends that BASE tube assemblies be tested in power producing AMTEC cells in which realistic operating temperature and sodium vapor pressure conditions can be established. The simplest and most expedient test which can be performed is in a cell known as a mini-electrode test cell (METC), in which a single BASE tube assembly is fabricated into a non-circulating cell. Testing in an METC will give an immediate answer to the question of potential degradation of ionic conductivity of the beta"-alumina during sealing. These cells have the ability be held at operating temperature conditions under open circuit conditions for two weeks or more. Such a long term test will provide additional data regarding degradation of the beta"-alumina adjacent to the seal of the seal materials themselves. Obviously, such short term tests won't be capable of providing significant life data, but can give a positive indication that additional testing in circulating sodium cells which can be tested for much longer periods of time is warranted.

9 Improved System Concepts

9.1 System Configuration

A limited amount of system design and analysis has been performed during 1999-2000, given the program focus on the evaluation of two alternative improved AMTEC design and fabrication approaches. However, some initial analysis was performed on the following topics:

- Combustor aerodynamics.
- Cell hot-side heat transfer.
- Recuperator heat transfer.
- Spoked condenser heat transfer.
- Impingement condenser heat transfer
- Preliminary weight estimates.
- Preliminary cost estimates

The two cell configurations being evaluated are designed to fit within the same overall system design. The overall system concept is illustrated schematically in Figure 9-1 and the two cell configurations are compared in Figure 9-2.

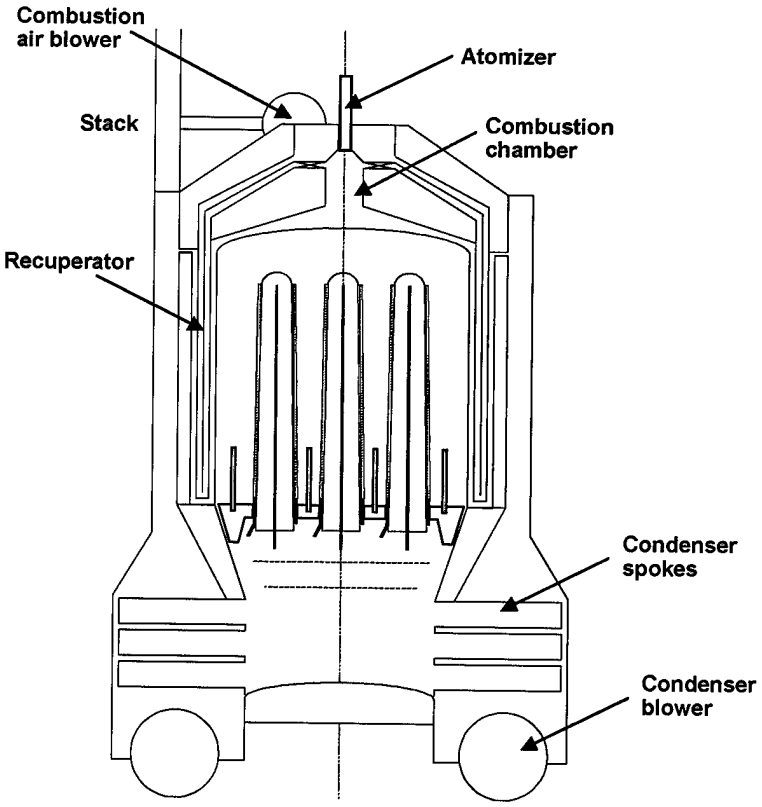

Figure 9-1 General Arrangement of 500 W Power System

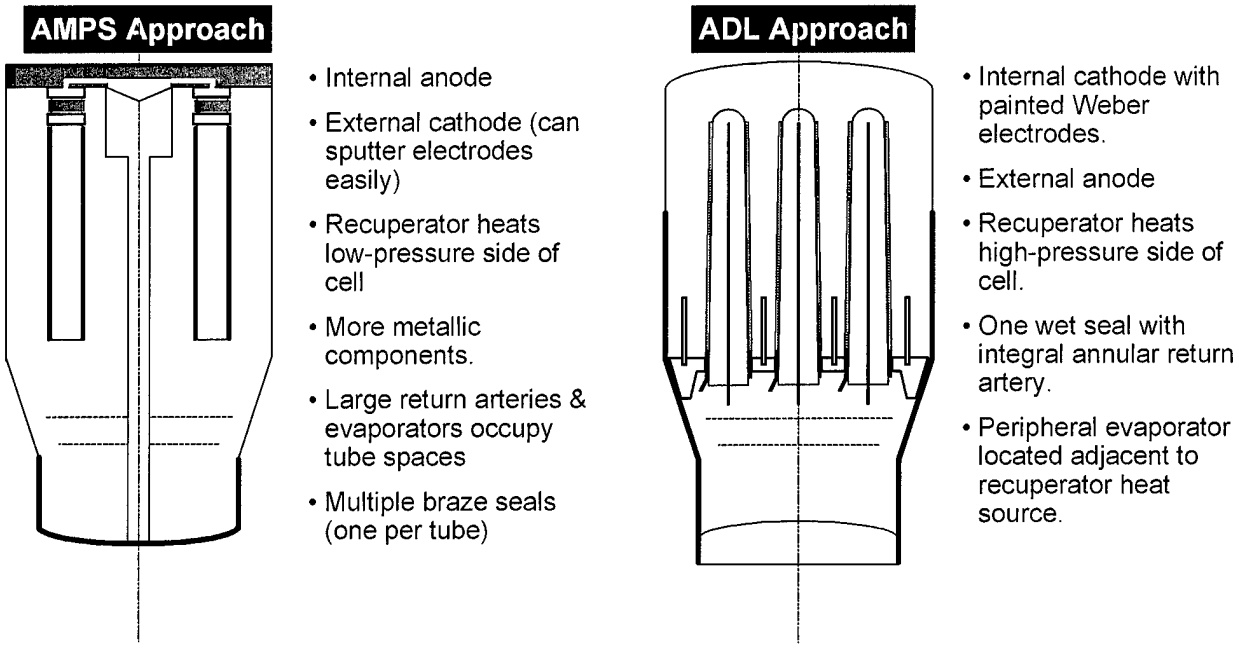

Figure 9-2 Comparison of Cell Configurations Being Evaluated

Each cell configuration has attractive features, which have not yet been fully evaluated. The activities planned for the remainder of this phase will allow a determination of a preferred architecture for terrestrial applications.

9.2 Combustion and Recuperation

Computational fluid dynamics models were developed for both the combustion chamber and recuperator. Sample results are shown in Figure 9-3.

The computational fluid dynamics models indicated that efficient combustion and recuperation systems are feasible for this system configuration. Of particular note is the increased geometric and structural compatibility between the combustion chamber and AMTEC cell hot side configurations. The volume of this combustion system is more consistent with the level of required heat release, and the temperature/heat flux requirements are less stringent than for the previous MAPPS design. Additional heat transfer area is also provided by locating the recuperator around the AMTEC tube bundle. The nested can recuperator configuration is less susceptible to thermally induced stresses, and more surface area is available than in the previous MAPPS design. Modeling also indicated that the heat transfer requirements of the condensing system may be met with several rows of spoked tubes. The design challenge will be in keeping the internal flow passages large for minimal pressure drop in the sodium vapor flow.

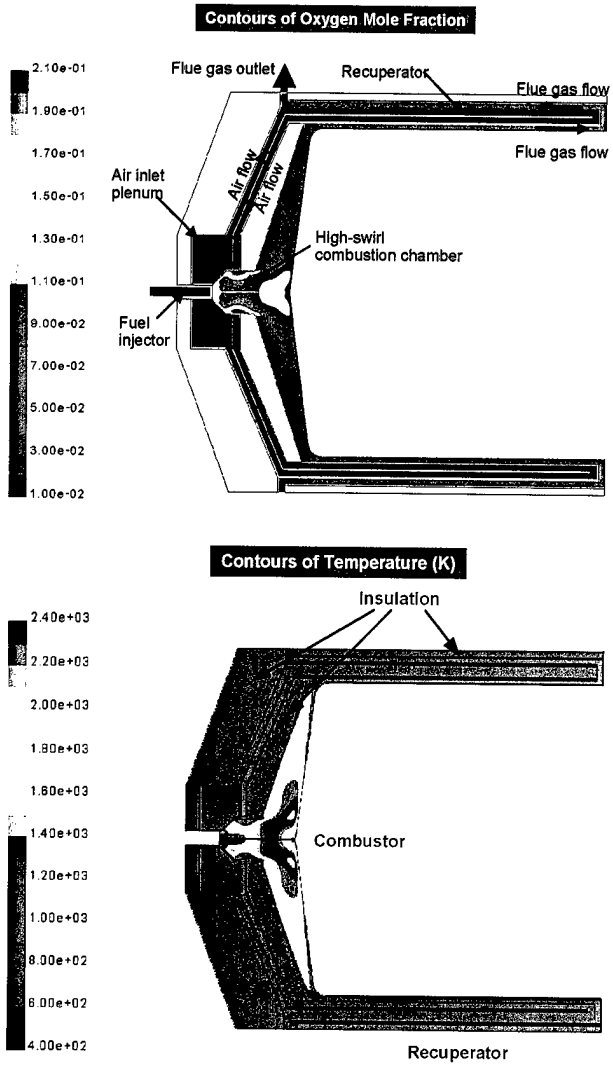

Figure 9-3 Results of Combustor/Recuperator CFD Analyses

9.3 Weight Estimates

Initial weight estimates for the new system concept indicated several areas in need of improvement (see Figure 9-4 and Table 9-1). The original design had a fully jacketed enclosure, a multi-pass recuperator and a high surface area condenser design.

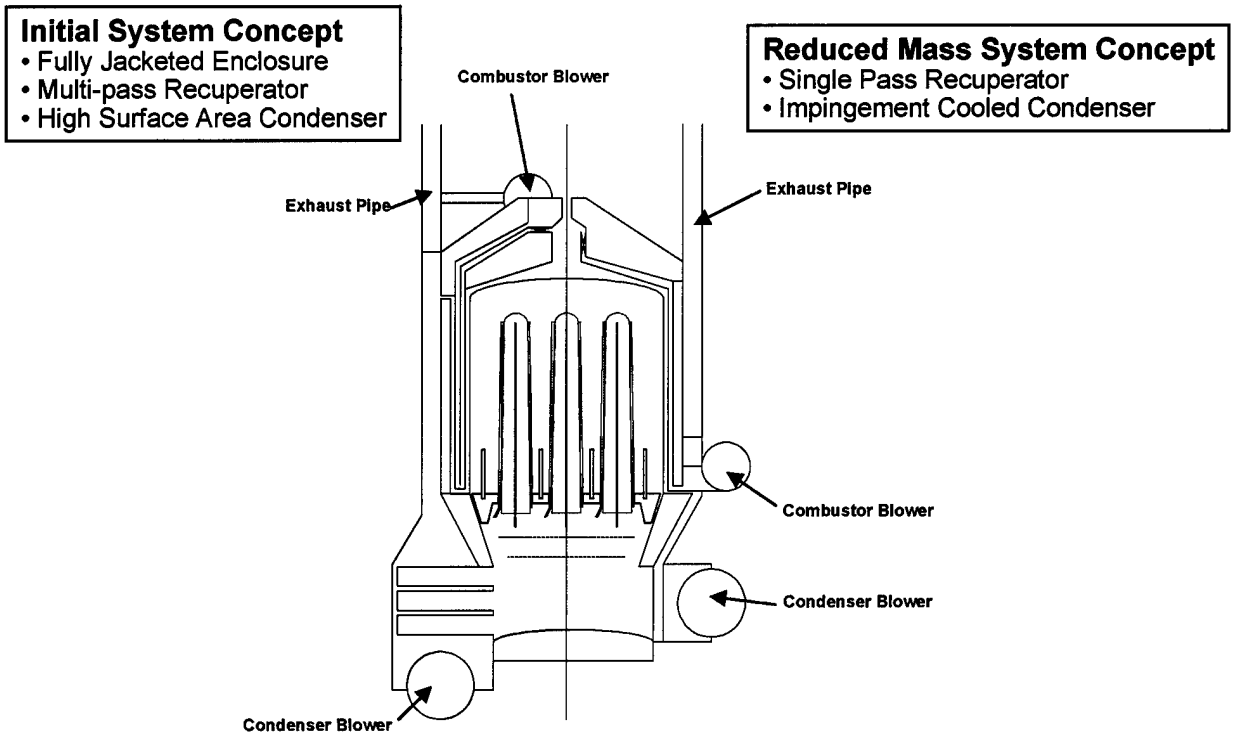

Figure 9-4 Original and Reduced Weight Concepts for System Arrangement

In a revised design, a single-pass recuperator is used and a higher-pressure drop, lower surface area, impingement cooled condenser design is employed. The estimated system weight can thus be reduced by ~40% at the expense of additional condenser air-side pressure drop (i.e. increased parasitic power). Further refinement of these and other estimates awaits the results of the 3D system modeling work. The impact of the difference in condenser design on various system parameters is shown in Table 9-2. The very significant weight reduction (from 1100 to 100 grams) obtained by moving to the impingement design comes at the price of a need for higher parasitic power (32 W versus 6 W) to provide the higher static pressure required by the impingement cooler.

A more detailed analysis of the system implications of the evolving AMTEC converter designs is required as the work progresses. Three-dimensional SINDA models of the cell designs will provide important input to this analyses. Only one-dimensional analyses have been available to date. In addition, the sizes and configurations of the monolithic and advanced tubular converters have only recently become available. A volume and weight tradeoff analysis is also required, as is a tradeoff analysis between surface area and pressure drop (parasitic power) for both the recuperator and the condenser systems.

Table 9-1 Weight Estimates for a 500 W System

Weight Summary	Initial System Concept		Reduced Mass Concept	
Component	Mass (g)	(%)	Mass (g)	(%)
AMTEC Module	11,170	50.6	8,049	60.5
Combustor Assembly	1,489	6.7	505	3.8
Recuperator Assembly	4,208	19.1	1,750	13.2
Housing Assembly	3,604	16.3	1,395	10.5
Support Components	1,600	7.2	1,600	12.0
Total	22,071	100.0	13,298	100.0

Table 9-2 Impact of Condenser Design on AMTEC Module Weight

	Spoked Design	Impingement
Pressure Drop ("H_2O)	0.2	1.6
Flow Rate (scfm)	45	32
Fan Power (W_e)	6	32
Weight* (grams)	1100	100

* Weight associated with AMTEC module.

9.4 Cost Estimates

A detailed estimate of material costs for a 500 W AMTEC power supply was prepared. The component details are provided in Table 9-3. Estimates were made for an AMTEC design of the ADL design, together with all system components (combustor, recuperator, condenser, blowers, fuel pump, exhaust system, housings, batteries, insulation, valves, hoses and valves).

Direct manufacturing cost estimates were extrapolated from the materials cost, based on ADL experience developed in performing detailed cost estimates of complex engineered products. In production volumes of order 10,000 units per year, it was assumed that materials costs would comprise 60% of the direct manufactured costs. Likewise, in volumes of greater than 100,000 units per year, materials costs were assumed to be 80% of the direct manufactured costs.

These summary costs are presented in Table 9-4. The direct manufactured costs was estimated to be in the range $8 - $11 per Watt, depending on production volume. Of this, the AMTEC module accounted for 55% of the system weight and 75% of the system cost. Most notably, the β"-alumina and the niobium account for 11% of the system weight and fully 50% of the system cost.

Table 9-3 Cost Estimate for a 500 W AMTEC Power Supply

Component	M g	Mtl $	M g	%	Mtl Cost $	%
AMTEC Module	**7457**	**$ 2,503.05**		**54.8**		**75.0**
Sodium			50	0.4	$0.33	0.0
Base Plate			576	4.2	$119.23	3.6
Beta Tubes			1154	8.5	$915.00	27.4
Anode Wicks/Current Collectors			614	4.5	$1.76	0.1
Niobium Tubes			408	3.0	$1,132.49	33.9
Cathode Electrode Wash			36	0.3	$0.40	0.0
Cathode Current Collectors			441	3.2	$84.54	2.5
Bus Bars			62	0.5	$11.97	0.4
Isolation Webs			395	2.9	$81.73	2.4
Assembly Glassing			132	1.0	$1.45	0.0
Evaporator Dome			542	4.0	$29.87	0.9
Evaporator Cylinder			1575	11.6	$86.84	2.6
Conic Cylinder			560	4.1	$30.85	0.9
High Tech Condenser			99	0.7	$0.22	0.0
Condenser Dome			69	0.5	$0.15	0.0
Feedthroughs			22	0.2	$4.15	0.1
Radiation Shields			128	0.9	$0.37	0.0
Radiation Supports			208	1.5	$0.60	0.0
Wicking Material			387	2.8	$1.11	0.0
Combustor Assembly	**833**	**$ 2.26**		**6.1**		**0.1**
Injector Mount			16	0.1	$0.04	0.0
Dome Conic			12	0.1	$0.03	0.0
Outer Dome Cylinder			42	0.3	$0.12	0.0
Inner Dome Cylinder			29	0.2	$0.08	0.0
Air Swirler			9	0.1	$0.03	0.0
Top Air Feed Plate			189	1.4	$0.42	0.0
Bottom Air Feed Plate			537	4.0	$1.54	0.0
Recuperator Assembly	**2055**	**$ 5.56**		**15.1**		**0.2**
Cylinder 1			1554	11.4	$4.46	0.1
Cylinder 2			400	2.9	$0.88	0.0
Combustion Air Separator						0.0
Combustion Air Topplate			56	0.4	$0.12	0.0
Combustion Air Bottomplate			45	0.3	$0.10	0.0
Exhaust Assembly	**591**	**$ 1.30**		**4.3**		**0.0**
Exhaust Duct			64	0.5	$0.14	0.0
Transition Topplate			96	0.7	$0.21	0.0
Transition Bottomplate			96	0.7	$0.21	0.0
Transition skin			329	2.4	$0.73	0.0
Combustion Air Inlet duct			6	0.0	$0.01	0.0
Condenser	**488**	**$ 1.08**		**3.6**		**0.0**
Conic Transition			205	1.5	$0.45	0.0
Plenum topplate			47	0.3	$0.10	0.0
Plenum bottom plate			79	0.6	$0.17	0.0
Plenum wraparound			157	1.2	$0.35	0.0
Insulation	**1260**	**$ 68.06**		**9.3**		**2.0**
Condenser Cap			142	1.0	$7.69	0.2
Recup to Condenser			118	0.9	$6.35	0.2
Recuperator Cap			720	5.3	$38.89	1.2
Recuperator Length			280	2.1	$15.12	0.5
Support Components	**920**	**$ 757.35**		**6.8**		**22.7**
Condenser blower			60	0.4	$170.00	5.1
Combustion Air blower			60	0.4	$180.00	5.4
Electrostatic injector			0	0.0	$40.00	1.2
fuel pump			20	0.1	$120.00	3.6
fuel hose			0	0.0	$4.92	0.1
Polypropylene air hose			0	0.0	$2.43	0.1
3-way Solenoid valve			20	0.1	$60.00	1.8
Fuel filter			20	0.1	$10.00	0.3
Air filter			20	0.1	$5.00	0.1
Needle Valve			20	0.1	$15.00	0.4
Battery			500	3.7	$50.00	1.5
Controls			200	1.5	$100.00	3.0
Total			**13604**	**100.0**	**$3,338.66**	**100.0**

Table 9-4 Summary Manufacturing Cost Estimates for a 500 W AMTEC Power Supply

Element	Materials $/W[1]	Moderate Volume[2] $/W	High Volume[3] $/W
AMTEC Module	5	8	6
System Components	2	3	2
TOTAL	7	11	8

[1] All costs rounded to whole $/W
[2] Of order 10,000 units/yr, materials cost is 60% of total cost
[3] Greater than 100,000 units/yr,materials cost is 80% of total cost

10 Conclusions

In the course of the program major advances have been made in developing designs and fabrication techniques for AMTEC cells to make the technology better suited to fuel-fired terrestrial applications. In addition, significant progress was made in designing and demonstrating small scale fuel handling, combustion and heat transfer systems for power systems at the 500 W size range.

Significant accomplishments in this program include:

- Development of fabrication and assembly procedures for a first-of-a-kind toroidal AMTEC cell configuration.
- Fabrication and successful testing of a 24-BASE tube toroidal engineering cell.
- Fabrication of a 96-BASE tube prototype toroidal cell.
- Validation of cell thermal/electrochemical models using data from engineering cell tests.
- Design, development and testing of an electrostatic atomizer system.
- Design, fabrication and successful testing of a JP-8 combustion system for a 500 W power supply, including demonstration of challenging heat transfer requirements. Fabrication of the combustion test system.
- Development of improved AMTEC converter and system concepts to reduce part count, improve manufacturability and reduce cost.
- Development of a design and successful fabrication and testing of a novel method of glazing BASE tubes to an alumina header.
- Demonstration of successful Internal Self Heat Pipe operation of both a single large tube cell and a multi-tube cell.
- Design, fabrication and testing of a 35 W engineering cell incorporating internal self-heat piping.

We conclude that AMTEC still has the potential to provide high reliability, long-lived, quiet power at small power ranges (between ten and a few hundred Watts). Many successful component designs, simulation and modeling tools and fabrication techniques have been demonstrated at small scale in the course of the work. Fabrication of larger, multi-tube AMTEC modules must still be regarded as at the developmental stage, however. The glass seals developed in the latter part of the program clearly offer a path to simpler manufacturing processes and more cost-effective and robust designs.

Based on the work conducted in the program, it appears that when configured in a JP-8 fired 500 Watt system, AMTEC currently offers:

- System power density of approximately 40 W/kg
- Net system efficiency of approximately 12% – 14% (fuel to net power out)
- Manufacturing cost of approximately $8 - $11 per Watt (depending on production volume)